Contract No:

This document was prepared in conjunction with work accomplished under Contract No. DE-AC09-08SR22470 with the U.S. Department of Energy (DOE) Office of Environmental Management (EM).

Disclaimer:

Degradation of Saltstone Disposal Unit Cementitious Materials

G. P. Flach

August 7, 2018

SRNL-STI-2018-00077, Revision 1

DISCLAIMER

Printed in the United States of America

Prepared for
U.S. Department of Energy

SRNL-STI-2018-00077
Revision 1

Keywords: *Z-Area*
Performance Assessment

Retention: *Permanent*

Degradation of Saltstone Disposal Unit Cementitious Materials

G. P. Flach

August 7, 2018

Prepared for the U.S. Department of Energy under contract number DE-AC09-08SR22470.

Savannah River National Laboratory™
OPERATED BY SAVANNAH RIVER NUCLEAR SOLUTIONS

REVIEWS AND APPROVALS

AUTHORS:

_____

G. P. Flach, Environmental Modeling Date

TECHNICAL REVIEW:

_____

T. L. Danielson, Environmental Modeling, Reviewed per E7 2.60 Date

APPROVAL:

_____

D. A. Crowley, Manager Date
Environmental Modeling

_____

L. T. Reid, Manager Date
Environmental Restoration Technologies

_____

K. H. Rosenberger, Manager Date
Closure and Disposal Assessment

REVISIONS

Revision 0 Issued April 4, 2018

Revision 1 Saltstone porosity and bulk density updated (SRR-CWDA-2018-00004 Rev. 1).

"Concrete for Cylinder SDUs" replaced with "Concrete for Existing Cylinder SDUs" and "Concrete for Future Cylinder SDUs" (SRR-CWDA-2018-00004 Rev. 1).

For SDU 7 Design case, HDPE thickness in floor reduced from 100 mil to 60 mil.

For SDU 7 Design Margin case, HDPE-GCL layer removed from floor.

For SDU 7 Design Margin case, floor and roof concrete are now initially damaged based on assumed unrepaired floor penetrations during construction (e.g. anchor bolt borings).

For SDU 1 and 4, HDPE-GCL layer added to roof.

HDPE degradation model revised to be consistent with cover system assumptions (SRRA107772-000009)

In Table 4-9, total ion concentration in g/L corrected to include nitrate/nitrite and carbonate contributions (g/L value not used in degradation calculations).

EXECUTIVE SUMMARY

The Saltstone facilities at the DOE Savannah River Site (SRS) are used to stabilize and dispose of low-level radioactive salt solution originating from liquid waste storage tanks at the site. The Saltstone Production Facility (SPF) receives treated salt solution and mixes the aqueous waste with dry cement, blast furnace slag, and fly ash to form a grout slurry which is mechanically pumped into concrete disposal cells that compose the Saltstone Disposal Facility (SDF). The solidified grout is termed "saltstone".

Cementitious materials play a prominent role in the design and long-term performance of the SDF. The saltstone grout exhibits low permeability and diffusivity, and thus represents a physical barrier to waste release. The waste form is also reducing, which creates a chemical barrier to waste release for certain key radionuclides, notably Tc-99. Similarly, the concrete shell of a saltstone disposal unit (SDU) represents an additional physical and chemical barrier to radionuclide release to the environment. Together the waste form and the SDU compose a robust containment structure at the time of facility closure. However, the physical and chemical state of cementitious materials will evolve over time through a variety of phenomena, leading to degraded barrier performance over Performance Assessment timescales of thousands to tens of thousands of years. Previous studies of cementitious material degradation in the context of low-level waste disposal have identified sulfate attack, carbonation-influenced steel corrosion, and decalcification (primary constituent leaching) as the chemical degradation phenomena of most significance under SRS exposure conditions.

In this study, degradation time scales for each of these three degradation phenomena are estimated for saltstone and SDU concrete associated with each SDU design under conservative, compliance, and best estimate assumptions. The "compliance value" (CV) is an intermediate result recommended for PA compliance case modeling that is more probable than the "conservative estimate" (CE) and more defensible than the "best estimate" (BE). The combined effects of multiple phenomena are then considered to determine the most limiting degradation time scale for each cementitious material component (e.g. roof, wall, floor). Degradation times are estimated using analytic solutions, supported by numerical simulation codes provided through the DOE Cementitious Barriers Partnership (CBP) Software Toolbox. Onset of degradation may be delayed due to clean cap grout or HDPE/GCL liners. Also considered is any physical and/or concrete degradation occurring during facility construction and/or operations, such as anchor penetrations and exposure to bleed water. Task Assistance Request G-TAR-Z-00006 further defines the task scope.

In the context of this analysis, the term "SDU 2" is used to represent all 150-foot diameter SDU structures: SDU 2A, SDU 2B, SDU 3A, SDU 3B, SDU 5A, and SDU 5B. Similarly, "SDU 7" refers to all future 375-foot diameter SDU structures: SDU 7, SDU 8, SDU 9, SDU 10, SDU 11, SDU 12, and (if needed) SDU 13.

Degradation times are summarized in Table 9-7 for existing, as-built SDUs (SDU 1, 4, 2, 6) and future, as-designed SDUs (SDU 7) conditions. Pessimistic degradation times are also provided for SDU 7 for postulated thinner as-built concrete barriers and unrepaired physical damage from various construction techniques (e.g. wall form wire anchors). Initial and fully-degraded hydraulic conductivity recommendations are summarized in Table 11-1.

TABLE OF CONTENTS

LIST OF TABLES

LIST OF FIGURES

LIST OF ABBREVIATIONS

BE	Best Estimate
CBP	Cementitious Barriers Partnership
CE	Conservative Estimate
CV	Compliance Value
DOE	Department of Energy
GCL	Geosynthetic Clay Liner
HDPE	High Density Polyethylene
MPAD	Most Probably And Defensible
PA	Performance Assessment
SPF	Saltstone Production Facility
SDF	Saltstone Disposal Facility
SDU	Saltstone Disposal Unit
SRNL	Savannah River National Laboratory
SRR	Savannah River Remediation LLC
SRS	Savannah River Site
VCO	Vault Concrete One (SDU 1/4 concrete)
VCT	Vault Concrete Two (SDU 2/6/7 concrete)
VU	Vanderbilt University

1.0 Introduction

The Saltstone facilities at the DOE Savannah River Site (SRS) are used to stabilize and dispose of low-level radioactive salt solution originating from liquid waste storage tanks at the site. The Saltstone Production Facility (SPF) receives treated salt solution and mixes the aqueous waste with dry cement, blast furnace slag, and fly ash to form a grout slurry which is mechanically pumped into concrete Saltstone Disposal Units (SDUs) that compose the Saltstone Disposal Facility (SDF). The solidified grout is termed "saltstone". The *Performance Assessment for the Saltstone Disposal Facility at the Savannah River Site* (SRR 2009) and subsequent Special Analyses (SRR 2013, 2014) provide further information about the general design and operation of the SDF.

Cementitious materials play a prominent role in the design and long-term performance of the SDF. Saltstone exhibits low permeability and diffusivity, and thus represents a physical barrier to waste release. The waste form is also reducing, which creates a chemical barrier to waste release for certain key radionuclides, notably Tc-99. Similarly, the concrete shell of an SDU represents an additional physical and chemical barrier to radionuclide release to the environment. Together the waste form and disposal cell compose a robust containment structure at the time of facility closure.

However, the physical and chemical state of cementitious materials will evolve over time through a variety of phenomena, leading to degraded barrier performance over Performance Assessment (PA) timescales of thousands to tens of thousands of years. Previous studies of cementitious material degradation in the context of low-level waste disposal have identified sulfate attack, carbonation-influenced steel corrosion, and decalcification (primary constituent leaching) as the chemical degradation phenomena of most relevance to SRS exposure conditions (Walton et al. 1990, Langton 2007, 2010a, Samson et al. 2009, Flach and Smith 2014, Flach 2015).

In this study, degradation time scales for each of these three degradation phenomena are estimated for saltstone and SDU concrete associated with each SDU design under conservative, compliance, and best estimate assumptions. The "compliance value" (CV) is an intermediate result that is more probable than the "conservative estimate" (CE) and more defensible than the "best estimate" (BE). The combined effects of multiple phenomena are then considered to determine the most limiting degradation time scale for each cementitious material. Degradation times are estimated using analytic solutions, supported by numerical simulation codes provided through the DOE Cementitious Barriers Partnership (CBP) Software Toolbox (http://cementbarriers.org). Also considered is any physical and/or concrete degradation occurring during facility construction and/or operations, such as anchor penetrations and exposure to bleed water. Task Assistance Request G-TAR-Z-00006 further defines the task scope.

This study consolidates and modifies preceding degradation analyses described by Flach (2013), Flach and Smith (2014) and Flach (2015), using updated inputs (Hommel 2018, Watkins 2018) and revised techniques. In the current analysis, the analytic method from Flach (2015) defines sulfate attack penetration rates, and CBP simulations provide supporting information. These roles were reversed in the previous analyses. With this revision, sulfate attack and carbonation penetration rates are predicted in a more similar manner. High Density Polyethylene (HDPE) and Geosynthetic Clay Liner (GCL) barriers were previously credited with slowing carbonation rates, based on hydraulic conductivity degradation reaching a certain threshold based on judgement. In the current analysis, the effects of HDPE and HDPE/GCL liners are estimated more rigorously using a two-layer diffusion model. The analysis has also been extended to include recommendations for computing effective hydraulic conductivity as a function of time, following Brown and Garrabrants (2017).

The previous set of analyses considered multiple degradation scenarios for the SDU 2 and 6 designs. In this study, only one scenario is considered for each of the SDU 1, 4, 2 and 6 designs. This "base case" scenario reflects currently known or expected conditions for each design. The analysis has also been expanded to include "Design" and "Design Margin" scenarios for future SDU 7. The expected Design (or base case) scenario represents as-designed dimensions and construction quality for SDU 7. The hypothetical Design Margin scenario reflects postulated thinner as-built concrete barriers and unrepaired physical damage from various construction techniques (e.g. wall form wire anchors). For each of the SDU 1, 4, 2, 6 and 7 scenarios, material degradation is defined for BE, CV, and CE input values.

CV results are generally recommended for PA compliance modeling, that is, comparison of deterministic predictions to performance objectives (e.g. 25 mrem/yr All-Pathways dose) to demonstrate compliance with regulations. BE and CE results are recommended for best-estimate prediction, sensitivity analysis, and uncertainty quantification. CV analysis inputs align with the "Nominal" or "MPAD" (Most Probable And Defensible) values in Hommel (2018).

The remaining discussion draws heavily, often verbatim, from Flach and Smith (2014) and Flach (2015). Notable modifications include reorganization of the sulfate attack narrative, new content on HDPE and HDPE/GCL liner degradation and effective hydraulic conductivity (Brown and Garrabrants 2017), and revised tables and results reflecting different input values from Hommel (2018) and Watkins (2018).

2.0 General Moving Reaction Front

The degradation mechanisms under consideration share the same basic functional form, wherein a chemical reaction zone moves slowly as a sharp front across the porous medium, and diffusion is the dominant transport mode for the fluid (gas or liquid) phase reactant, as shown in Figure 2-1.

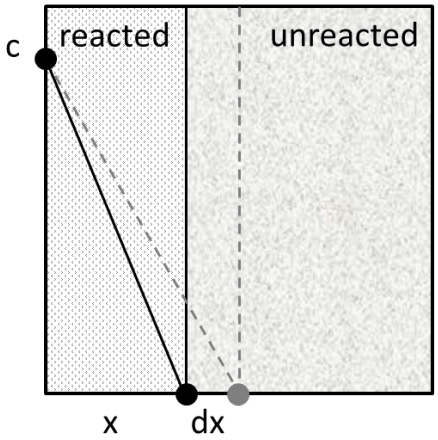

Figure 2-1 Generic moving reaction front controlled by diffusion.

The differential molar balance for this generic moving front system is

$$Sn\tau D_m \frac{c}{x} dt = R(1-n)\rho_s dx \qquad (2\text{-}1)$$

where

S = saturation of fluid phase delivering reactant to the moving front [cm^3 phase / cm^3 void]

n = porosity [cm^3 void / cm^3 total]

τ = tortuosity, defined here as the ratio of effective to molecular diffusion coefficient (< 1) [-]

D_m = molecular diffusion coefficient for fluid phase [cm^2/yr]

x = penetration depth [cm]

t = elapsed time [yr]

c = concentration of fluid phase reactant at the exposure surface [mol / cm^3 phase]

R = reaction capacity of solid [mol / g solid], i.e., moles of fluid phase reactant consumed per mass of solid

ρ_s = solid / mineral density [g/cm^3 solid].

Assuming a constant diffusion coefficient, integration of Equation (2-1) yields the following analytic expression for penetration depth:

$$x = \left[\frac{2Sn\tau D_m ct}{(1-n)\rho_s R}\right]^{1/2} = \left[\frac{2Sn\tau D_m ct}{\rho_b R}\right]^{1/2} \quad (2\text{-}2)$$

where

ρ_b = bulk density [g/cm^3].

Inspection of Equation (2-2) indicates that movement of the reaction front is proportional or inversely proportional to the square root of all quantities in the righthand expression. Equation (2-2) can be used to define the relative effect of a parameter change compared to a baseline result. For example, relative to a reference concentration (c_1) and penetration depth (x_1), a modified exposure concentration (c_2) produces an altered penetration depth (x_2) given by

$$x_2 = \left[\frac{c_2}{c_1}\right]^{1/2} x_1 \quad (2\text{-}3)$$

The effective reaction capacity of a numerical reactive transport model can be derived using Equation (2-2) for a selected penetration depth (x_0) and time (t_0) as

$$R = \frac{2Sn\tau D_m ct_0}{(1-n)\rho_s x_0^2} = \frac{2Sn\tau D_m ct_0}{\rho_b x_0^2} \quad (2\text{-}4)$$

Equation (2-4) is useful for translating numerical simulation results into the equivalent analytic form given by Equation (2-2), assuming the numerical model exhibits the underlying behavior implied by Equation (2-2). Alternatively, Equation (2-2) can be written as

$$x = At^{1/2} \quad (2\text{-}5)$$

where the rate constant A is defined by

$$A = \left[\frac{2Sn\tau D_m c}{(1-n)\rho_s R}\right]^{1/2} = \left[\frac{2Sn\tau D_m c}{\rho_b R}\right]^{1/2} \quad (2\text{-}6)$$

and empirically derived from a numerical simulation result (t_0,x_0) as

$$A = \frac{x_0}{t_0^{1/2}} \quad (2\text{-}7)$$

The time t_0 associated with a certain penetration depth x_0 is

$$t_0 = \frac{x_0^2}{A^2} \quad (2\text{-}8)$$

Equations (2-2) through (2-8) are generally applicable to all three degradation mechanisms being considered in this study (provided that the diffusion coefficient is fixed), although the specifics differ. In the case of sulfate attack, sulfate dissolved in the liquid phase diffuses into the porous medium, and reacts with the solid forming ettringite or gypsum. In the case of carbonation, carbon dioxide in the gas phase diffuses in, reacts with the solid forming calcite, and the pH is lowered. In the case of decalcification, the

'reaction' is calcium in the solid dissolving into the liquid phase; the dissolved calcium then diffuses out of the porous medium. The report sections that follow address the specific analyses performed for sulfate attack, carbonation, and decalcification.

Implicit in Equations (2-2) and (2-5) is the assumption of a constant diffusion coefficient. If physical damage is occurring behind the reaction front, then the diffusion coefficient may increase and the front may penetrate deeper than indicated by a $\sqrt{t}$ dependence. The $\sqrt{t}$ dependence is a result of increasing distance between the boundary and reaction front. If damage occurs around the reaction front, then the diffusion distance may effectively not increase beyond some maximum distance, δ [cm], and penetration will be proportional to time instead of $\sqrt{t}$ at long times. Assuming penetration initially follows Equation (2-5), this alternative relationship is described by

$$x = \frac{\delta}{t_\delta} t = \frac{\delta}{\delta^2/A^2} t = \frac{A^2}{\delta} t \tag{2-9}$$

where

δ = penetration through time t_δ [cm]

t_δ = time at which penetration reaches δ [yr].

Equations (2-5) and (2-9) are schematically depicted in Figure 2-2.

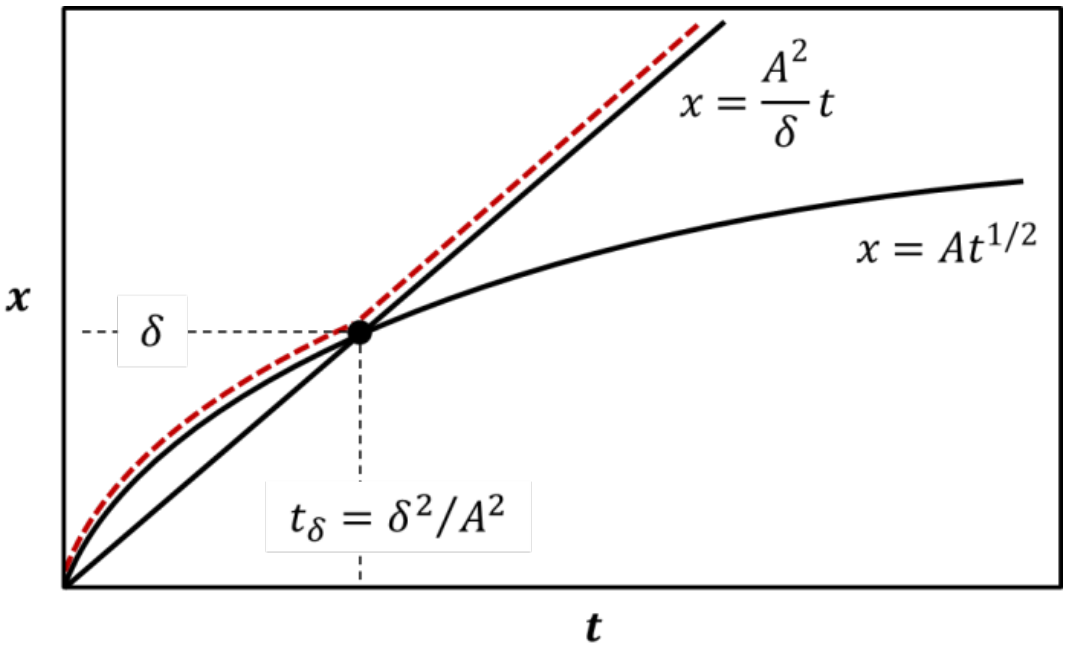

Figure 2-2 Square-root and linear penetration with respect to time.

Solving Equation (2-9) for time yields

$$t = \frac{\delta x}{A^2} \tag{2-10}$$

compared to

$$t = \frac{x^2}{A^2} \tag{2-11}$$

for a fixed diffusion coefficient from Equation (2-5).

To account for the feedback effects of physical damage on diffusion rates, the minimum of Equations (2-10) and (2-11) may be taken as the estimated degradation time t_0 for a specified material thickness x_0:

$$t_0 = min\left[\frac{x_0^2}{A^2}, \frac{\delta x_0}{A^2}\right] \tag{2-12}$$

The minimum time curve is shown in Figure 2-2 as a dashed red line. Selection of δ is discussed later in the context of specific degradation phenomena: sulfate attack, carbonation-influenced steel corrosion, and decalcification.

3.0 Sulfate Attack

Sodium sulfate attack involves ingress of sulfate ions through concrete pore water and reactions with calcium bearing minerals, including calcium hydroxide and $C\text{-}S\text{-}H$, that produce expansive products, principally ettringite and gypsum. Physical degradation occurs when sufficient ettringite and/or gypsum form to cause internal cracking.

3.1 Ettringite formation

The chemical formula for ettringite has been expressed in several equivalent forms including

$$Ca_6Al_2(SO_4)_3(OH)_{12} \cdot 26H_2O = 6CaO \cdot Al_2O_3 \cdot 3SO_3 \cdot 32H_2O = 3CaO \cdot Al_2O_3 \cdot 3CaSO_4 \cdot 32H_2O \quad (3\text{-}1)$$

and in the shorthand of cement chemist notation (http://en.wikipedia.org/wiki/Cement_chemist_notation)

$$C_6A\bar{S}_3H_{32} \quad (3\text{-}2)$$

Cement paste is calcium-rich compared to aluminum, so the latter is the limiting solid-phase reactant. The reaction capacity for ettringite formation based on aluminum availability can be estimated from laboratory characterization of Saltstone concrete.

SIMCO (2012) deduced mineral compositions for hydrated SDU concretes based on characterization of the dry mix components and thermodynamic considerations; these data summarized in Table 9 of SIMCO (2012) are reproduced in Table 3-1. The only aluminum-bearing phase is monosulfoaluminate (AFm). Equivalent chemical formulas for AFm in conventional and cement chemist notations include (Matschei et al. 2007)

$$Ca_4Al_2(SO_4)(OH)_{12} \cdot 6H_2O = 4CaO \cdot Al_2O_3 \cdot SO_3 \cdot 12H_2O \quad (3\text{-}3)$$

and

$$C_4A\bar{S}H_{12} \quad (3\text{-}4)$$

Table 3-2 presents a calculation of reaction capacity based on Table 3-1 and the stoichiometry indicated by Expressions (3-1) through (3-4). The availability of AFm for reaction is assumed to be 100% on the basis that formation of ettringite from AFm is thermodynamically favorable when additional sulfate enters the system (Matschei et al. 2007).

Table 3-1 SIMCO (2012) characterization of SDU concretes.

Mineral phase	SDU 1/4 (g/kg)	SDU 2/6/7 (g/kg)
$C\text{-}S\text{-}H$	118.8	81.2
CH (Portlandite)	7.2	-
AFm	18.4	10.0
C_4FH_{13}	9.9	-

Table 3-2 Ettringite reaction capacity of AFm based on SIMCO (2012).

Parameter	SDU 1/4	SDU 2/6/7	Units	Comments
Mass concentration of AFm	18.4	10.0	g / kg solid	SIMCO (2012) Table 9
Molecular weight of AFm	622	622	g / mol	Approximate value calculated from chemical formula using round numbers for element molecular weights
Molar concentration of AFm	2.96e-2 2.96e-5	1.61e-2 1.61e-5	mol / kg solid mol / g solid	Calculated
Moles Al per mole AFm	2	2	mol Al / mol AFm	See Expression (3-3)
Molar concentration of Al	5.92e-5	3.22e-5	mol / g solid	Calculated
Moles SO_4 reacted per mol Al	1.5	1.5	mol SO_4 / mol Al	See Expression (3-1)
Reaction capacity, R	**8.87e-5**	**4.82e-5**	mol SO_4 / g solid	Calculated

Ettringite reaction capacity can be similarly estimated from concrete characterization performed independently by Vanderbilt University (VU) on different concrete samples (Arnold et al. 2010), as summarized by input to the CBP LeachXS/Orchestra sulfate attack module (Flach 2015). These calculations are presented in Table 3-3. VU characterization is expressed on an elemental basis, thus the mass concentration of Al is directly specified.

Table 3-3 Ettringite reaction capacity based on VU characterization of total aluminum.

Parameter	SDU 1/4	SDU 2/6/7	Units	Comments
Mass concentration of Al	5373 5.373	6108 6.108	mg / kg solid g / kg solid	"Concrete_data.xls" input file
Molecular weight of Al	27	27	g / mol	
Molar concentration of Al	1.99e-1 1.99e-4	2.26e-1 2.26e-4	mol / kg solid mol / g solid	Calculated
Moles SO_4 reacted per mol Al	1.5	1.5	mol SO_4 / mol Al	See Expression (3-1)
Reaction capacity, R	**2.99e-4**	**3.39e-4**	mol SO_4 / g solid	Calculated

The Al reaction capacities in Table 3-2 and Table 3-3 differ because different samples were tested, and more significantly, because of differing assumptions for the availability of aluminum for reaction due to independent model calibration/validation efforts.

3.2 Gypsum formation

The chemical formula for gypsum can be expressed as

$$CaSO_4 \cdot 2H_2O = CaO \cdot SO_3 \cdot 2H_2O \quad (3\text{-}5)$$

or in cement chemist notation as

$$C\bar{S}H_2 \quad (3\text{-}6)$$

Unlike ettringite, calcium availability defines the reaction capacity for gypsum formation. The availability of calcium for gypsum formation is assumed to be less than 100% and limited to that present as calcium hydroxide (Portlandite) following the sulfate attack model of Tixier and Mobasher (2003a, b).

SIMCO Technologies Inc. models $C\text{-}S\text{-}H$ gel as a mixture of calcium hydroxide and the calcium silicate hydrate (CSH) mineral (Samson 2010, Table 7):

$$C\text{-}S\text{-}H = 1.65CaO \cdot SiO_2 \cdot 1.65H_2O = 0.65Ca(OH)_2 + CaH_2SiO_4 \quad (3\text{-}7)$$

In cement chemist notation, Equation (3-7) becomes

$$C\text{-}S\text{-}H = 0.65CH + CSH \quad (3\text{-}8)$$

Table 3-4 presents a calculation of the reaction capacity for gypsum formation based on Ca available explicitly as $Ca(OH)_2 = CH$ and implicitly as the CH portion of $C\text{-}S\text{-}H$.

Table 3-4 Gypsum reaction capacity based on SIMCO (2012).

Parameter	SDU 1/4	SDU 2/6/7	Units	Comments
Mass concentration of CH	7.2	-	g / kg solid	SIMCO (2012) Table 9
Molecular weight of CH	74	74	g / mol	$Ca(OH)_2$
Molar concentration of CH	9.73e-2 9.73e-5	-	mol / kg solid mol / g solid	Calculated
Moles of Ca per mole of CH	1	1	mol Ca / mol CH	$CH = Ca(OH)_2$
Molar concentration of Ca as CH	9.73e-5	-	mol / g solid	Calculated
Mass conc. of SIMCO $C\text{-}S\text{-}H$	118.8	81.2	g / kg solid	SIMCO (2012) Table 9
Molecular weight of SIMCO $C\text{-}S\text{-}H$	182.1	182.1	g / mol	$1.65CaO \cdot SiO_2 \cdot 1.65H_2O$
Molar conc. of SIMCO $C\text{-}S\text{-}H$	6.52e-1 6.52e-4	4.46e-1 4.46e-4	mol / kg solid mol / g solid	Calculated
Moles of Ca as CH per mole of $C\text{-}S\text{-}H$	0.65	0.65	mol Ca / mol $C\text{-}S\text{-}H$	$0.65CH + CSH$
Molar conc. of Ca as $C\text{-}S\text{-}H$	4.24e-4	2.90e-4	mol / g solid	Calculated
Total molar concentration of Ca	5.21e-4	2.90e-4	mol / g solid	Calculated
Moles SO_4 reacted per mol Ca	1	1	mol SO_4 / mol Al	See Expression (3-5)
Reaction capacity, R	**5.21e-4**	**2.90e-4**	mol SO_4 / g solid	Calculated

A similar calculation can be performed based on VU characterization of VCO ("Vault Concrete One", SDU 1/4) and VCT ("Vault Concrete Two", SDU 2/6/7) concretes (Arnold et al. 2010), and the resulting initial mineral assemblage in CBP LeachXS/Orchestra sulfate attack module simulations. Inspection of LeachXS/Orchestra simulation output listed in the Appendix of Flach (2015) indicates that both Portlandite and siliceous hydrogarnet are consumed during sulfate ingress, so both minerals are assumed to contribute to gypsum reaction capacity. Chemical formulas for siliceous hydrogarnet include

$$C_3AS_{0.8}H_{4.4} = 3CaO \cdot Al_2O_3 \cdot 0.8SiO_2 \cdot 4.4H_2O \quad (3\text{-}9)$$

Table 3-5 presents a calculation of gypsum reaction capacity based on Ca being available in calcium hydroxide and siliceous hydrogarnet.

Table 3-5 Gypsum reaction capacity based on VU characterization and LeachXS initialization.

Parameter	SDU 1/4	SDU 2/6/7	Units	Comments
Porosity	0.115	0.11	cm^3 void / cm^3 tot.	"Concrete_data.xls" input file
Saturation	1	1	cm^3 liq. / cm^3 void	Saturated exposure conditions
Solid density	2400	2310	kg / m^3 solid	"Concrete_data.xls" input file
Bulk density	2124 2.124	2056 2.056	kg / m^3 total g / cm^3 total	Calculated
Molar conc. of CH on a liquid basis	18.7	12.4	mol / L liquid	LeachXS initialization from "output_profiles.dat" (Appendix of Flach (2015); unreacted concrete at depth)
Molar conc. of CH on a total volume basis	2.15 2.15e-3	1.36 1.36e-3	mol / L total mol / cm^3 total	Calculated
Molar conc. of CH on a solid basis	1.01e-3	6.63e-4	mol / g solid	Calculated
Moles of Ca per mole CH	1	1	mol Ca / mol CH	$CH = Ca(OH)_2$
Molar conc. of Ca in CH on a solid basis	1.01e-3	6.63e-4	mol / g solid	Calculated
Molar conc. of $C_3AS_{0.8}H_{4.4}$ on a liquid basis	1.15	1.09	mol / L liquid	LeachXS initialization from "output_profiles.dat" (Appendix of Flach (2015); unreacted concrete at depth)
Molar conc. of $C_3AS_{0.8}H_{4.4}$ on a total volume basis	1.32e-1 1.32e-4	1.20e-1 1.20e-4	mol / L total mol / cm^3 total	Calculated
Molar conc. of $C_3AS_{0.8}H_{4.4}$ on a solid basis	6.23e-5	5.83e-5	mol / g solid	Calculated
Moles of Ca per mole $C_3AS_{0.8}H_{4.4}$	3	3	mol Ca / mol $C_3AS_{0.8}H_{4.4}$	$3CaO \cdot Al_2O_3 \cdot 0.8SiO_2 \cdot 4.4H_2O$
Molar conc. of Ca in $C_3AS_{0.8}H_{4.4}$ on a solid basis	1.87e-4	1.75e-4	mol / g solid	Calculated
Total molar conc. of Ca	1.20e-3	8.38e-4	mol / g solid	Calculated
Moles SO_4 reacted per mol Ca	1	1	mol SO_4 / mol Al	See Expression (3-5)
Reaction capacity, R	**1.20e-3**	**8.38e-4**	mol SO_4 / g solid	Calculated

As with Al reaction capacity, Ca reaction capacity differs between Table 3-4 and Table 3-5 due to differing assumptions for mineral availability. The LeachXS/Orchestra output file "output_profiles.dat" did not list the concentrations of C-S-H components `C-S-H_tobermorite` and `C-S-H_jennite`. Presumably these minerals provided additional reaction capacity for gypsum formation. An upper bound on reaction capacity can be calculated by assuming all Ca present in the system is available for reaction. This calculation is presented in Table 3-6. The increases in reaction capacity are modest at +16% for SDU 1/4 concrete and +29% for SDU 2/6/7 concrete.

Table 3-6 Gypsum reaction capacity based on VU characterization of total calcium.

Parameter	SDU 1/4	SDU 2/6/7	Units	Comments
Mass concentration of Ca	55579 55.579	43193 43.193	mg / kg solid g / kg solid	"Concrete_data.xls" input file
Molecular weight of Ca	40	40	g / mol	
Molar concentration of Ca	1.39 1.39e-3	1.08 1.08e-3	mol / kg solid mol / g solid	Calculated
Moles SO_4 reacted per mol Ca	1	1	mol SO_4 / mol Al	See Expression (3-5)
Reaction capacity, R	**1.39e-3**	**1.08e-3**	mol SO_4 / g solid	Calculated

3.3 Total reaction capacity

The total capacity of the solid to react with infiltrating sulfate is taken to be the sum of the capacities for reaction with AFm and any other aluminum phases (to form ettringite) and Portlandite (to form gypsum). Table 3-7 summarizes total reaction capacities based on independent material characterization performed by SIMCO Technologies and Vanderbilt University. The actual total reaction capacity based on VU characterization is expected to lie between the lower ("Portlandite calcium") and upper ("total calcium") estimates.

Table 3-7 Total reaction capacities.

Reaction capacity, R (mol SO_4 reacted / g solid)	SDU 1/4	SDU 2/6/7	Comments
SIMCO characterization			
Ettringite formation	8.87e-5	4.82e-5	Table 3-2
Gypsum formation	5.21e-4	2.90e-4	Table 3-4
Ettringite+gypsum formation	**6.10e-4**	**3.38e-4**	Total capacity
VU characterization			
Ettringite formation	2.99e-4	3.39e-4	Table 3-3
Gypsum formation, Portlandite calcium	1.20e-3	8.38e-4	Table 3-5
Gypsum formation, total calcium	1.39e-3	1.08e-3	Table 3-6
Ettringite+gypsum formation, Portlandite calcium	**1.50e-3**	**1.18e-3**	Lower estimate of total capacity
Ettringite+gypsum formation, total calcium	**1.69e-3**	**1.42e-3**	Upper estimate of total capacity

3.4 Penetration rate coefficients

Table 3-8 and Table 3-9 present sulfate attack rate coefficients calculated using Equation (2-6) for SDU 1/4 and SDU 2/6/7 concrete, respectively. Because SDU 1 and 4 wall concretes are assumed to be fully degraded at PA time zero for the CV and CE cases, obviating the need for degradation estimates except for the BE case, penetration rate coefficient calculations are not shown in Table 3-8 for these components. However, the rate coefficients for the SDU 1/4 wall BE, CV and CE cases were calculated herein to be 0.651, 2.118 and 2.118 cm/√yr, respectively.

Note that a higher reaction capacity is associated with a lower rate coefficient, because more time is required to consume more solid-phase reactant for a given fluid-phase reactant transport rate. Thus, the rate coefficients based on SIMCO characterization are higher than those based on VU characterization. The SIMCO rate coefficients are adopted for further analysis as a pessimistic assumption. Flach (2015) compared sulfate penetration depths based on Equation (2-2) to those simulated by the CBP Software Toolbox version 1.0 sulfate attack module, and concluded that the two methods produced similar results.

Table 3-8 Penetration rate coefficients for sulfate attack on SDU 1/4 concrete.

Parameter	SDU 1/4 Floor			SDU 1/4 Roof			Units
	BE	CV	CE	BE	CV	CE	
Porosity (a)	0.106	0.106	0.106	0.106	0.106	0.106	cm^3 void / cm^3 total
Bulk density (a)	2.28	2.28	2.28	2.28	2.28	2.28	g solid / cm^3 total
Saturation	1	1	1	1	1	1	cm^3 liquid / cm^3 void
Effective diffusion coefficient (a)	3.5E-08	5.3E-08	6.0E-08	6.0E-08	9.7E-08	1.2E-07	cm^2/s
	1.1	1.7	1.9	1.9	3.1	3.8	cm^2/yr
Exposure concentration (b)	0.1	0.1	0.1	0.1	0.1	0.1	mol / L
	1.0E-04	1.0E-04	1.0E-04	1.0E-04	1.0E-04	1.0E-04	mol / cm^3
SIMCO Technologies, Inc. characterization							
Reaction capacity	6.10E-04	6.10E-04	6.10E-04	6.10E-04	6.10E-04	6.10E-04	mol SO_4 reacted / g solid
Rate coefficient	**0.130**	**0.160**	**0.170**	**0.170**	**0.216**	**0.240**	cm / √yr
Vanderbilt University characterization							
Reaction capacity, lower estimate	1.50E-03	1.50E-03	1.50E-03	1.50E-03	1.50E-03	1.50E-03	mol SO_4 reacted / g solid
Rate coefficient, lower estimate	0.083	0.102	0.108	0.108	0.138	0.153	cm / √yr
Reaction capacity, upper estimate	1.69E-03	1.69E-03	1.69E-03	1.69E-03	1.69E-03	1.69E-03	mol SO_4 reacted / g solid
Rate coefficient, upper estimate	0.078	0.096	0.102	0.102	0.130	0.144	cm / √yr

Table 3-8 notes:
(a) Hommel (2018), Table 1.
(b) Average SO_4 concentration of Tank 50 salt solution from 2007 to 2014 is 0.05M (Simner 2015). Pore water concentration in cured saltstone is 2x higher than in mixing fluid concentration (SIMCO 2010, Tables 3 and 8).

Table 3-9 Penetration rate coefficients for sulfate attack on SDU 2/6/7 concrete.

Parameter	SDU 2/6/7 Concrete			SDU 2/6/7 Column			Units
	BE	CV	CE	BE	CV	CE	
Porosity (a)	0.11	0.11	0.11	0.211	0.211	0.211	cm^3 void / cm^3 total
Bulk density (a)	2.18	2.18	2.18	2.06	2.06	2.06	g solid / cm^3 total
Saturation	1	1	1	1	1	1	cm^3 liquid / cm^3 void
Effective diffusion coefficient (a)	3.5E-08	5.3E-08	6.0E-08	1.2E-07	3.9E-07	5.0E-07	cm^2/s
	1.1	1.7	1.9	3.8	12.3	15.8	cm^2/yr
Exposure concentration (b)	0.1	0.1	0.1	0.1	0.1	0.1	mol / L
	1.0E-04	1.0E-04	1.0E-04	1.0E-04	1.0E-04	1.0E-04	mol / cm^3
SIMCO Technologies, Inc. characterization							
Reaction capacity	3.38E-04	3.38E-04	3.38E-04	3.38E-04	3.38E-04	3.38E-04	mol SO_4 reacted / g solid
Rate coefficient	**0.182**	**0.223**	**0.238**	**0.479**	**0.863**	**0.977**	cm / √yr
Vanderbilt University characterization							
Reaction capacity, lower estimate	1.18E-03	1.18E-03	1.18E-03	1.18E-03	1.18E-03	1.18E-03	mol SO_4 reacted / g solid
Rate coefficient, lower estimate	0.097	0.120	0.127	0.257	0.463	0.524	cm / √yr
Reaction capacity, upper estimate	1.42E-03	1.42E-03	1.42E-03	1.42E-03	1.42E-03	1.42E-03	mol SO_4 reacted / g solid
Rate coefficient, upper estimate	0.089	0.109	0.116	0.234	0.421	0.477	cm / √yr

Table 3-9 notes:
(a) Hommel (2018), Table 1.
(b) Average SO_4 concentration of Tank 50 salt solution from 2007 to 2014 is 0.05M (Simner 2015). Pore water concentration in cured saltstone is 2x higher than in mixing fluid concentration (SIMCO 2010, Tables 3 and 8).

3.5 Sulfate attack prior to facility closure

Between construction and disposal unit closure, SDU wall concrete may experience significant desiccation from exposure to the atmosphere. When subsequently exposed to grout slurry and bleed water, sulfate may rapidly penetrate the dry concrete due to strong capillary suction, causing early and accelerated sulfate attack prior to facility closure (Phifer et al. 2007). Wall sections adjoining sheet drains may be exposed to bleed water multiple times. Drying could also potentially lead to fine-scale shrinkage cracking at wall surfaces, and provide a means for accelerated sulfate intrusion (Phifer et al. 2007).

However, a waterproof coating was applied to the inside wall of SDU 2. This coating is assumed to fully protect SDU 2 wall concrete from sulfate attack during operations, but not delay the onset of post-closure sulfate attack. Also, SDU 1 and 4 wall concretes are assumed to be already fully degraded, consistent with recent PA modeling (Flach and Smith 2014), obviating further consideration of these components.

Floor concrete is much less likely to dry out because the bottom contacts the damp subsurface, initial saltstone placement will cover the top surface, and its initial saturation may be higher due to more conducive curing conditions (e.g. horizontal surface for holding external moisture). Roof concrete will generally be protected by clean grout, which may or may not be credited for delaying the onset of sulfate attack after facility closure (Section 7.0). Also, high humidity conditions inside an SDU during operations will tend to re-saturate roof concrete over time. Therefore, the potential for sulfate attack on SDU floor and roof concrete during operations is considered relatively insignificant.

The components remaining to be considered are the SDU 6 and 7 walls. Following the approach of Flach (2013), initial degradation depth from accelerated sulfate attack is estimated by considering surface cracking and capillary suction. The extent of presumed sulfate attack damage depends on the timescales of chemical reaction and diffusive transport. If the chemical reaction rate is relatively slow, then sulfate entering the system by capillary suction will penetrate to the same depth as the bleed water intrusion before reacting. If the reaction rate is fast, then sulfate will be consumed at a reaction front at a shallower depth.

For the *slow* reaction scenario, bleed water is assumed to displace all pore water in its path in a plug-flow manner. With this simple model, the penetration depth is

$$\delta_s = (S_f - S_i)L \tag{3-10}$$

where S_i and S_f are the initial and final saturations, and L is the wall thickness. The final saturation is assumed to be 100%. Sappington and Phifer (2005) analyzed concrete rubble exposed to atmospheric conditions (uncovered) at the Savannah River Site and observed an average saturation of 73%, which is adopted as a representative initial saturation.

For the *fast* reaction scenario, the penetration depth depends on the reaction capacity of the solid. Based on SIMCO (2012) characterization, the reaction capacity for conversion of AFm to ettringite, ignoring potential reaction of sulfate with calcium-bearing phases to form gypsum, is given in Table 3-2 as. 4.82e-5 mol SO_4 / g solid. The penetration depth is

$$\delta_f = \frac{(S_f - S_i)nc}{\rho_b R} L \tag{3-11}$$

where n is porosity, c is sulfate concentration, ρ_b is bulk density, and R is reaction capacity.

Reality is assumed to lie between the *slow* and *fast* end-members and coincide with their geometric mean, including hypothetical drying shrinkage cracks to depth δ_c:

$$\delta = \sqrt{(\delta_c + \delta_s)(\delta_c + \delta_f)} \quad (3\text{-}12)$$

Levitt (2003, p. 5) states that the drying shrinkage "has typical crack apertures in the range 0.1-0.5mm, tapering to zero at depths of about 10mm." Thus, interior walls are assumed to have surface cracks to a depth of δ_c = 1.0 cm (10 mm) and be physically degraded to at least this depth prior to any sulfate exposure.

As-built dimensions are used for SDU 6. For future SDU 7, two scenarios are considered (Watkins 2018). The SDU 7 "Design" case reflects the current design. The SDU 7 "Design Margin" case assumes thinner components to accommodate potential design changes and/or construction deviations. Input parameters and results for these three cases are summarized by Table 3-10 through Table 3-12. Because the SDU 6 and 7 walls are tapered, each wall is divided into 5 vertical segments consistent with recent PA simulations of these units. The average thickness of each segment is used for the parameter L. Initial damage due to early sulfate attack is estimated to be around 1 to 2 inches.

Table 3-10 Degradation of SDU 6 wall concrete segments due to early sulfate attack.

Parameter	Wall 1	Wall 2	Wall 3	Wall 4	Wall 5	Units
Thickness, L	22.37	19.08	15.66	12.28	10.33	in
	56.83	48.45	39.77	31.19	26.23	cm
Initial saturation, S_i (a)	0.73	0.73	0.73	0.73	0.73	mL liquid / mL void
Final saturation, S_f	1	1	1	1	1	mL liquid / mL void
Change in saturation, ΔS	0.27	0.27	0.27	0.27	0.27	mL liquid / mL void
Porosity, n (b)	0.11	0.11	0.11	0.11	0.11	mL void / mL total
Surface crack depth, δ_c (c)	1	1	1	1	1	cm
	0.39	0.39	0.39	0.39	0.39	in
Slow reaction						
Penetration fraction	0.27	0.27	0.27	0.27	0.27	
Penetration distance, δ_s	15.34	13.08	10.74	8.42	7.08	cm
Total degraded thickness	16.34	14.08	11.74	9.42	8.08	cm
$\delta_c + \delta_s$	6.43	5.54	4.62	3.71	3.18	in
Fast reaction						
Bulk density, ρ_b (b)	2.18	2.18	2.18	2.18	2.18	g/mL
Bleed water conc., c (d)	0.075	0.075	0.075	0.075	0.075	mol/L
	7.50E-05	7.50E-05	7.50E-05	7.50E-05	7.50E-05	mol/mL
Reaction capacity, R (e)	4.82E-05	4.82E-05	4.82E-05	4.82E-05	4.82E-05	mol SO4 / g solid
	1.1E-04	1.1E-04	1.1E-04	1.1E-04	1.1E-04	mol/mL
	0.11	0.11	0.11	0.11	0.11	mol/L
Penetration fraction	0.02	0.02	0.02	0.02	0.02	
Penetration distance, δ_f	1.20	1.03	0.84	0.66	0.56	cm
Total degraded thickness	2.20	2.03	1.84	1.66	1.56	cm
$\delta_c + \delta_f$	0.87	0.80	0.73	0.65	0.61	in
Initial damage						
Geometric mean value	6.00	5.34	4.65	3.96	3.55	cm
$\sqrt{(\delta_c + \delta_s)(\delta_c + \delta_f)}$	2.36	2.10	1.83	1.56	1.40	in
Intact wall thickness	50.82	43.11	35.12	27.23	22.68	cm
	20.01	**16.97**	**13.83**	**10.72**	**8.93**	in

Table 3-10 notes:
(a) Sappington and Phifer (2005)
(b) Hommel (2018)
(c) Levitt (2003), page 5
(d) Bleed water concentration taken as the midpoint between feed water (0.05 mol/L, Simner 2015) and porewater (~2x, SIMCO 2010)
(e) Table 3-2. Reaction capacity for conversion of AFm to ettringite. Potential reaction of sulfate with calcium-bearing phases to form gypsum ignored. Based on SIMCO (2012) characterization.

Table 3-11 Degradation of SDU 7 Design wall concrete segments due to early sulfate attack.

Parameter	Wall 1	Wall 2	Wall 3	Wall 4	Wall 5	Units
Thickness, L	22.60	19.78	16.85	13.95	12.28	in
	57.42	50.24	42.80	35.44	31.19	cm
Initial saturation, S_i (a)	0.73	0.73	0.73	0.73	0.73	mL liquid / mL void
Final saturation, S_f	1	1	1	1	1	mL liquid / mL void
Change in saturation, ΔS	0.27	0.27	0.27	0.27	0.27	mL liquid / mL void
Porosity, n (b)	0.11	0.11	0.11	0.11	0.11	mL void / mL total
Surface crack depth, δ_c (c)	1	1	1	1	1	cm
	0.39	0.39	0.39	0.39	0.39	in
Slow reaction						
Penetration fraction	0.27	0.27	0.27	0.27	0.27	
Penetration distance, δ_s	15.50	13.56	11.55	9.57	8.42	cm
Total degraded thickness	16.50	14.56	12.55	10.57	9.42	cm
$\delta_c + \delta_s$	6.50	5.73	4.94	4.16	3.71	in
Fast reaction						
Bulk density, ρ_b (b)	2.18	2.18	2.18	2.18	2.18	g/mL
Bleed water conc., c (d)	0.075	0.075	0.075	0.075	0.075	mol/L
	7.50E-05	7.50E-05	7.50E-05	7.50E-05	7.50E-05	mol/mL
Reaction capacity, R (e)	4.82E-05	4.82E-05	4.82E-05	4.82E-05	4.82E-05	mol SO4 / g solid
	1.1E-04	1.1E-04	1.1E-04	1.1E-04	1.1E-04	mol/mL
	0.11	0.11	0.11	0.11	0.11	mol/L
Penetration fraction	0.02	0.02	0.02	0.02	0.02	
Penetration distance, δ_f	1.22	1.06	0.91	0.75	0.66	cm
Total degraded thickness	2.22	2.06	1.91	1.75	1.66	cm
$\delta_c + \delta_f$	0.87	0.81	0.75	0.69	0.65	in
Initial damage						
Geometric mean value	6.05	5.48	4.89	4.30	3.96	cm
$\sqrt{(\delta_c + \delta_s)(\delta_c + \delta_f)}$	2.38	2.16	1.93	1.69	1.56	in
Intact wall thickness	51.37	44.76	37.90	31.14	27.23	cm
	20.22	**17.62**	**14.92**	**12.26**	**10.72**	in

Table 3-11 notes:
(a) Sappington and Phifer (2005)
(b) Hommel (2018)
(c) Levitt (2003), page 5
(d) Bleed water concentration taken as the midpoint between feed water (0.05 mol/L, Simner 2015) and porewater (~2x, SIMCO 2010)
(e) Table 3-2. Reaction capacity for conversion of AFm to ettringite. Potential reaction of sulfate with calcium-bearing phases to form gypsum ignored. Based on SIMCO (2012) characterization.

Table 3-12 Degradation of SDU 7 Design Margin wall concrete segments due to early sulfate attack.

Parameter	Wall 1	Wall 2	Wall 3	Wall 4	Wall 5	Units
Thickness, L	18.49	15.43	12.25	9.12	7.30	in
	46.96	39.19	31.12	23.16	18.55	cm
Initial saturation, S_i (a)	0.73	0.73	0.73	0.73	0.73	mL liquid / mL void
Final saturation, S_f	1	1	1	1	1	mL liquid / mL void
Change in saturation, ΔS	0.27	0.27	0.27	0.27	0.27	mL liquid / mL void
Porosity, n (b)	0.11	0.11	0.11	0.11	0.11	mL void / mL total
Surface crack depth, δ_c (c)	1	1	1	1	1	cm
	0.39	0.39	0.39	0.39	0.39	in
Slow reaction						
Penetration fraction	0.27	0.27	0.27	0.27	0.27	
Penetration distance, δ_s	12.68	10.58	8.40	6.25	5.01	cm
Total degraded thickness	13.68	11.58	9.40	7.25	6.01	cm
$\delta_c + \delta_s$	5.39	4.56	3.70	2.86	2.37	in
Fast reaction						
Bulk density, ρ_b (b)	2.18	2.18	2.18	2.18	2.18	g/mL
Bleed water conc., c (d)	0.075	0.075	0.075	0.075	0.075	mol/L
	7.50E-05	7.50E-05	7.50E-05	7.50E-05	7.50E-05	mol/mL
Reaction capacity, R (e)	4.82E-05	4.82E-05	4.82E-05	4.82E-05	4.82E-05	mol SO4 / g solid
	1.1E-04	1.1E-04	1.1E-04	1.1E-04	1.1E-04	mol/mL
	0.11	0.11	0.11	0.11	0.11	mol/L
Penetration fraction	0.02	0.02	0.02	0.02	0.02	
Penetration distance, δ_f	0.99	0.83	0.66	0.49	0.39	cm
Total degraded thickness	1.99	1.83	1.66	1.49	1.39	cm
$\delta_c + \delta_f$	0.79	0.72	0.65	0.59	0.55	in
Initial damage						
Geometric mean value	5.22	4.60	3.95	3.29	2.89	cm
$\sqrt{(\delta_c + \delta_s)(\delta_c + \delta_f)}$	2.06	1.81	1.56	1.29	1.14	in
Intact wall thickness	41.74	34.58	27.17	19.87	15.66	cm
	16.43	**13.61**	**10.70**	**7.82**	**6.16**	in

Table 3-12 notes:
(a) Sappington and Phifer (2005)
(b) Hommel (2018)
(c) Levitt (2003), page 5
(d) Bleed water concentration taken as the midpoint between feed water (0.05 mol/L, Simner 2015) and porewater (~2x, SIMCO 2010)
(e) Table 3-2. Reaction capacity for conversion of AFm to ettringite. Potential reaction of sulfate with calcium-bearing phases to form gypsum ignored. Based on SIMCO (2012) characterization.

4.0 Carbonation

Carbonation, more properly termed carbonatation, commonly refers to the reaction of carbon dioxide with calcium hydroxide (Portlandite) to form calcium carbonate (calcite):

$$Ca(OH)_2 + H_2O + CO_2 \rightarrow CaCO_3 + 2H_2O \quad (4\text{-}1)$$

or in cement chemist shorthand notation

$$CH + H + \overline{C} \rightarrow C\overline{C} + 2H \quad (4\text{-}2)$$

More generally, carbonation in the context of concrete may include other reactions of carbon dioxide with calcium-bearing minerals, such as calcium-silicate-hydrate gel ($C\text{-}S\text{-}H$). Carbonation increases mechanical strength and decreases alkalinity to a pH around 8.5 in cementitious materials. While the former is generally beneficial, corrosion of embedded steel accelerates as pH approaches carbonated conditions, approximately $pH < 10$. The volume of the corrosion products far exceeds that of the uncorroded steel, which typically introduces sufficient internal pressure to cause cracking and spalling of the surrounding concrete. Going forward "carbonation" is used as shorthand for "carbonation-influenced corrosion of steel", keeping mind that carbonation itself does not appreciably degrade the hydraulic and transport properties on cementitious materials. Rather, carbonation only leads to physical damage in the presence of embedded steel (e.g. reinforcing bars). Most concrete components of the various SDUs contain reinforcing steel, notable exceptions including the upper and lower mud mats in the SDU 2 design. Saltstone grout also contains embedded steel in the form of metal support columns (SDU 2 and 4) and roof trusses (SDU 4). Steel corrosion is discussed further in Section 5.0.

4.1 Analytic solution

Papadakis et al. (1989) developed an analytical solution for carbonation penetration depth with the same basic form as Equation (2-2). Using the nomenclature of this report, the expression is

$$x = \left[\frac{2\theta D_e c_{CO_2} t}{c_{Ca(OH)_2} + 3c_{CSH}}\right]^{1/2} \quad (4\text{-}3)$$

where

x = penetration depth [cm]

θ = gas content, Sn [cm^3 phase / cm^3 total]

D_e = effective diffusion coefficient for gas phase, τD_m [cm^2/yr]

c_{CO_2} = carbon dioxide concentration [mol / cm^3 gas]

t = elapsed time [yr]

$c_{Ca(OH)_2}$ = Portlandite concentration [mol / cm^3 total]

c_{CSH} = CSH concentration, $CSH \equiv 3CaO \cdot 2SiO_2 \cdot 3H_2O$ [mol / cm^3 total].

In the context of Equation (2-6), $c_{Ca(OH)_2} + 3c_{CSH} = (1-n)\rho_s R = \rho_b R$. Equation (4-3) considers only transport of carbon dioxide through the gas phase, which is appropriate for unsaturated concrete in typical

applications. However, fully saturated conditions are also of interest for the SDF and Equation (4-3) can be generalized to include delivery of dissolved carbon dioxide to the reaction front as

$$x = \left[\frac{2\left(\theta_g D_{e,g} c_{CO_2,g} + \theta_\ell D_{e,\ell} c_{CO_2,\ell}\right)t}{c_{Ca}}\right]^{1/2} = At^{1/2} \tag{4-4}$$

where the subscripts g and ℓ denote the gas and liquid phases, respectively, and

$$A \equiv \left[\frac{2\left(\theta_g D_{e,g} c_{CO_2,g} + \theta_\ell D_{e,\ell} c_{CO_2,\ell}\right)}{c_{Ca}}\right]^{1/2} \tag{4-5}$$

Also, the denominator of Equation (4-3) is equivalent to the cumulative molar concentration of Ca in $Ca(OH)_2$ and CSH, and denoted by c_{Ca} in these equations. Equation (4-4) is used to predict carbonation depth under saturated and unsaturated conditions in this study.

4.2 Gaseous and dissolved carbon dioxide concentrations

Millings (2012) estimated the average and median partial pressure of CO_2 in the vadose zone at the Savannah River Site to be roughly $p_{CO2} = 10^{-2}$ = 0.01 atm, compared to an atmospheric partial pressure of 0.00039 atm. Using the ideal gas law at 20ºC, the molar concentration of carbon dioxide in the vadose zone becomes 4.16E-07 mol/cm^3 gas. The concentration of dissolved CO_2 in cement pore water at the cement-soil interface can be estimated by analyzing a calcium carbonate (calcite) system in equilibrium with gaseous CO_2:

$$\begin{gathered} H_2O \rightleftharpoons H^+ + OH^- \\ CO_2(g) + H_2O \rightleftharpoons H_2CO_3 \\ CO_2(g) + H_2O \rightleftharpoons HCO_3^- + H^+ \\ H_2CO_3 \rightleftharpoons HCO_3^- + H^+ \\ HCO_3^- \rightleftharpoons CO_3^{2-} + H^+ \\ CaCO_3(s) \rightleftharpoons Ca^{2+} + CO_3^{2-} \end{gathered} \tag{4-6}$$

For a partial pressure of 0.01 atm, pH= 7.3 and the dominant form of dissolved carbon is HCO_3^- at a concentration c_{aq} = 3.07E-06 mol/ cm^3 liquid. The total concentration of dissolved carbon is c_{aq} = 3.41E-06 mol/ cm^3 (Table 4-1). The p_{CO2} data reported by Millings (2012) range from roughly $10^{-2.5}$ to $10^{-1.5}$ atm. The corresponding total concentration of dissolved carbon based on the calculation shown in Table 4-1 ranges from $c_{aq} = 2.2 \times 10^{-3}$ to 5.6×10^{-3} mol/ cm^3. This variation is relatively small compared to other uncertainties in the calculations of carbonation penetration rates, and ignored.

The transport properties and solid phase concentrations for the SDU 1/4 floor and wall concrete and SDU 2/6/7 concrete are available from the Hommel (2018) and SIMCO (2012). Similar data for the Saltstone grout are provided in Hommel (2018) and SIMCO (2010) / Langton (2010b). These input data to Equations (4-4) and (4-5) are summarized in Table 4-2, Table 4-3 and Table 4-4 for the BE, CV and CE cases, respectively. The solid phase concentration of calcium in SDU 1 and 4 roof concrete is approximated by scaling the SDU 1/4 floor/wall concrete value using the CaO ratios computed in Table 4-5 based on the composition of the unhydrated binders (SIMCO 2012, Table 3; SRR 2009, Tables 3.2-1 and 3.2-2).

Table 4-1 Chemical equilibrium for calcium carbonate (calcite) at 0.01 atm CO_2.

Reactions					
1)	$H_2O \leftrightarrow H^+ + OH^-$				
2)	$CO_2(g) + H_2O \leftrightarrow H_2CO_3$				
3)	$CO_2(g) + H_2O \leftrightarrow HCO_3^- + H^+$				
4)	$H_2CO_3 \leftrightarrow HCO_3^- + H^+$				
5)	$HCO_3^- \leftrightarrow CO_3^{2-} + H^+$				
6)	$CaCO_3(s) \leftrightarrow Ca^{2+} + CO_3^{2-}$				
Specifications		value	units	$-\log_{10}$	Comments
1)	p_{CO2}	0.010000	atm	2.00	Millings, M. *Summary of Carbon Dioxide in Water Table Wells and the Vadose Zone at SRS*, SRNL-L3200-2012-00017, May 30, 2012.
Equations		@25C	units	$-\log_{10}K$	Comments
1)	$K_w = [H^+][OH^-]$	1.00E-14	M^2	14	e.g. Table 3.4 (25C), R. A. Freeze and J. A. Cherry, Groundwater, Prentice-Hall, 1979
2)	$K_{CO2} = [H_2CO_3]/p_{CO2}$	3.39E-02	M/atm	1.47	Table 4-1, J. I. Drever, The Geochemistry of Natural Waters, 2nd edition, Prentice-Hall, 1988
3)	$K_1 = [H^+][HCO_3^-]/[H_2CO_3]$	4.47E-07	M	6.35	Table 4-1, J. I. Drever, The Geochemistry of Natural Waters, 2nd edition, Prentice-Hall, 1988
	$K_1 = [H^+][HCO_3^-]/p_{CO2}$		M^2/atm	7.82	same as Table 5-1, Stumm and Morgan, Aquatic Chemistry, Wiley, 1970
4)	$K_2 = [H^+][CO_3^{2-}]/[HCO_3^-]$	4.68E-11	M	10.33	Table 5-1, Stumm and Morgan (1970)
5)	$K_{s0} = [Ca^{2+}][CO_3^{2-}]$	4.47E-09	M^2	8.35	Table 5-1, Stumm and Morgan (1970)
6)	$2*[Ca^{2+}] + [H^+] = [HCO_3^-] + 2*[CO_3^{2-}] + [OH^-]$				Charge balance
Variables		value	units	value	units
1)	$[H_2CO_3]$	3.39E-04	M	3.39E-07	mol/cm^3
2)	$[H^+]$	4.93E-08	M	7.31	pH
3)	$[OH^-]$	2.03E-07	M	6.69	pOH
4)	$[HCO_3^-]$	3.07E-03	M	3.07E-06	mol/cm^3
5)	$[CO_3^{2-}]$	2.91E-06	M	2.91E-09	mol/cm^3
6)	$[Ca^{2+}]$	1.54E-03	M	1.54E-06	mol/cm^3
	$[H_2CO_3]+[HCO_3^-]+[CO_3^{2-}]$	**3.41E-03**	M	3.41E-06	mol/cm^3

Table 4-2 Input data and rate coefficients for BE carbonation calculations.

Parameter	SDU 2/6/7	SDU 1/4	SDU 4 Roof	SDU 1 Roof	Saltstone	Units
p_{CO_2} (a)	0.01	0.01	0.01	0.01	0.01	atm
$c_{CO_2,g}$ (b)	4.16e-7	4.16e-7	4.16e-7	4.16e-7	4.16e-7	mol/cm^3 gas
$c_{CO_2,\ell}$ (c)	3.41e-6	3.41e-6	3.41e-6	3.41e-6	3.41e-6	mol/cm^3 liquid
n (d)	0.11	0.106	0.106	0.106	0.656	cm^3 void / cm^3 total
ρ_b (d)	2.18	2.28	2.28	2.28	0.932	g/cm^3 total
$D_{m,g}$ (e)	0.165	0.165	0.165	0.165	0.165	cm^2/s
τ (f)	1.52E-03	1.52E-03	2.61E-03	2.61E-03	2.96E-04	-
$D_{e,g}$ (g)	2.51E-04	2.51E-04	4.30E-04	4.30E-04	4.88E-05	cm^2/s
$D_{e,\ell}$ (d)	3.5E-08	3.5E-08	6.0E-08	6.0E-08	6.8E-09	cm^2/s
$[Ca(OH)_2]$	0 (h)	7.2 (h)	-	-	0 (i)	g/kg
$M_{Ca(OH)_2}$(j)	74	74	-	-	74	g/mol
$c_{Ca(OH)_2}$ (k)	0	2.22e-4	-	-	0	mol/cm^3 total
$[CSH]$	81.2 (h)	118.8 (h)	-	-	147.4 (i)	g/kg
M_{CSH} (l)	182.1	182.1	-	-	182.1	g/mol
c_{CSH} (m)	9.72e-4	1.49e-3	-	-	7.54e-4	mol/cm^3 total
c_{Ca}	1.60e-3(n)	2.68e-3(n)	2.15e-3(o)	1.85e-3(o)	1.24e-3(n)	mol/cm^3 total
S_g (p)	7.e-6 (~0)	7.e-6(~0)	7.e-6 (~0)	7.e-6 (~0)	0.0004	cm^3 gas / cm^3 void
S_ℓ (q)	1	1	1	1	0.9996	cm^3 liquid / cm^3 void
θ_g (q)	7.2e-7	7.0e-7	7.0e-7	7.0e-7	2.4e-4	cm^3 gas / cm^3 total
θ_ℓ (q)	0.110	0.106	0.106	0.106	0.656	cm^3 liquid / cm^3 total
A (r)	**0.023**	**0.017**	**0.025**	**0.027**	**0.032**	cm/√yr

Table 4-2 notes:
(a) Millings (2012)
(b) p_{CO_2} and ideal gas law at 20ºC
(c) Sum of H_2CO_3, HCO_3^-, and CO_3^{2-} concentrations from Table 4-1
(d) Hommel (2018), Table 1
(e) Marrero and Mason (1972), Table 20, N_2-CO_2 system
(f) Calculated from liquid-phase effective diffusion coefficients in Hommel (2018, Table 1) assuming a molecular diffusion coefficient of 2.3e-5 cm^2/s (Holz et al. 2000)
(g) $D_{e,g} = \tau D_{m,g}$
(h) SIMCO (2012), Tables 9 and 13, 28 day cure
(i) SIMCO (2010), Tables 6 and 13, WS-2 grout
(j) $M_{Ca(OH)_2}$= 40 + 2(16+1) g/mol
(k) $c_{Ca(OH)_2} = [Ca(OH)_2]\rho_b / M_{Ca(OH)_2}$
(l) The stoichiometry of CSH in cement paste is variable. SIMCO assumes $CSH \rightarrow 0.65Ca(OH)_2 + CaH_2SiO_4 = 1.65CaO \cdot SiO_2 \cdot 1.65H_2O$ in STADIUM modeling (Samson 2010, Table 7). M_{CSH} = 1.65(40) + 3.3(1) + 1(28) + 5.3(16) g/mol
(m) $c_{CSH} = [CSH]\rho_b / M_{CSH}$
(n) $c_{Ca} = c_{Ca(OH)_2} + 1.65 \cdot c_{CSH}$; see note (l)
(o) Scaled from "SDU 1/4" concrete using CaO ratio from Table 4-5
(p) Computed from van Genuchten (1980) water retention curve and 1500 cm suction
(q) $S_g + S_\ell = 1$, $\theta_g = S_g n$, and $\theta_\ell = S_\ell n$
(r) Equation (4-5)

Table 4-3 Input data and rate coefficients for CV carbonation calculations.

Parameter	SDU 2/6/7	SDU 1/4	SDU 4 Roof	SDU 1 Roof	Saltstone	Units
p_{CO_2} (a)	0.01	0.01	0.01	0.01	0.01	atm
$c_{CO_2,g}$ (b)	4.16e-7	4.16e-7	4.16e-7	4.16e-7	4.16e-7	mol/cm^3 gas
$c_{CO_2,\ell}$ (c)	3.41e-6	3.41e-6	3.41e-6	3.41e-6	3.41e-6	mol/cm^3 liquid
n (d)	0.11	0.106	0.106	0.106	0.656	cm^3 void / cm^3 total
ρ_b (d)	2.18	2.28	2.28	2.28	0.932	g/cm^3 total
$D_{m,g}$ (e)	0.165	0.165	0.165	0.165	0.165	cm^2/s
τ (f)	2.30E-03	2.30E-03	4.22E-03	4.22E-03	5.65E-04	-
$D_{e,g}$ (g)	3.80E-04	3.80E-04	6.96E-04	6.96E-04	9.33E-05	cm^2/s
$D_{e,\ell}$ (d)	5.3E-08	5.3E-08	9.7E-08	9.7E-08	1.3E-08	cm^2/s
$[Ca(OH)_2]$	0 (h)	7.2 (h)	-	-	0 (i)	g/kg
$M_{Ca(OH)_2}$(j)	74	74	-	-	74	g/mol
$c_{Ca(OH)_2}$ (k)	0	2.22e-4	-	-	0	mol/cm^3 total
$[CSH]$	81.2 (h)	118.8 (h)	-	-	147.4 (i)	g/kg
M_{CSH} (l)	182.1	182.1	-	-	182.1	g/mol
c_{CSH} (m)	9.72e-4	1.49e-3	-	-	7.54e-4	mol/cm^3 total
c_{Ca}	1.60e-3(n)	2.68e-3(n)	2.15e-3(o)	1.85e-3(o)	1.24e-3(n)	mol/cm^3 total
S_g (p)	0.02	0.02	0.02	0.02	0.02	cm^3 gas / cm^3 void
S_ℓ (q)	0.98	0.98	0.98	0.98	0.98	cm^3 liquid / cm^3 void
θ_g (q)	0.0022	0.00212	0.00212	0.00212	0.0131	cm^3 gas / cm^3 total
θ_ℓ (q)	0.1078	0.10388	0.10388	0.10388	0.6429	cm^3 liquid / cm^3 total
A (r)	**0.120**	**0.091**	**0.138**	**0.149**	**0.165**	cm/√yr

Table 4-3 notes:
(a) Millings (2012)
(b) p_{CO_2} and ideal gas law at 20ºC
(c) Sum of H_2CO_3, HCO_3^-, and CO_3^{2-} concentrations from Table 4-1
(d) Hommel (2018), Table 1
(e) Marrero and Mason (1972), Table 20, N_2-CO_2 system
(f) Calculated from liquid-phase effective diffusion coefficients in Hommel (2018, Table 1) assuming a molecular diffusion coefficient of 2.3e-5 cm^2/s (Holz et al. 2000)
(g) $D_{e,g} = \tau D_{m,g}$
(h) SIMCO (2012), Tables 9 and 13, 28 day cure
(i) SIMCO (2010), Tables 6 and 13, WS-2 grout
(j) $M_{Ca(OH)_2}$= 40 + 2(16+1) g/mol
(k) $c_{Ca(OH)_2} = [Ca(OH)_2]\rho_b / M_{Ca(OH)_2}$
(l) The stoichiometry of CSH in cement paste is variable. SIMCO assumes $CSH \rightarrow 0.65Ca(OH)_2 + CaH_2SiO_4 = 1.65CaO \cdot SiO_2 \cdot 1.65H_2O$ in STADIUM modeling (Samson 2010, Table 7). M_{CSH} = 1.65(40) + 3.3(1) + 1(28) + 5.3(16) g/mol
(m) $c_{CSH} = [CSH]\rho_b / M_{CSH}$
(n) $c_{Ca} = c_{Ca(OH)_2} + 1.65 \cdot c_{CSH}$; see note (l)
(o) Scaled from "SDU 1/4" concrete using CaO ratio from Table 4-5
(p) Postulated condition
(q) $S_g + S_\ell = 1$, $\theta_g = S_g n$ and $\theta_\ell = S_\ell n$
(r) Equation (4-5)

Table 4-4 Input data and rate coefficients for CE carbonation calculations.

Parameter	SDU 2/6/7	SDU 1/4	SDU 4 Roof	SDU 1 Roof	Saltstone	Units
p_{CO_2} (a)	0.01	0.01	0.01	0.01	0.01	atm
$c_{CO_2,g}$ (b)	4.16e-7	4.16e-7	4.16e-7	4.16e-7	4.16e-7	mol/cm^3 gas
$c_{CO_2,\ell}$ (c)	3.41e-6	3.41e-6	3.41e-6	3.41e-6	3.41e-6	mol/cm^3 liquid
n (d)	0.11	0.106	0.106	0.106	0.656	cm^3 void / cm^3 total
ρ_b (d)	2.18	2.28	2.28	2.28	0.932	g/cm^3 total
$D_{m,g}$ (e)	0.165	0.165	0.165	0.165	0.165	cm^2/s
τ (f)	2.61E-03	2.61E-03	5.22E-03	5.22E-03	1.48E-03	-
$D_{e,g}$ (g)	4.30E-04	4.30E-04	8.61E-04	8.61E-04	2.44E-04	cm^2/s
$D_{e,\ell}$ (d)	6.0E-08	6.0E-08	1.2E-07	1.2E-07	3.4E-08	cm^2/s
$[Ca(OH)_2]$	0 (h)	7.2 (h)	-	-	0 (i)	g/kg
$M_{Ca(OH)_2}$(j)	74	74	-	-	74	g/mol
$c_{Ca(OH)_2}$ (k)	0	2.22e-4	-	-	0	mol/cm^3 total
$[CSH]$	81.2 (h)	118.8 (h)	-	-	147.4 (i)	g/kg
M_{CSH} (l)	182.1	182.1	-	-	182.1	g/mol
c_{CSH} (m)	9.72e-4	1.49e-3	-	-	7.54e-4	mol/cm^3 total
c_{Ca}	1.60e-3(n)	2.68e-3(n)	2.15e-3(o)	1.85e-3(o)	1.24e-3(n)	mol/cm^3 total
S_g (p)	0.05	0.05	0.05	0.05	0.05	cm^3 gas / cm^3 void
S_ℓ (q)	0.95	0.95	0.95	0.95	0.95	cm^3 liquid / cm^3 void
θ_g (q)	0.0055	0.0053	0.0053	0.0053	0.033	cm^3 gas / cm^3 total
θ_ℓ (q)	0.1045	0.1007	0.1007	0.1007	0.623	cm^3 liquid / cm^3 total
A (r)	**0.199**	**0.151**	**0.238**	**0.257**	**0.415**	cm/√yr

Table 4-4 notes:
(a) Millings (2012)
(b) p_{CO_2} and ideal gas law at 20ºC
(c) Sum of H_2CO_3, HCO_3^-, and CO_3^{2-} concentrations from Table 4-1
(d) Hommel (2018), Table 1
(e) Marrero and Mason (1972), Table 20, N_2-CO_2 system
(f) Calculated from liquid-phase effective diffusion coefficients in Hommel (2018, Table 1) assuming a molecular diffusion coefficient of 2.3e-5 cm^2/s (Holz et al. 2000)
(g) $D_{e,g} = \tau D_{m,g}$
(h) SIMCO (2012), Tables 9 and 13, 28 day cure
(i) SIMCO (2010), Tables 6 and 13, WS-2 grout
(j) $M_{Ca(OH)_2}$= 40 + 2(16+1) g/mol
(k) $c_{Ca(OH)_2} = [Ca(OH)_2]\rho_b / M_{Ca(OH)_2}$
(l) The stoichiometry of CSH in cement paste is variable. SIMCO assumes $CSH \rightarrow 0.65Ca(OH)_2 + CaH_2SiO_4 = 1.65CaO \cdot SiO_2 \cdot 1.65H_2O$ in STADIUM modeling (Samson 2010, Table 7). M_{CSH} = 1.65(40) + 3.3(1) + 1(28) + 5.3(16) g/mol
(m) $c_{CSH} = [CSH]\rho_b / M_{CSH}$
(n) $c_{Ca} = c_{Ca(OH)_2} + 1.65 \cdot c_{CSH}$; see note (l)
(o) Scaled from "SDU 1/4" concrete using CaO ratio from Table 4-5
(p) Postulated condition
(q) $S_g + S_\ell = 1$, $\theta_g = S_g n$ and $\theta_\ell = S_\ell n$
(r) Equation (4-5)

Table 4-5 Estimated calcium content in SDU 1 and 4 roof concrete relative to SDU 1/4 floor concrete.

Binder	CaO (%)	SDU 1/4 Floor (lbs/yd^3)	SDU 4 Roof (lbs/yd^3)	SDU 1 Roof (lbs/yd^3)
Type I/II cement Lafarge	64.8	419	466	400
Type IV cement Lehigh	63.8	0	0	0
GGBFS Holcim	37.8	278	0	0
Force 10000 SF Grace	0.6	0	0	0
Class F Fly Ash SEFA	1.32	0	62	70
CaO_{roof}/CaO_{floor}	-	-	0.80	0.69

The molar concentrations of CO_2 in the gas and liquid phases are observed to be similar (within an order of magnitude), whereas the effective diffusion coefficient for gas phase transport is 4 to 5 orders of magnitude larger than its counterpart for the liquid phase. Therefore, gas phase transport generally controls the carbonation process, and liquid phase transport is commonly neglected in the literature (e.g. Papadakis et al. 1989). The exception is saturated conditions, where liquid phase transport is the only mechanism delivering CO_2 to the reaction front. The carbonation rate is very slow under these conditions. As a specific example, Rast and Rinker (2012) reported a carbonation depth of 1-2 mm for a concrete core taken from a 50-year-old Hanford waste tank. The rate of carbonation is also minimal under dry conditions, because water is required to support the aqueous reaction $Ca(OH)_2 + H_2O + CO_2 \rightarrow CaCO_3 + 2H_2O$. The maximum rate of carbonation occurs at intermediate conditions, roughly 50% relative humidity (e.g. Papadakis et al. 1989, Walton et al. 1990). The carbonation rate is very sensitive to liquid saturation near full saturation.

4.3 Saturation state

Relative humidity and saturation are related through thermodynamic relationships and a material specific water retention curve. Total suction is related to water vapor pressure through the equilibrium thermodynamic relationship (Richards 1965, cited in Fredlund and Rahardjo 1993, Equations 4.1 and 4.3)

$$\psi = \left(P_g - P_\ell\right)/\rho g + \pi = \psi_c + \pi = -\frac{RT}{gM_w} ln\left(\frac{P_v}{P_0}\right) = -\frac{RT}{gM_w} ln(RH) \qquad (4\text{-}7)$$

known as the Kelvin relationship where

ψ = total suction [m]

P_g = gas pressure [Pa]

P_ℓ = liquid pressure [Pa]

ρ = liquid density [kg/m^3]

g = gravitational acceleration [m/s^2]

π = osmotic suction [m]

ψ_c = capillary or matric suction [m]

R = universal (molar) gas constant [J/mol-K = m^{3}Pa/mol-K]

T = temperature [K]

M_w = molar mass of water [kg/mol]

P_v = water vapor pressure [Pa]

P_0 = vapor pressure at saturation [Pa]

RH = relative humidity, P_v/P_0 [-]

Considering this expression, water vapor pressure can be viewed as a master variable defining the pressure state of both the gas and liquid phases (Hall and Hoff 2002). The osmotic suction can be estimated from the Morse equation (http://en.wikipedia.org/wiki/Osmotic_pressure)

$$\rho g \pi = iMRT \tag{4-8}$$

where

ρ = liquid density [kg/m^3]

g = gravitational acceleration [m/s^2]

π = osmotic suction [m]

i = van't Hoff factor [-]

M = molarity of the solution [mol/m^3]

R = universal (molar) gas constant [J/mol-K = m^{3}Pa/mol-K]

T = temperature [K].

Equation (3.6) assumes a dilute solution, but can be used with increasing approximation for more concentrated solutions. The dimensionless van't Hoff factor is approximately one (http://en.wikipedia.org/wiki/Van_%27t_Hoff_factor). Capillary suction is related to saturation through a water retention curve commonly expressed in the form (van Genuchten 1980)

$$S_e = \frac{S - S_r}{1 - S_r} = \frac{\theta - \theta_r}{\theta_s - \theta_r} = \left[\frac{1}{1 + (\alpha\psi_c)^n}\right]^m \tag{4-9}$$

where

S = saturation [m^3 liquid / m^3 void]

S_r = material specific fitting parameter [m^3 liquid / m^3 void]

θ = water content [m^3 liquid / m^3 total]

θ_r = material specific fitting parameters [m^3 liquid / m^3 total]

θ_s = saturated water content = porosity [m^3 liquid / m^3 total]

α = material specific fitting parameter [1/m]

ψ_c = capillary or matric suction [m]

n, m= material specific fitting parameters [-]

and the subscripts e and r denote "effective" and "residual". Note that S_r and θ_r are correlated (not independent) parameters. It is commonly assumed that $m = 1 - 1/n$. Figure 4-1 illustrates water retention curves characteristic of SDU concrete (Phifer et al. 2006) and 20°C cure temperature ARP/MCU saltstone (Dixon 2011).

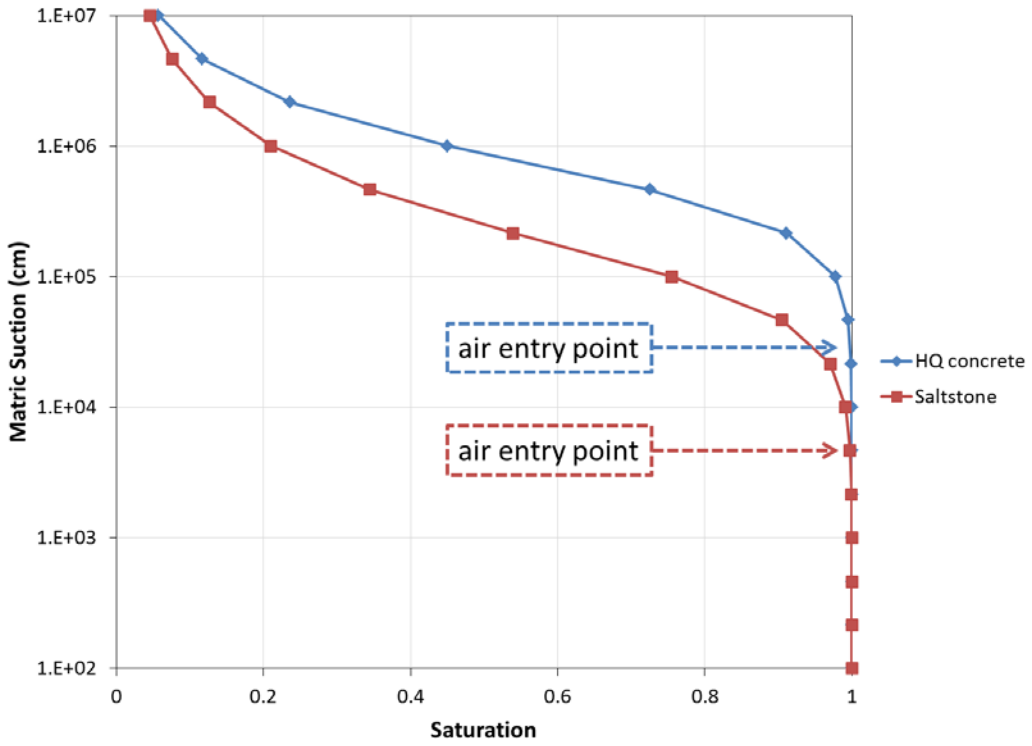

Figure 4-1 Water retention curves for SDU concrete and saltstone.

As mentioned previously, the saturation state of a cementitious material strongly affects the rate of carbonation, particularly near full saturation. The anticipated saturation states for SDF cementitious materials can be assessed using Equations (4-7) through (4-9) and estimated soil suction and relative humidity values.

Once buried under a low-permeability cover system, the SDF will initially be exposed to soil conditions approaching gravity equilibrium (no infiltration), where the matric suction head is equal to the height above the water table. Soil moisture contains dissolved solids, but the concentrations are dilute such that osmotic suction is negligible compared to that within cementitious materials. Any infiltration above zero produces capillary suction levels that are lower than under gravity equilibrium. Thus, as the cover system degrades over time, soil suction levels will decrease. With this consideration, the maximum suction head

anticipated for SDUs is roughly 1500 cm, the approximate height of the SDUs above the water table (15 meters). From Figure 4-1 the air entry head is observed to exceed 1500 cm for SDF grout and 10,000 cm for SDF concrete. Thus, SDF concrete is expected to be saturated for all time. Ignoring osmotic effects, saltstone could potentially be slightly unsaturated immediately after cap placement, but if so, would then become saturated by the time the soil suction levels fall below approximately 1500 cm. Table 4-6 shows saturation calculated from the water retention curves depicted in Figure 4-1 for the expected maximum capillary suction of approximately 1500 cm, and 10x higher and lower levels as points of reference.

Table 4-6 Saltstone and concrete saturation for selected capillary suctions.

Parameter	Saltstone			Concrete		
Saturated water content, θ_s	0.58	0.58	0.58	0.1	0.1	0.1
Residual water content, θ_r	0	0	0	0	0	0
van Genuchten (1980) α (1/cm)	1.008E-05	1.008E-05	1.008E-05	2.086E-06	2.086E-06	2.086E-06
van Genuchten (1980) n	1.67131	1.67131	1.67131	1.9433	1.9433	1.9433
$m = 1 - 1/n$	0.402	0.402	0.402	0.485	0.485	0.485
Capillary suction, ψ_c (cm)	15000	1500	150	15000	1500	150
Saturation, S	**0.983**	**1.000**	**1.000**	**0.999**	**1.000**	**1.000**

The chemical compositions of pore water in SDU concrete and saltstone have been characterized by SIMCO (2010, 2012) and are reproduced in Table 4-7 through Table 4-9. Nitrogen ions, denoted N^-, include NO_2^- and NO_3^- in these tables. The osmotic suctions associated with these molar concentrations are shown in Table 4-10 based on Equation (4-8). Over time dissolved species will advect and/or diffuse out of cementitious materials, thus lowering the initial molar concentrations, to levels approaching zero with sufficient time. Table 4-10 includes calculations for two additional concentrations: half the initial values and zero. The total suction is assumed to be 1500 cm in all cases based on the exposure to soil conditions. The relative humidity corresponding to 1500 cm is 99.89% from Equation (4-7). In comparison, carbonation rates reported in the literature are typically focused on 50-70% relative humidity, which is reflective of atmospheric exposure conditions and maximum penetration. For the initial and intermediate molar concentrations, the osmotic suctions exceed the total suction and the capillary suctions are negative-valued (Equation (4-7), total suction is composed of capillary and osmotic suction). The latter implies the pore water pressure is positive, in contrast to pure water that is under tension (negative pressure). Therefore, saturation is 100% when dissolved species are present at these concentrations. The practical implication is that saltstone is expected to be fully saturated at early times, when soil suction levels are the highest, because of osmotic suction. At later times when the molar concentration of the pore fluid drops, soil (total) suction levels will also be lower such that saltstone will remain saturated, even with pure water in its pore space. Thus, the pore spaces of both concrete and grout are expected to be fully saturated for all time once these materials are in the subsurface.

Table 4-7 Pore fluid composition for SDU 2/6/7 concrete (SIMCO 2012, Table 11).

	28d V2	MW	28d V2	28d V2	water
Ion	mmol/L	g/mol	mol/L	g/L	g/L
OH^-	113.9	17	0.114	1.94	
Na^+	26.5	23	0.027	0.61	
K^+	35.8	39	0.036	1.40	
SO_4^{2-}	0	96	0.000	0.00	
Ca^{2+}	2	40	0.002	0.08	
Cl^-	4.2	35	0.004	0.15	
N			0.000	0.00	
CO_3^{2-}			0.000	0.00	
Total			**0.182**	4.2 (0.4 wt%)	998

Table 4-8 Pore fluid composition for SDU 1/4 concrete (SIMCO 2012, Table 11).

	28d V4	MW	28d V4	28d V4	water
Ion	mmol/L	g/mol	mol/L	g/L	g/L
OH^-	244.4	17	0.244	4.15	
Na^+	73.9	23	0.074	1.70	
K^+	140.7	39	0.141	5.49	
SO_4^{2-}	0.1	96	0.000	0.01	
Ca^{2+}	1.8	40	0.002	0.07	
Cl^-	4.8	35	0.005	0.17	
N			0.000	0.00	
CO_3^{2-}			0.000	0.00	
Total			**0.466**	11.6 (1.1 wt%)	998

Table 4-9 Pore fluid composition for saltstone (SIMCO 2010, Table 8).

	28d WS-2	MW	28d WS-2	28d WS-2	water
Ion	mmol/L	g/mol	mol/L	g/L	g/L
OH^-	383.9	17	0.384	6.53	
Na^+	4144.2	23	4.144	95.32	
K^+	120.5	39	0.121	4.70	
SO_4^{2-}	111.7	96	0.112	10.72	
Ca^{2+}	0.1	40	0.000	0.00	
Cl^-	11.9	35	0.012	0.42	
N	3552.1	60.4	3.552	214.52	
CO_3^{2-}	46.8	60	0.047	2.81	
Total			**8.371**	335.0 (25.1 wt%)	998

Table 4-10 Relative humidity and capillary suction corresponding to a total suction of 1500 cm.

Parameter	Saltstone			Concrete-V2			Concrete-V4			Units
temperature, T	20	20	20	20	20	20	20	20	20	C
	293.15	293.15	293.15	293.15	293.15	293.15	293.15	293.15	293.15	K
relative humidity, RH	99.89%	99.89%	99.89%	99.89%	99.89%	99.89%	99.89%	99.89%	99.89%	
saturation pressure, P_0	23.46	23.46	23.46	23.46	23.46	23.46	23.46	23.46	23.46	millibar
	2346	2346	2346	2346	2346	2346	2346	2346	2346	Pa
water vapor pressure, P_v	2344	2344	2344	2344	2344	2344	2344	2344	2344	Pa
gas constant, R	8.314	8.314	8.314	8.314	8.314	8.314	8.314	8.314	8.314	J/K-mol
molecular mass of water, M_w	18	18	18	18	18	18	18	18	18	g/mol
gravitational acceleration, g	9.81	9.81	9.81	9.81	9.81	9.81	9.81	9.81	9.81	m/s^2
density of water, ρ	998	998	998	998	998	998	998	998	998	kg/m^3
pg	9790.38	9790.38	9790.38	9790.38	9790.38	9790.38	9790.38	9790.38	9790.38	Pa/m
total suction, ψ	15	15	15	15	15	15	15	15	15	m
	1500	1500	1500	1500	1500	1500	1500	1500	1500	cm
	146856	146856	146856	146856	146856	146856	146856	146856	146856	Pa
	1.5	1.5	1.5	1.5	1.5	1.5	1.5	1.5	1.5	bar
van't Hoff factor, i	1	1	1	1	1	1	1	1	1	
molarity, M	8.37	4.185	0	0.18	0.09	0	0.47	0.235	0	mol/L
osmotic suction, Π	20399775	10199887	0	438705	219352	0	1145507	572754	0	Pa
	2083.66	1041.83	0.00	44.81	22.40	0.00	117.00	58.50	0.00	m
	208366	104183	0	4481	2240	0	11700	5850	0	cm
	204.0	102.0	0.0	4.4	2.2	0.0	11.5	5.7	0.0	bar
capillary (matric) suction, Ψ_c	-2069	-1027	15	-30	-7	15	-102	-44	15	m
	-206866	-102683	1500	-2981	-740	1500	-10200	-4350	1500	cm
	-20252919	-10053032	146856	-291849	-72497	146856	-998651	-425898	146856	Pa
	-202.5	-100.5	1.5	-2.9	-0.7	1.5	-10.0	-4.3	1.5	bar
saturated water content, θ_s	0.58	0.58	0.58	0.1	0.1	0.1	0.1	0.1	0.1	
residual water content, θ_r	0	0	0	0	0	0	0	0	0	
van Genuchten (1980) α	1.008E-05	1.008E-05	1.008E-05	2.086E-06	2.086E-06	2.086E-06	2.086E-06	2.086E-06	2.086E-06	1/cm
van Genuchten (1980) n	1.67131	1.67131	1.67131	1.9433	1.9433	1.9433	1.9433	1.9433	1.9433	
m=1-1/n	0.402	0.402	0.402	0.485	0.485	0.485	0.485	0.485	0.485	
capillary suction, Ψ_c	-206866	-102683	1500	-2981	-740	1500	-10200	-4350	1500	cm
saturation	1.000	1.000	1.000	1.000	1.000	1.000	1.000	1.000	1.000	

While saturated pores preclude gas-phase CO_2 transport and relatively fast carbonation, these processes may occur should either cementitious material be fractured, depending on matric suction levels and crack aperture. For a perfectly wetting fluid, the capillary rise between two vertical parallel surfaces is

$$h = \frac{2\sigma}{\rho g b} \tag{4-10}$$

where

h = capillary rise [m]

σ = surface tension [N/m]

ρ = density [kg/m^3]

g = gravitation acceleration [m/s^2]

b = aperture [m].

In the context of a vertical fracture subjected to a given pressure head, $P/\rho g$ [m], in the surrounding matrix, the aperture will be liquid-filled under the condition (Wang and Narasimhan 1985)

$$\frac{P}{\rho g} > -\frac{2\sigma}{\rho g b} \tag{4-11}$$

In other words, the fracture will be liquid-filled for positive pressure head and suction (negative pressure) head less than $2\sigma/\rho g b$. Alternatively, the maximum aperture that can be liquid-filled for a given capillary suction head, ψ_c [m], is

$$b = \frac{2\sigma}{\rho g \psi_c} \tag{4-12}$$

For ψ_c = 1500 cm = 15m, the result is b = 1 μm = 0.04 mil. Hence fractures, if present, are expected to be unsaturated unless very narrow. If these hypothetical fractures were connected, then they would provide a means for gas-phase transport of CO_2 through the porous medium.

4.4 Penetration rate coefficients

Returning to Equations (4-4) and (4-5), three conditions are considered for predicting carbonation rates in SDU concrete and saltstone, as shown in Table 4-2 through Table 4-4. The best-estimate (BE) rate is calculated assuming a capillary suction of 1500 cm and pure water occupying pore space, i.e., neglecting osmotic effects. Under these conditions SDF concrete is fully liquid saturated and SDF grout is liquid saturated at 99.96% (practically saturated). The best-estimate (BE) label is somewhat of a misnomer because suction levels will be less than 1500 cm for much of the performance period and osmotic effects are present. Thus, saltstone is expected to be liquid saturated. Rather, the label is used in a relative sense compared to the other two scenarios.

The compliance-value and conservative-estimate rates account for uncertainty in water retention curves, and/or the postulation that entrapped air creates a connected pathway for gas-phase transport. Figure 4-2 shows water retention curves for a variety of actual and hypothetical materials. The “HQ Concrete” and

"Saltstone" curves from Figure 4-1 are reproduced in Figure 4-2. Three soils, "Clay", "Clay-Sand" and "Backfill" from Phifer et al. (2006), are shown as points of reference. The remaining curves are hypothetical variations on Table 4-6 where the α parameter has been increased to lower the air-entry pressures of concrete and saltstone. At high saturations, the setting $\alpha = 0.0001$ cm^{-1} applied to either concrete or saltstone produces a pessimistic condition that lies midway between the two cementitious materials and the soils, which are surrogates for a severely degraded state of concrete or saltstone. At a capillary suction of 1500 cm, liquid saturation for this hypothetical condition is approximately 98% (equivalently 2% gas saturation). Alternatively, saturations of 98% liquid / 2% gas can be tied to pessimistic assumptions about entrapped air. Entrapped air typically occupies 0.5 to 2% of concrete by volume (Daniel and Lobo 2005). Air pockets are generally expected to be isolated, and thus not connected. A pessimistic assumption is that entrapped air at 2% forms a fully connected pathway for gas-phase transport. The compliance-value calculation assumes 98% liquid saturation / 2% gas saturation due to a much higher than expected α parameter, or connected macro-voids due to entrapped air. The conservative-estimate assumes 95% liquid saturation / 5% gas saturation due to combined effects, or conditions otherwise more pessimistic than the CV case.

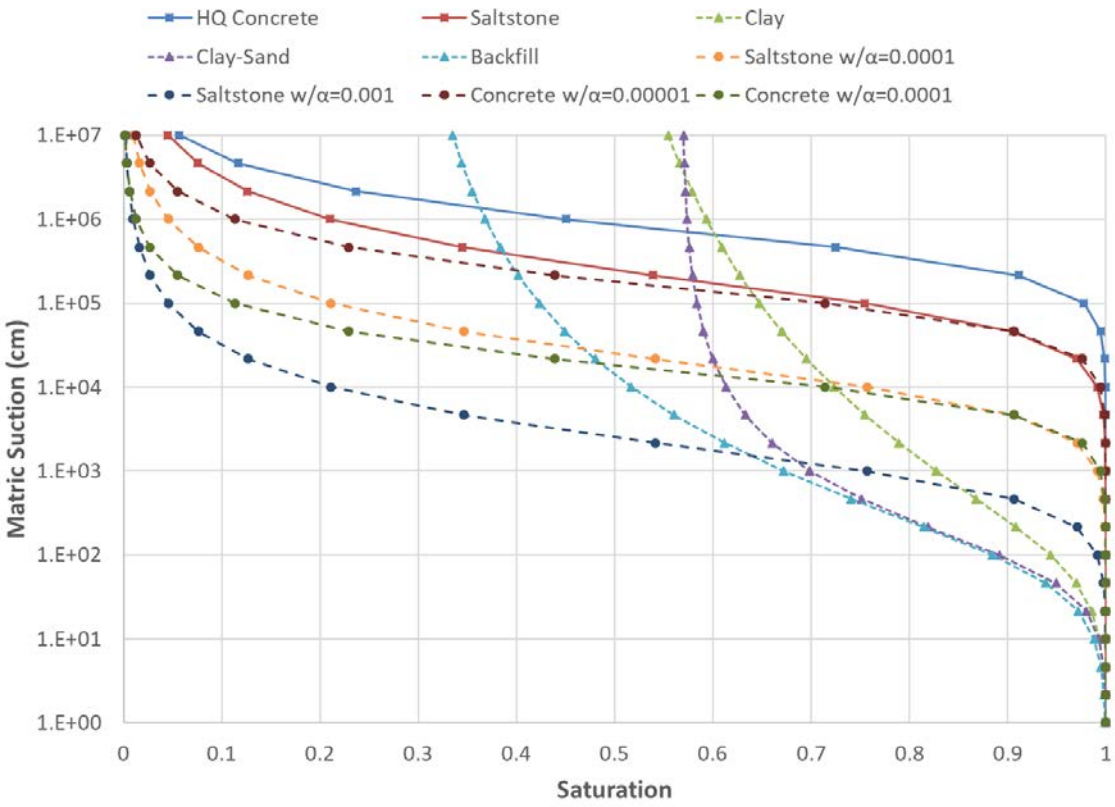

Figure 4-2 Water retention curves for various reference materials.

Table 4-2 through Table 4-4 indicate the carbonation rate coefficient A [cm/√yr] from Equation (4-5) for the BE, CV, and CE conditions. The carbonation rate coefficient can be used in Equation (2-8) to predict degradation time t_0 for a specified material thickness x_0.

As a point of reference, Brown et al. (2012) performed detailed simulations of carbonation in "VCT" concrete, which is essentially Saltstone SDU 2/6/7 concrete, using LeachXS™/ORCHESTRA in a developmental CBP Software Toolbox carbonation module (Brown et al. 2013a, b). The carbonation depth was defined as the location where pH < 9. Figure 4-3 is a reproduction of simulation results for various CO_2 concentrations based on 30% porosity, 90% liquid saturation, and a diffusion coefficient of 1.E-6 m^2/s. These settings are more conservative than any of the cases considered in Table 4-2 through Table 4-4. Focusing on the 1% CO_2 curve (0.01 atm), the numerical simulations are observed to exhibit an initial time lag before the carbonation front advances from the exposure surface. After √t = 15 √yr (t = 225 yr), the carbonation front stalls at about 1.25 cm. Using t_0 = 225 yr and x_0 = 1.25 cm in Equation (2-7), the equivalent carbonation rate constant is A = 0.083 cm/√yr. The latter is significantly lower than the conservative-estimate value in Table 4-4, which indicates that the analytic solution given by Equation (4-4) and other input assumptions are biased in the pessimistic direction. The reason is that the analytic model does not allow calcium to diffuse from the unreacted zone, where concentration is controlled by $Ca(OH)_2$ and $C\text{-}S\text{-}H$ solubility and high, to the reacted zone, where concentration is controlled by $CaCO_3$ solubility and low. Transport of calcium to the reaction front increases the effective reaction capacity at that location (while depleting it deeper), slowing the penetration front.

Because SDU 1 and 4 wall concretes are assumed to be fully degraded at PA time zero for the CV and CE cases, obviating the need for degradation estimates except for the BE case, penetration rate coefficient calculations are not shown in Table 4-2 through Table 4-4 for these components. However, the rate coefficients for the SDU 1/4 wall BE, CV and CE cases are calculated herein to be 0.087, 1.212 and 1.886 cm/√yr, respectively.

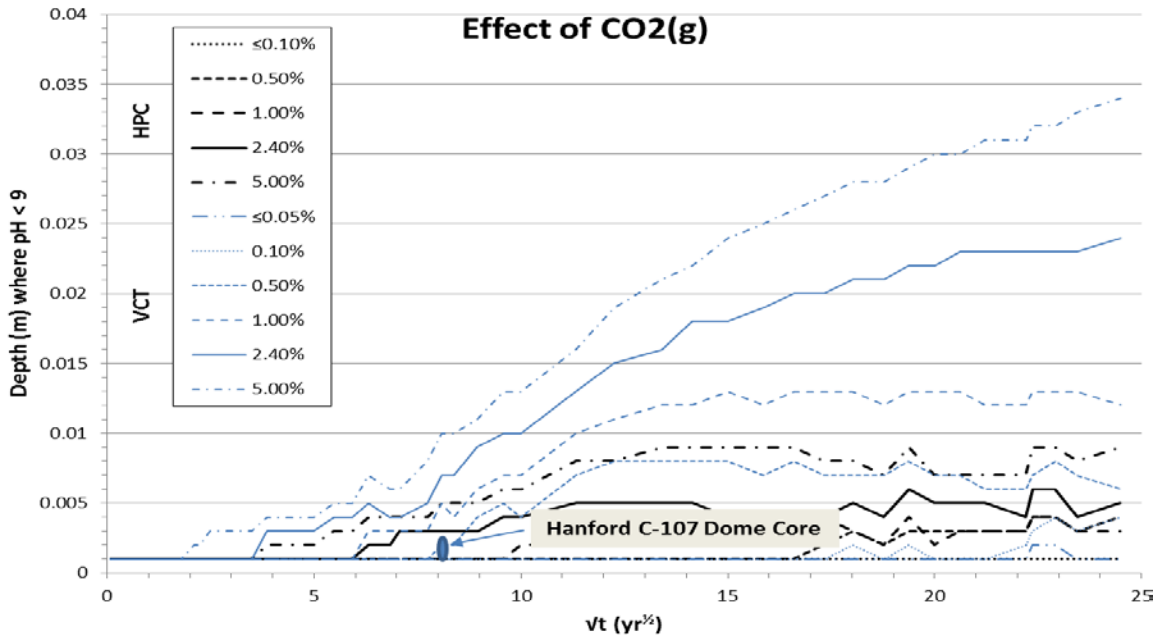

Figure 4-3 Carbonation simulation results as a function of soil-gas CO2 concentration for 90% concrete saturation from Brown et al (2012) (VCT = SDU 2 concrete, HPC = high performance concrete).

5.0 Steel Corrosion

As noted in the preceding section, steel corrosion products (rust) are expansive and when present inside concrete (e.g. corroded rebar) can exert stresses that cause cracking. Under high pH conditions, such as found in uncarbonated concrete, a passivating layer forms on steel surfaces leading to relatively slow corrosion rates. Specifically, the passive corrosion rate is typically 0.1 μm/yr (ACI 222R-01) and might range between 0.01 and 1 μm/yr (see Ahmad 2003, Equation (14) and surrounding discussion). Much higher corrosion rates, roughly 1000x (ACI 222R-01, Ahmad 2003), occur at lower pH, found in concrete following the arrival of a carbonation front. Degradation of concrete barriers via corrosion of embedded steel is analyzed in this study in the manner typical of civil engineering applications focused on structural service life. That is, corrosion is assumed to be negligible prior to carbonation and extensive damage is assumed to coincide with carbonation.

Neglecting passive steel corrosion prior to carbonation is deemed an acceptable simplifying assumption considering the time scale of combined carbonation and external sulfate attack on concrete. In the degradation timing analysis that follows, concrete barriers become fully degraded after roughly a thousand years from a combination of sulfate attack and carbonation. The corrosion depth for passivated steel over this time frame would be nominally 0.1 mm and conservatively 1 mm, which is not expected to cause significant damage. That is, passive steel corrosion is expected to be a non-limiting degradation phenomenon and is thus not explicitly considered in the degradation calculations that follow.

6.0 Decalcification

Decalcification in this application refers to leaching of Ca^{2+} in pore water to exterior soil, where the concentration is assumed to be zero (Walton et al. 1990, Langton 2007, 2010a). Leaching may occur through diffusion and/or advection.

6.1 Penetration rate coefficients for diffusive decalcification

For diffusion-controlled release between a sharp dissolution front and the soil interface, the penetration depth follows the general Equation (2-2) as

$$x = \left[\frac{2\theta D_e c_{Ca^{2+}} t}{c_{Ca}}\right]^{1/2} = At^{1/2} \quad (6\text{-}1)$$

where

x = penetration depth [cm]

θ = liquid content, Sn [cm^3 liquid / cm^3 total]

D_e = effective diffusion coefficient for liquid phase, τD_m [cm^2/yr]

t = elapsed time [yr]

$c_{Ca^{2+}}$ = dissolved Ca^{2+} concentration [mol / cm^3 liquid]

c_{Ca} = calcium concentration in solid phase [mol / cm^3 total]

and

$$A \equiv \left[\frac{2\theta D_e c_{Ca^{2+}}}{c_{Ca}}\right]^{1/2} \quad (6\text{-}2)$$

Table 6-1 through Table 6-3 present BE, CV and CE input parameters for use in Equations (6-1) and (6-2). Most parameter values come from Table 4-2 through Table 4-4. The concentration of Ca^{2+} varies through the leaching process; alkali metals leach first, followed by $(OH)_2$, and then CSH (Walton et al. 1990). In this analysis, dissolution of C-S-H gel is assumed to control the concentration of Ca^{2+} over most of the leaching process, considering the fact that little or no Portandite is expected in SDF cementitious materials (Table 6-1 through Table 6-3). C-S-H dissolves incongruently in that calcites leach preferentially in comparison to silicates. SIMCO (2012, Table 11) measured $c_{Ca^{2+}}$ in SDU concrete ranging from 1.8 to 2.0 mmol/L, or 1.8 - 2.0 $\times 10^{-6}$ mol/cm^3, which is consistent with Clodic and Meike (1997, Table 15, Ca/Si = 0.9). A value of 2.0 $\times 10^{-6}$ mol/cm^3 is assumed in Table 6-1 through Table 6-3. The rate coefficients for decalcification controlled by diffusion are low, indicating a slow process. Because these rate coefficients are small compared to those for other phenomena, uncertainty in $c_{Ca^{2+}}$ is ignored.

Because SDU 1 and 4 wall concretes are assumed to be fully degraded at PA time zero for the CV and CE cases, obviating the need for degradation estimates except for the BE case, penetration rate coefficient calculations are not shown in Table 6-1 through Table 6-3 for these components. However, the rate coefficients for the SDU 1/4 wall BE, CV and CE cases are calculated herein to be 0.066, 0.216 and 0.216 cm/√yr, respectively.

Table 6-1 Input data and rate coefficients for BE diffusion-limited decalcification.

Parameter	SDU 2/6/7	SDU 1/4	SDU 4 Roof	SDU 1 Roof	Saltstone	Units
$c_{Ca^{2+}}$ (a)	2.0e-6	2.0e-6	2.0e-6	2.0e-6	2.0e-6	mol/cm^3 liquid
n (b)	0.11	0.106	0.106	0.106	0.656	cm^3 void / cm^3 total
ρ_b (b)	2.18	2.28	2.28	2.28	0.932	g/cm^3 total
D_e (b)	3.5e-8	3.5e-8	6.0e-8	6.0e-8	6.8e-9	cm^2/s
$[Ca(OH)_2]$	0 (c)	7.2 (c)	-	-	0 (d)	g/kg
$M_{Ca(OH)_2}$ (e)	74	74	-	-	74	g/mol
$c_{Ca(OH)_2}$ (f)	0	2.22e-4	-	-	0	mol/cm^3 total
$[CSH]$	81.2 (c)	118.8 (c)	-	-	147.4 (d)	g/kg
M_{CSH} (g)	182.1	182.1	-	-	182.1	g/mol
c_{CSH} (h)	9.72e-4	1.49e-3	-	-	7.54e-4	mol/cm^3 total
c_{Ca}	1.60e-3 (i)	2.68e-3 (i)	2.15e-3 (j)	1.85e-3 (j)	1.24e-3 (i)	mol/cm^3 total
S_ℓ (k)	1	1	1	1	0.9996	cm^3 liquid / cm^3 void
θ_ℓ (l)	0.110	0.106	0.106	0.106	0.656	cm^3 liquid / cm^3 total
A (m)	**0.017**	**0.013**	**0.019**	**0.021**	**0.021**	cm/√yr

Table 6-1 notes:
(a) Approximate solubility of CSH (SIMCO 2012, Clodic and Meike 1997)
(b) Hommel (2018), Table 1
(c) SIMCO (2012), Tables 9 and 13, 28 day cure
(d) SIMCO (2010), Tables 6 and 13, WS-2 grout
(e) $M_{Ca(OH)_2}$= 40 + 2(16+1) g/mol
(f) $c_{Ca(OH)_2} = [Ca(OH)_2]\rho_b/M_{Ca(OH)_2}$
(g) The stoichiometry of CSH in cement paste is variable. SIMCO assumes $CSH \rightarrow 0.65Ca(OH)_2 + CaH_2SiO_4 = 1.65CaO \cdot SiO_2 \cdot 1.65H_2O$ in STADIUM modeling (Samson 2010, Table 7). M_{CSH} = 1.65(40) + 3.3(1) + 1(28) + 5.3(16) g/mol
(h) $c_{CSH} = [CSH]\rho_b/M_{CSH}$
(i) $c_{Ca} = c_{Ca(OH)_2} + 1.65 \cdot c_{CSH}$; see note (g)
(j) Scaled from "SDU 1/4" concrete using CaO ratio from Table 4-5
(k) computed from van Genuchten (1980) water retention curve and 1500 cm suction
(l) $\theta_\ell = S_\ell n$
(m) Equation (6-2).

Table 6-2 Input data and rate coefficients for CV diffusion-limited decalcification.

Parameter	SDU 2/6/7	SDU 1/4	SDU 4 Roof	SDU 1 Roof	Saltstone	Units
$c_{Ca^{2+}}$ (a)	2.0e-6	2.0e-6	2.0e-6	2.0e-6	2.0e-6	mol/cm^3 liquid
n (b)	0.11	0.106	0.106	0.106	0.656	cm^3 void / cm^3 total
ρ_b (b)	2.18	2.28	2.28	2.28	0.932	g/cm^3 total
D_e (b)	5.3e-8	5.3e-8	9.7e-8	9.7e-8	1.3e-8	cm^2/s
$[Ca(OH)_2]$	0 (c)	7.2 (c)	-	-	0 (d)	g/kg
$M_{Ca(OH)_2}$ (e)	74	74	-	-	74	g/mol
$c_{Ca(OH)_2}$ (f)	0	2.22e-4	-	-	0	mol/cm^3 total
$[CSH]$	81.2 (c)	118.8 (c)	-	-	147.4 (d)	g/kg
M_{CSH} (g)	182.1	182.1	-	-	182.1	g/mol
c_{CSH} (h)	9.72e-4	1.49e-3	-	-	7.54e-4	mol/cm^3 total
c_{Ca}	1.60e-3 (i)	2.68e-3 (i)	2.15e-3 (j)	1.85e-3 (j)	1.24e-3 (i)	mol/cm^3 total
S_ℓ (k)	1	1	1	1	0.9996	cm^3 liquid / cm^3 void
θ_ℓ (l)	0.110	0.106	0.106	0.106	0.656	cm^3 liquid / cm^3 total
A (m)	**0.021**	**0.016**	**0.025**	**0.026**	**0.029**	cm/√yr

Table 6-2 notes:
(a) Approximate solubility of CSH (SIMCO 2012, Clodic and Meike 1997)
(b) Hommel (2018), Table 1
(c) SIMCO (2012), Tables 9 and 13, 28 day cure
(d) SIMCO (2010), Tables 6 and 13, WS-2 grout
(e) $M_{Ca(OH)_2}$= 40 + 2(16+1) g/mol
(f) $c_{Ca(OH)_2} = [Ca(OH)_2]\rho_b/M_{Ca(OH)_2}$
(g) The stoichiometry of CSH in cement paste is variable. SIMCO assumes $CSH \rightarrow 0.65Ca(OH)_2 + CaH_2SiO_4 = 1.65CaO \cdot SiO_2 \cdot 1.65H_2O$ in STADIUM modeling (Samson 2010, Table 7). M_{CSH} = 1.65(40) + 3.3(1) + 1(28) + 5.3(16) g/mol
(h) $c_{CSH} = [CSH]\rho_b/M_{CSH}$
(i) $c_{Ca} = c_{Ca(OH)_2} + 1.65 \cdot c_{CSH}$; see note (g)
(j) Scaled from "SDU 1/4" concrete using CaO ratio from Table 4-5
(k) computed from van Genuchten (1980) water retention curve and 1500 cm suction
(l) $\theta_\ell = S_\ell n$
(m) Equation (6-2).

Table 6-3 Input data and rate coefficients for CE diffusion-limited decalcification.

Parameter	SDU 2/6/7	SDU 1/4	SDU 4 Roof	SDU 1 Roof	Saltstone	Units
$c_{Ca^{2+}}$ (a)	2.0e-6	2.0e-6	2.0e-6	2.0e-6	2.0e-6	mol/cm^3 liquid
n (b)	0.11	0.106	0.106	0.106	0.656	cm^3 void / cm^3 total
ρ_b (b)	2.18	2.28	2.28	2.28	0.932	g/cm^3 total
D_e (b)	6.0e-8	6.0e-8	1.2e-7	1.2e-7	3.4e-8	cm^2/s
$[Ca(OH)_2]$	0 (c)	7.2 (c)	-	-	0 (d)	g/kg
$M_{Ca(OH)_2}$ (e)	74	74	-	-	74	g/mol
$c_{Ca(OH)_2}$ (f)	0	2.22e-4	-	-	0	mol/cm^3 total
$[CSH]$	81.2 (c)	118.8 (c)	-	-	147.4 (d)	g/kg
M_{CSH} (g)	182.1	182.1	-	-	182.1	g/mol
c_{CSH} (h)	9.72e-4	1.49e-3	-	-	7.54e-4	mol/cm^3 total
c_{Ca}	1.60e-3 (i)	2.68e-3 (i)	2.15e-3 (j)	1.85e-3 (j)	1.24e-3 (i)	mol/cm^3 total
S_ℓ (k)	1	1	1	1	0.9996	cm^3 liquid / cm^3 void
θ_ℓ (l)	0.110	0.106	0.106	0.106	0.656	cm^3 liquid / cm^3 total
A (m)	**0.023**	**0.017**	**0.027**	**0.029**	**0.048**	cm/√yr

Table 6-3 notes:
(a) Approximate solubility of CSH (SIMCO 2012, Clodic and Meike 1997)
(b) Hommel (2018), Table 1
(c) SIMCO (2012), Tables 9 and 13, 28 day cure
(d) SIMCO (2010), Tables 6 and 13, WS-2 grout
(e) $M_{Ca(OH)_2}$= 40 + 2(16+1) g/mol
(f) $c_{Ca(OH)_2} = [Ca(OH)_2]\rho_b/M_{Ca(OH)_2}$
(g) The stoichiometry of CSH in cement paste is variable. SIMCO assumes $CSH \rightarrow 0.65Ca(OH)_2 + CaH_2SiO_4 = 1.65CaO \cdot SiO_2 \cdot 1.65H_2O$ in STADIUM modeling (Samson 2010, Table 7). M_{CSH} = 1.65(40) + 3.3(1) + 1(28) + 5.3(16) g/mol
(h) $c_{CSH} = [CSH]\rho_b/M_{CSH}$
(i) $c_{Ca} = c_{Ca(OH)_2} + 1.65 \cdot c_{CSH}$; see note (g)
(j) Scaled from "SDU 1/4" concrete using CaO ratio from Table 4-5
(k) computed from van Genuchten (1980) water retention curve and 1500 cm suction
(l) $\theta_\ell = S_\ell n$
(m) Equation (6-2).

6.2 Penetration rate coefficients for advective decalcification

While diffusion may control the decalcification of thinner features at earlier times, specifically in concrete barriers, advection is more likely to control decalcification of the saltstone monolith, considering its greater dimensions and higher hydraulic conductivity. Assuming one-dimensional downward flow, a quasi-steady state advective mass balance for decalcification is

$$U \cdot c_{Ca^{2+}} \cdot t = c_{Ca} \cdot h \tag{6-3}$$

where

U = Darcy velocity (volumetric water flux) [cm/yr]

t = elapsed time [yr]

h = monolith height [cm]

and the concentrations are as defined for Equation (6-1). Equation (6-3) assumes that advection occurs uniformly through the entire thickness, the dissolution front advances uniformly, and the exit concentration coincides with Ca^{2+} solubility. Solving for time yields

$$t = \frac{c_{Ca}}{c_{Ca^{2+}}} \cdot \frac{h}{U} \equiv \left(\frac{1}{A_U}\right) \cdot h \tag{6-4}$$

where A_U [cm/yr] is the rate coefficient for this advection-based degradation:

$$A_U = \frac{c_{Ca^{2+}}}{c_{Ca}} U \tag{6-5}$$

Equation (6-4) is more limiting than Equation (6-1) for saltstone. Note that A_U is inversely proportion to time t, instead of $\sqrt{t}$ for diffusion-limited decalcification.

Table 6-5 presents advection-limited decalcification rate coefficients for saltstone. The reaction capacity inputs are taken from Section 6.1. The saturated hydraulic conductivity of saltstone is defined by Hommel (2018).

The hydraulic head gradient in vadose zone soil tends to be one or less, such that the flowrate is equal to or less than the saturated hydraulic conductivity, per Darcy's law:

$$U \leq -K_{sat} \frac{dH}{dz} \tag{6-6}$$

For a cementitious monolith placed in the vadose zone, the head gradient can be higher as infiltration flows around the lower permeability obstacle. An upper bound on the gradient can be computed by assuming that water is ponded on the SDU roof up to the ground surface, and the underside of the floor is at gravity equilibrium (Section 4.3) with the water table. Table 6-4 shows this calculation using bounding values for all inputs. The result is a gradient of roughly 5 ft/ft. The assumptions for the BE, CV, and CE scenarios are dH/dz = 1, 3, and 5 ft/ft, respectively.

Table 6-4 Bounding hydraulic head gradient calculation.

Parameter	Bounding Value	Units	Comments
Maximum distance, roof to ground surface (a)	45	ft	
SDU 1distance, floor to roof (b)	27	ft	
SDU 4 distance, floor to roof (c)	30	ft	
SDU 2 distance, floor to roof (d)	22	ft	
SDU 6/7 distance, floor to roof (e)	43	ft	
Minimum distance, floor to roof	22	ft	SDU 2
Maximum distance, water table to floor (f)	48	ft	SDU 1
Pressure head at roof	45	ft	
Elevation of roof	22	ft	reference is floor
Head at roof	67	ft	
Pressure head at floor	-48	ft	
Elevation of floor	0	ft	reference is floor
Head at floor	-48	ft	
Head difference	115	ft	
Gradient (g)	**5.2**	ft/ft	

Table 6-4 notes:
(a) Jones and Phifer (2008), Figures 6 and 7
(b) SRR (2009), Section 3.2.1.1.2
(c) SRR (2009), Section 3.2.1.2.2
(d) SRR (2009), Section 3.2.1.3.2
(e) Watkins (2018)
(f) SRR (2009), Table 4.2-13
(g) Head difference / Floor to roof distance

Table 6-5 Input data and rate coefficients for advection-limited decalcification of saltstone.

Parameter	BE Saltstone	CV Saltstone	CE Saltstone	Units
$c_{Ca^{2+}}$ (a)	2.0e-6	2.0e-6	2.0e-6	mol/cm^3 liquid
$[Ca(OH)_2]$ (b)	0	0	0	g/kg
$M_{Ca(OH)_2}$ (c)	74	74	74	g/mol
$c_{Ca(OH)_2}$ (d)	0	0	0	mol/cm^3 total
$[CSH]$ (b)	147.4	147.4	147.4	g/kg
M_{CSH} (e)	182.1	182.1	182.1	g/mol
c_{CSH} (f)	7.54E-04	7.54E-04	7.54E-04	mol/cm^3 total
c_{Ca} (g)	1.24E-03	1.24E-03	1.24E-03	mol/cm^3 total
K_{sat} (h)	1.0e-10	5.0e-10	2.0e-9	cm/s
dH/dz (i)	1	3	5	cm/cm
A_U (j)	**5.1E-06**	**7.6E-05**	**5.1E-04**	cm/yr

Table 6-5 notes:
(a) Approximate solubility of CSH (SIMCO 2012, Clodic and Meike 1997)
(b) SIMCO (2010), Tables 6 and 13, WS-2 grout
(c) $M_{Ca(OH)_2}$= 40 + 2(16+1) g/mol
(d) $c_{Ca(OH)_2} = [Ca(OH)_2]\rho_b/M_{Ca(OH)_2}$
(e) The stoichiometry of CSH in cement paste is variable. SIMCO assumes $CSH \rightarrow 0.65Ca(OH)_2 + CaH_2SiO_4 = 1.65CaO \cdot SiO_2 \cdot 1.65H_2O$ in STADIUM modeling (Samson 2010, Table 7). M_{CSH} = 1.65(40) + 3.3(1) + 1(28) + 5.3(16) g/mol
(f) $c_{CSH} = [CSH]\rho_b/M_{CSH}$
(g) $c_{Ca} = c_{Ca(OH)_2} + 1.65 \cdot c_{CSH}$; see note (e)
(h) Hommel (2018), Table 1
(i) Postulated values
(j) Equation (6-5)

7.0 Clean grout cap

Saltstone Disposal Units 1 and 4 are expected to be closed with a layer of clean grout between saltstone grout and the underside of the roof. The potential presence of a clean cap grout in SDU 2, 6 and 7 is not credited. The lag time for sulfate in saltstone grout to effectively reach the roof and initiate sulfate attack is estimated using the analytic solution for diffusion into a semi-infinite medium (Myer 1971, Equation 6.4.29; Flach et al. 2009, Equation 19b):

$$c = c_0 erfc\left(\frac{x}{2\sqrt{D_e t}}\right) \tag{7-1}$$

where

c = interior concentration [mol/L]

c_0 = boundary concentration [mol/L]

x = penetration depth [cm]

D_e = effective diffusion coefficient for liquid phase, τD_m [cm^2/yr]

t = elapsed time [yr].

The ratio c/c_0 is assumed to be 10%, 20%, and 50% for the CE, CV, and BE cases. When these trigger values are reached, sulfate attack is assumed to occur as though the underside of the roof were exposed to the unattenuated sulfate concentration, c_0. The penetration depth is defined to be the minimum thickness of the clean grout: 6 inches (WSRC 2008a) and 15 inches (WSRC 2008b) for SDU 1 and 4, respectively. Effective diffusion coefficients are defined in Hommel (2018). The resulting delayed onset times for sulfate attack are shown in Table 7-1 and Table 7-2.

Table 7-1 Delayed sulfate attack onset times for SDU 1 roof concrete.

Parameter	BE	CV	CE	Units
Effective diffusion coefficient, D_e	6.0E-08 1.89	9.7E-08 3.06	1.2E-07 3.78	cm2/s cm2/yr
Penetration depth, x	6 15.24	6 15.24	6 15.24	in cm
Relative concentration, c/c_0	0.5	0.2	0.1	-
Penetration time, t	**135**	**23**	**11**	yr

Table 7-2 Delayed sulfate attack onset times for SDU 4 roof concrete.

Parameter	BE	CV	CE	Units
Effective diffusion coefficient, D_e	6.0E-08 1.89	9.7E-08 3.06	1.2E-07 3.78	cm2/s cm2/yr
Penetration depth, x	15 38.1	15 38.1	15 38.1	in cm
Relative concentration, c/c_0	0.5	0.2	0.1	-
Penetration time, t	**843**	**144**	**71**	yr

8.0 HDPE/GCL Liners

High Density Polyethylene (HDPE) and Geosynthetic Clay Liner (GCL) barriers reside between the SDU 2/6/7 upper and lower mud mats beneath reinforced floors, and an HDPE liner resides outside the SDU 2 concrete wall. Initially these barriers have very low permeability and intrinsic diffusion coefficient, and hinder carbonation-influenced steel corrosion. However, these properties gradually increase as HDPE degrades and eventually the HDPE components no longer function as a significant barrier to gaseous and dissolved CO_2 ingress.

Flach and Smith (2014) modeled the influence of HDPE/GCL barriers as a binary effect on carbonation: a liner delayed the onset of carbonation until its effective failure time was reached, after which the liner had no effect on CO_2 ingress. Failure was defined as liner hydraulic conductivity reaching 100 times its initial value in the PA system model, based on engineering judgement. In this study, liners are again considered to delay the onset of carbonation, but effective liner failure times are defined using a more rigorous approach. Furthermore, Revision 0 based HDPE degradation on Phifer (2005), Jones and Phifer (2008) and Flach et al. (2009). In this Revision 1 analysis, HDPE is assumed to degrade in a similar manner as in the SDF cover system, per Benson and Benavides (2018) and Tian et al. (2017).

Figure 8-1 extends Figure 2-1 by adding a liner outside the concrete barrier. The liner material may be HDPE, HDPE/GCL or other nonreactive material with respect to solute ingress. Under quasi-steady conditions, the concentration profile across the composite medium will be piecewise linear as depicted in Figure 8-1.

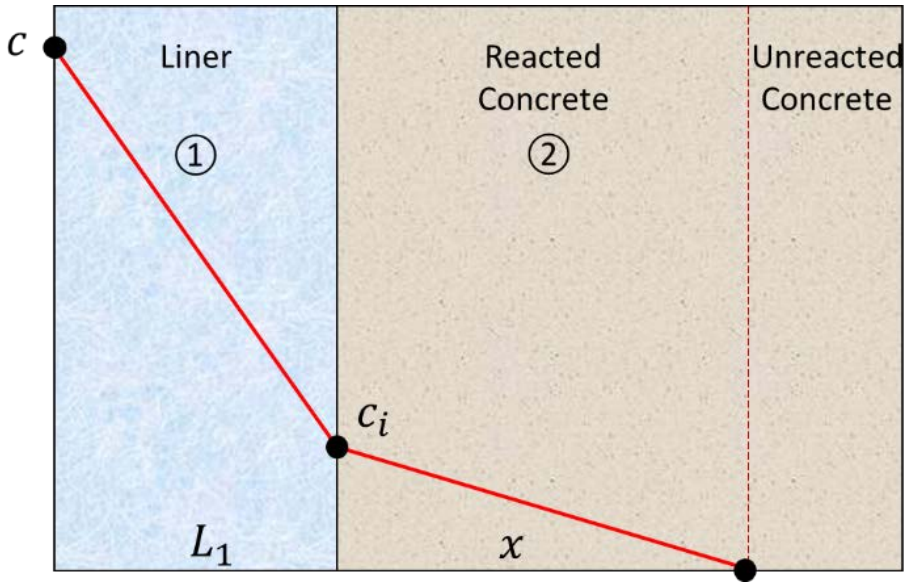

Figure 8-1 Solute diffusing through a liner and concrete and reacting at a sharp front.

The quasi-steady condition is equivalent to assuming negligible solute mass compared to the reaction capacity of the concrete. For a constant exposure concentration c, the maximum solute mass divided by reaction capacity is

$$\frac{[(SnL)_1 + (Snx)_2]c}{(1-n)\rho_s Rx} \tag{8-1}$$

where symbols are defined as in Equation.(2-1) . For a thin or low-porosity liner, the first term in the numerator can be neglected leaving:

$$\frac{Snc}{(1-n)\rho_s R} = \frac{\theta c}{\rho_b R} \tag{8-2}$$

Using SDU 2 BE carbonation values from SRNL-STI-2013-00118 Rev. 2 Table 3-2, Equation (8-2) evaluates to

$$\frac{\left(0.11\,\frac{\text{cm3 liquid}}{\text{cm3}}\right)\left(3.41\text{e-}6\,\frac{\text{mol}}{\text{cm3 liquid}}\right)}{\left(1.63\text{e-}3\,\frac{\text{mol}}{\text{cm3}}\right)} = 0.0002 \ll 1 \tag{8-3}$$

Thus, the quasi-steady assumption is quite good for this representative example.

Fick's law for solute flux can be written in a variety of forms (e.g. Flach et al. 2016, Section 4.2):

$$F = -Sn\tau D_m \frac{dc}{dx} = -SnD_e \frac{dc}{dx} = -\theta D_e \frac{dc}{dx} = -D_i \frac{dc}{dx} \tag{8-4}$$

For brevity, the subscript i will be dropped from the intrinsic diffusion coefficient, D_i. At the interface between the liner and concrete, the left and right fluxes must be equal:

$$D_1 \frac{c - c_i}{L_1} = D_2 \frac{c_i}{x} \tag{8-5}$$

Solving for the interface concentration c_i yields:

$$D_1 \frac{c}{L_1} - D_1 \frac{c_i}{L_1} = D_2 \frac{c_i}{x} \tag{8-6}$$

$$\frac{D_1}{L_1} c = \left[\frac{D_1}{L_1} + \frac{D_2}{x}\right] c_i \tag{8-7}$$

$$c_i = \frac{\frac{D_1}{L_1}}{\frac{D_1}{L_1} + \frac{D_2}{x}} c \tag{8-8}$$

A differential mass balance at reaction front is

$$D_2 \frac{c_i}{x} dt = \rho_b R dx \tag{8-9}$$

Substituting the right-hand side of Equation (8-8) for c_i produces

$$\frac{D_2}{x} \frac{\frac{D_1}{L_1}}{\frac{D_1}{L_1} + \frac{D_2}{x}} c dt = \rho_b R dx \tag{8-10}$$

$$\frac{D_1 D_2}{D_1 x + D_2 L_1} c dt = \rho_b R dx \tag{8-11}$$

$$\frac{D_1 D_2 c}{\rho_b R} dt = (D_1 x + D_2 L_1) dx \tag{8-12}$$

$$\frac{D_2 c}{\rho_b R} dt = \left(x + \frac{D_2}{D_1} L_1 \right) dx \tag{8-13}$$

Assuming the diffusion coefficients are constant through time, differential Equation (8-13) can be readily solved by integration:

$$\frac{D_2 c}{\rho_b R} \int_0^t dt = \int_0^x \left(x + \frac{D_2}{D_1} L_1 \right) dx \tag{8-14}$$

$$\frac{D_2 ct}{\rho_b R} = \left. \frac{\left(x + \frac{D_2}{D_1} L_1 \right)^2}{2} \right|_0^x \tag{8-15}$$

Evaluating the right-hand side of Equation (8-15) and solving for x yields

$$\frac{D_2 ct}{\rho_b R} = \frac{\left(x + \frac{D_2}{D_1} L_1 \right)^2}{2} - \frac{\left(\frac{D_2}{D_1} L_1 \right)^2}{2} \tag{8-16}$$

$$\frac{2 D_2 ct}{\rho_b R} + \left(\frac{D_2}{D_1} L_1 \right)^2 = \left(x + \frac{D_2}{D_1} L_1 \right)^2 \tag{8-17}$$

$$x + \frac{D_2}{D_1} L_1 = \left[\frac{2 D_2 ct}{\rho_b R} + \left(\frac{D_2}{D_1} L_1 \right)^2 \right]^{1/2} \tag{8-18}$$

$$x = \left[\frac{2 D_2 ct}{\rho_b R} + \left(\frac{D_2}{D_1} L_1 \right)^2 \right]^{1/2} - \frac{D_2}{D_1} L_1 \tag{8-19}$$

In the more general case, the liner may degrade such that its intrinsic diffusion coefficient is a function of time, $D_1(t)$, and Equation (8-11) becomes

$$\frac{D_1(t) D_2}{D_1(t) x + D_2 L_1} c dt = \rho_b R dx \tag{8-20}$$

$$dx = \frac{D_1(t) D_2}{D_1(t) x + D_2 L_1} \frac{c}{\rho_b R} \cdot dt \tag{8-21}$$

The coefficient on the right-hand side of Equation (8-21) is the instantaneous speed of the reaction front, $S(x,t)$:

$$dx = S(x,t)dt \tag{8-22}$$

Equation (8-22) can be solved numerically using a predictor-corrector approach. An initial estimate of the reaction front position at time t^{n+1} (predictor step) is

$$x^{n+1\prime} = x^n + S(x^n, t^n)dt \tag{8-23}$$

Using this value, the speed at time t^{n+1} can be estimated as

$$S(x^{n+1\prime}, t^{n+1}) \tag{8-24}$$

A refined estimate of the front position at t^{n+1} (corrector step) is

$$x^{n+1} = x^n + \frac{S(x^{n+1\prime}, t^{n+1}) + S(x^n, t^n)}{2}dt \tag{8-25}$$

Figure 8-2 and Figure 8-3 illustrate carbonation penetration depths as a function of time for 100 mil and 60 mil HDPE, respectively (Watkins 2018). The GCL layer is assumed to be 200 mil (Flach et al. 2009) based on a minimum 0.75 lbs/ft^2 sodium bentonite (SRR 2009 Section 3.2.1.3.2) with a density of approximately 47 lbs/ft^3 (e.g. https://www.reade.com/products/bentonite-montmorillonite-clay-powder). The first (blue) curve is penetration depth for no liner, computed from Equation (2-2). The second (red) curve is computed using Equation (8-25), considering either an HDPE or HDPE + GCL liner. The third (green) curve is Equation (2-2) shifted by the delayed onset time shown in Table 8-1. The delayed onset times were manually selected to achieve approximate agreement at intermediate times between the two-layer numerical solution (red curve) and shifted single-layer analytic solution (green curve). All calculations use SDU 2/6/7 parameter values from Table 4-2 through Table 4-4. The intrinsic diffusion coefficient for HDPE is based on Benson and Benavides (2018) and Tian et al. (2017). The GCL component is assumed to reduce the gas phase saturation by 50% compared to the HDPE-only case.

At time zero, HDPE is assumed to have five 10-millimeter diameter holes per hectare (approximately five holes per SDU 6/7 roof area). No further damage is assumed until antioxidants are depleted around year 750, after which stress crack resistance (SCR) declines from 100% to 50% at year 1975 or beyond (Tian et al. 2017, 80 mil HDPE). By extrapolation, 0% SCR is projected to occur no sooner than year 3200. In this analysis, HDPE saturated hydraulic conductivity and diffusion coefficient are assumed to increase geometrically between years 750 and 3200, with the fully-degraded end state being comparable to backfill soil. These assumptions are common to the BE, CV and CE scenarios. Accordingly, the three cases have similar times for HPDE failure and onset of carbonation. However, the rates of carbonation vary significantly between the BE, CV and CE cases.

Table 8-1 Delayed carbonation onset times for SDU 2/6/7 concrete (yr).

Configuration	BE case	CV case	CE case
100 mil HDPE	1900	1700	1600
100 mil HDPE + 200 mil GCL	1700	1800	1750
60 mil HDPE	1850	1700	1600
60 mil HDPE + 200 mil GCL	1600	1750	1700

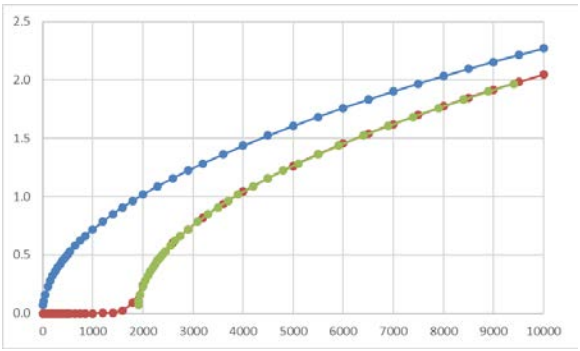

(a) BE 100 mil HDPE

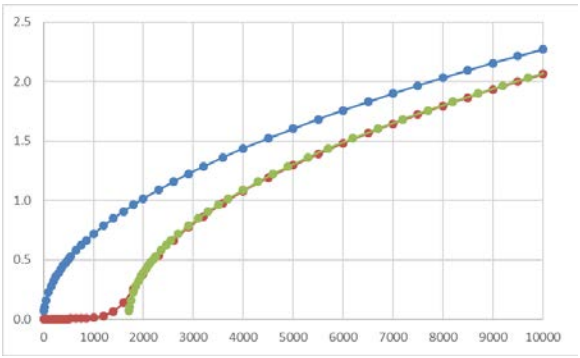

(d) BE 100 mil HDPE + GCL

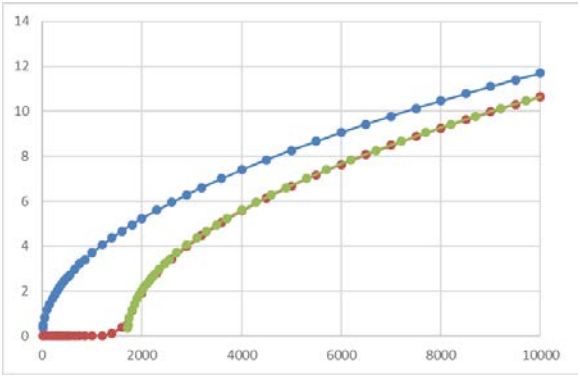

(b) CV 100 mil HDPE

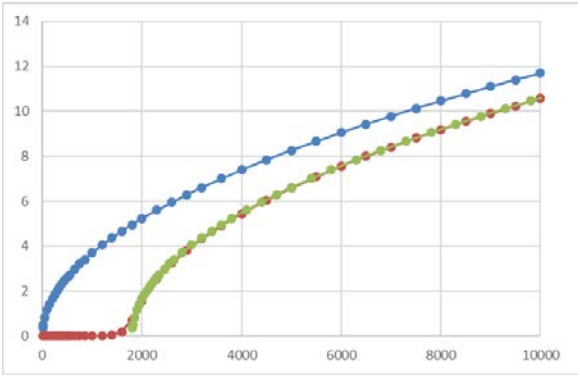

(e) CV 100 mil HDPE + GCL

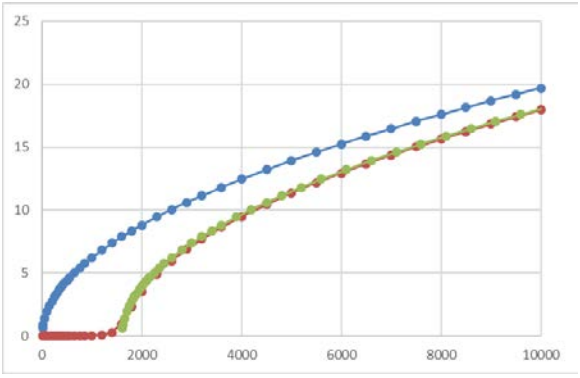

(c) CE 100 mil HDPE

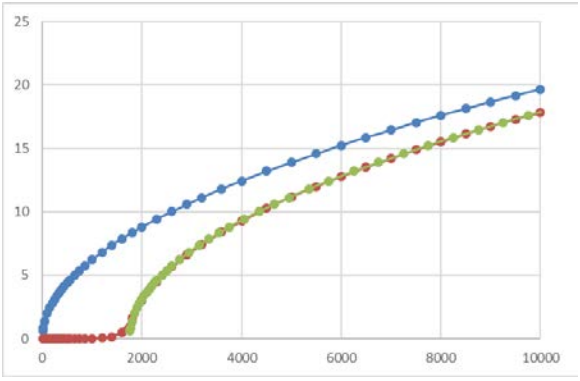

(f) CE 100 mil HDPE + GCL

Figure 8-2 Carbonation penetration for SDU2/6/7 concrete without liner, with liner, and delayed onset approximation (cm vs. yr): 100 mil HDPE cases.

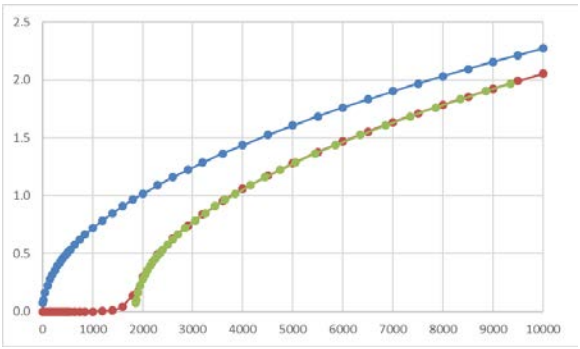

(a) BE 60 mil HDPE

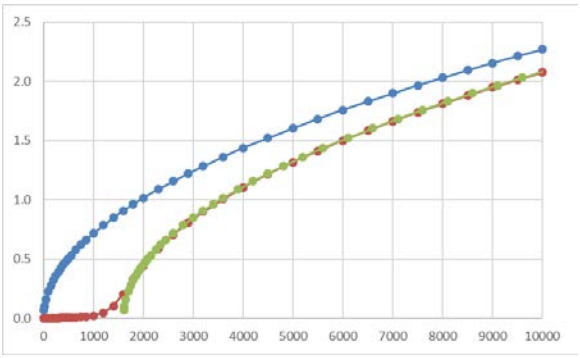

(d) BE 60 mil HDPE + GCL

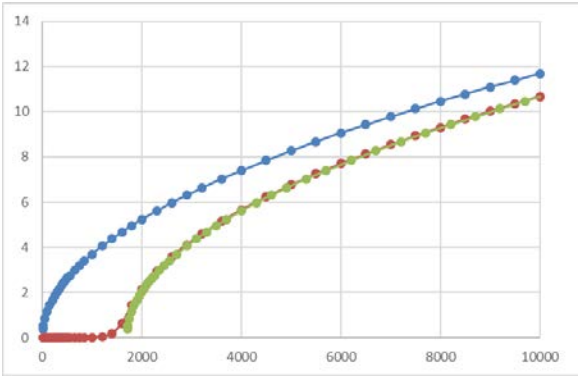

(b) CV 60 mil HDPE

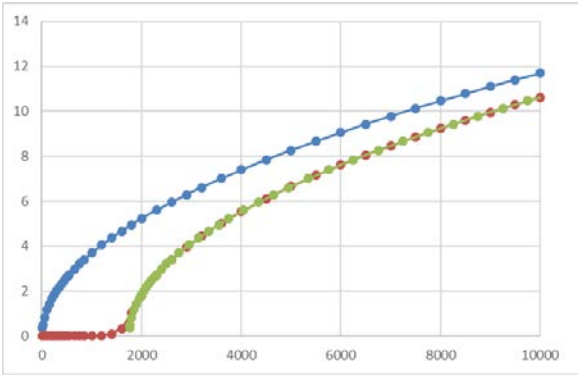

(e) CV 60 mil HDPE + GCL

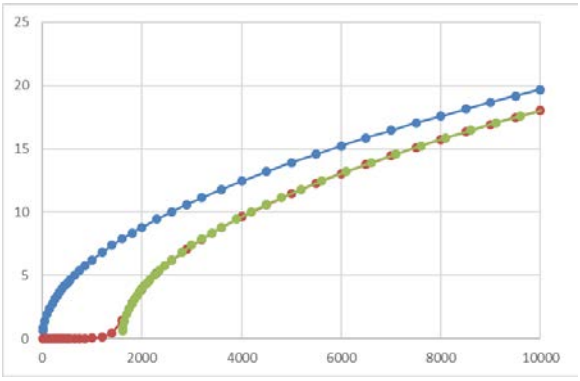

(c) CE 60 mil HDPE

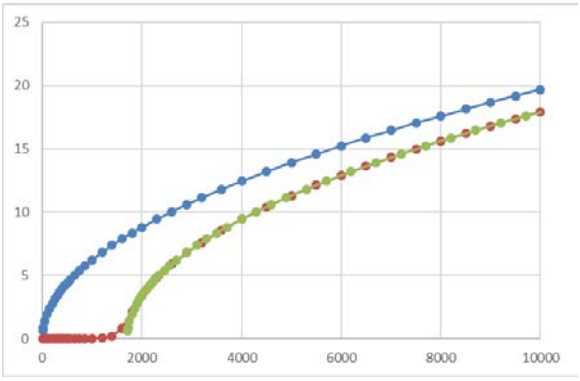

(f) CE 60 mil HDPE + GCL

Figure 8-3 Carbonation penetration for SDU2/6/7 concrete without liner, with liner, and delayed onset approximation (cm vs. yr): 60 mil HDPE cases.

9.0 Cementitious Material Degradation Times

Along with sulfate attack, carbonation-influenced steel corrosion, and decalcification, biodegradation was also considered as a potential degradation phenomenon of significance. However, Turick and Berry (2012) concluded that while biodegradation of SDU concrete is likely, it would be concentrated near outer surfaces with penetration limited by the high pH and osmotic pressure of saltstone grout pore fluid, at least for early times. Therefore, biodegradation is neglected going forward. The penetration rate coefficients for diffusion-controlled decalcification (Section 6.0) are smaller than those for sulfate attack (Section 3.0) and carbonation (Section 4.0). Thus, decalcification does not drive concrete degradation; nonetheless, penetration depths are computed for information. For saltstone grout, the sole degradation mechanism carried forward is advection-controlled decalcification.

Carbonation advances through concrete from the outside in (triggering fast steel corrosion, Section 5.0), while sulfate attack, arising from sulfate in saltstone pore water, occurs from the inside moving outward. Complete concrete degradation is assumed to occur when the two reaction fronts meet. In some cases, one or the other degradation mechanism is delayed, due to clean cap grout (Section 7.0) or an HDPE/GCL liner (Section 8.0). If the delay is long enough for one process, the other may fully penetrate the thickness in question. Sulfate attack and carbonation are generally assumed to begin at facility closure, time zero with respect to the Performance Assessment, on the general basis that the operational period is short compared to PA timeframes and can be neglected compared to analysis uncertainties. However, early sulfate attack on SDU 6 and 7 wall concrete is considered in Section 3.5. Although degradation estimates are provided for SDU 1 and 4 wall concretes, these components are assumed to be already fully degraded at PA t = 0 for the CV and CE cases, rendering the degradation times irrelevant to system performance.

Penetration times for sulfate attack and carbonation are computed using Equation (2-12). Penetration rate coefficients (A [cm/√yr]) are given in Sections 3.4 and 4.4. The maximum diffusion distance, δ [cm], is generally assumed to be 2.54 cm = 1 inch. The choice of δ = 2.54 cm produces sulfate attack results like those generated previously from the Cementitious Barriers Partnership numerical simulations (Flach and Smith 2014, Flach 2015). With respect to carbonation, the maximum diffusion distance is assumed to be correlated with the spacing of reinforcing steel and thickness of concrete cover. The typical thickness of concrete cover over reinforcing steel is 5 cm, based on American Concrete Institute (ACI) code 318 (http://en.wikipedia.org/wiki/Concrete_cover). δ = 2.54 cm is conservative in comparison. An exception to δ = 1 inch is the SDU 2 floor and upper mud mat system. Because the 4-inch thick upper mud mat does not contain rebar, carbonation is assumed to cause no damage to this material. Therefore, the minimum diffusion distance is 10.16 cm = 4 inches. The SDU 6/7 upper mud mat is not credited because this component did/will not undergo quality inspections during construction, unlike SDU 2.

Table 9-1 through Table 9-6 summarize degradation time calculations for Saltstone Disposal Units for three confidence levels: conservative estimate (CE), compliance value (CV), and best estimate (BE). As noted in the Introduction, the compliance value is defined to be an intermediate result that is more probable than the conservative estimate and more defensible than the best estimate ("MPAD", "Nominal" in SRR-CWDA-2018-00004). The dimensions of the SDU 1, 4, 2 and 6 designs reflect as-built conditions (WSRC 2008a, b, Watkins 2018). For future SDU 7, two scenarios are considered (Watkins 2018). The SDU 7 "Design" case reflects the current design. The SDU 7 "Design Margin" case assumes thinner components to accommodate potential design changes and/or construction deviations. Table 9-7 summarizes degradation times for all SDUs.

9.1 Calculation details

The SDU 1 and 4 "Grout" thicknesses include saltstone and clean grout. The 12-inch "FloorUMM" thickness for SDU 2 denotes the combination of an 8-inch floor with rebar and a 4-inch upper mud mat without rebar.

The SDU 4 roof is supported by trusses that will extend into the clean cap grout and upper saltstone when disposal cells are filled. To account for the presence of embedded steel, the upper 3.45 feet of clean grout and saltstone ("Top saltstone") degrades by carbonation-induced steel corrosion. The remaining saltstone thickness, except for the vertical roof support columns, degrades by advection-controlled decalcification.

The SDU 4 trusses are supported by concrete-filled steel pipes. These degrade by carbonation advancing inside the pipe column through concrete and outside the column through grout; both processes lead to accelerated steel corrosion. Carbonation occurs faster through the grout, so only the outer carbonation front is calculated. Carbonation through the column region is assumed to start after the earlier of the roof and floor degradation times, such that columns degrade symmetrically from the top and bottom. Performance Assessment analysts anticipate discretizing the columns in 2 foot segments for flow and transport simulations; therefore, degradation times are computed for 24-inch increments. The main calculation table indicates the degradation times for the first pair of column segments. Degradation times for all column segments (denoted "grout1", "grout2", etc.) are indicated by a summary list adjoining the main table. Because the carbonation front advances at a constant rate (past 2.54 cm), the elapsed time for the carbonation front to pass through a segment is the same for all segments.

The SDU 2, 6 and 7 roofs are supported by reinforced concrete columns. These degrade immediately by sulfate attack from the outside diameter inward. Because the columns degrade uniformly from top to bottom, they are not subdivided into segments as with SDU 4. Early sulfate attack during operations is ignored because the longevity of the internal columns is already shorter than the roof and floor. Therefore, column degradation does not control waste release.

The SDU 6 and 7 walls are partially degraded at PA time zero, due to early sulfate attack during operations (Section 3.5). After facility closure, the wall segments 1 through 5 degrade at a slower rate (Section 3.4). The degraded thickness Δx is assumed to vary linearly with time for $t_0 < t < t_1$,

$$\Delta x = \frac{t - t_0}{t_1 - t_0} L \tag{9-1}$$

where L is initial thickness and t_1 is the time of complete degradation. Time t_0 is defined by the constraint

$$\Delta x_{t=0} = \frac{-t_0}{t_1 - t_0} L \tag{9-2}$$

The solution is

$$t_0 = \frac{t_1}{1 - L/\Delta x_{t=0}} < 0 \tag{9-3}$$

or in terms of undegraded thickness at $t = 0$

$$t_0 = t_1(1 - L/L_{t=0}) < 0 \tag{9-4}$$

To support subsequent numerical flow and transport modeling, values for t_0 are included in Table 9-4 through Table 9-6.

Table 9-1 Degradation timing for SDU 1 concrete and saltstone.

Degradation mechanism:	Thickness:		SA	Carb	SA	Carb	SA	Carb	Sulfate attack						Carbonation						
			CE		CV		BE		A (cm/√yr)			Time (yr)			max δ	A (cm/√yr)			Time (yr)			max δ
Component	(in)	(cm)	(cm)	(cm)	(cm)	(cm)	(cm)	(cm)	CE	CV	BE	CE	CV	BE	(cm)	CE	CV	BE	CE	CV	BE	(cm)
Roof delay											*clean grout:*	11	**23**	135				*HDPE-GCL:*	1750	1800	1700	
Roof degradation	6	15.2	15.2	0	15.2	0	15.2	0	0.240	0.216	0.170	671	830	1342	2.54	0.257	0.149	0.027	0	0	0	2.54
Roof delay+degradation			-1067		-947		-223					683	**853**	1477					1750	**1800**	1700	
Floor delay											*immediate contact:*	0	**0**	0				*no liner:*	0	**0**	0	
Floor degradation	24	61.0	34.0	26.9	45.9	15.0	59.3	1.6	0.170	0.160	0.130	2996	4579	8957	2.54	0.151	0.091	0.017	2996	4579	8957	2.54
Floor delay+degradation			0		0		0					2996	**4579**	8957					2996	**4579**	8957	
Wall delay											*immediate contact:*	0	**0**	0				*no liner:*	0	**0**	0	
Wall degradation	18	45.7	25.5	20.2	34.4	11.3	44.3	1.4	2.118	2.118	0.651	14	19	266	2.54	1.886	1.212	0.087	14	19	266	2.54
Wall delay+degradation			0		0		0					14	**19**	266					14	**19**	266	
Grout delay																						
Grout degradation	294	746.8																				
Grout delay+degradation																						

Degradation mechanism:	Thickness:		Decalcification									Limiting		
			A (cm/√yr)			Time (yr)			max δ	CE	CV	BE		
Component	(in)	(cm)	CE	CV	BE	CE	CV	BE	(cm)	(yr)	(yr)	(yr)		
Roof delay					*HDPE-GCL:*	1750	1800	1700		**11**	**23**	**135**		
Roof degradation	6	15.24	0.029	0.026	0.021	44594	55168	89189	2.54		Roof			
Roof delay+degradation						46344	56968	90889		**683**	**853**	**1477**		
Floor delay					*no liner:*	0	0	0		**0**	**0**	**0**		
Floor degradation	24	60.96	0.017	0.016	0.013	516493	584709	885416	2.54		Floor			
Floor delay+degradation						516493	584709	885416		**2996**	**4579**	**8957**		
Wall delay					*no liner:*	0	0	0		**0**	**0**	**0**		
Wall degradation	18	45.72	0.216	0.216	0.066	2489	2489	26387	2.54		Wall			
Wall delay+degradation						2489	2489	26387		**14**	**19**	**266**		
Grout delay			A_U (cm/yr)			683	853	1477		**683**	**853**	**1477**		
Grout degradation	294	746.8	5.1E-04	7.6E-05	5.1E-06	1473777	9.8E+06	1.5E+08			Grout			
Grout delay+degradation						1.5E+06	**9.8E+06**	1.5E+08		**1.5E+06**	**9.8E+06**	**1.5E+08**		

Table 9-2 Degradation timing for SDU 4 concrete and saltstone.

Degradation mechanism:			*SA*	*Carb*	*SA*	*Carb*	*SA*	*Carb*	**Sulfate attack**							**Carbonation**						
	Thickness:		CE		CV		BE		**A (cm/√yr)**			**Time (yr)**			**max δ**	**A (cm/√yr)**			**Time (yr)**			**max δ**
Component	(in)	(cm)	(cm)	(cm)	(cm)	(cm)	(cm)	(cm)	CE	CV	BE	CE	CV	BE	(cm)	CE	CV	BE	CE	CV	BE	(cm)
Roof delay										*clean grout:*		71	**144**	843			*HDPE-GCL:*		1750	1800	1700	
Roof degradation	4	10.16	10.2	0	10.2	0	10	0.13	0.240	0.216	0.170	447	554	883	2.54	0.238	0.138	0.025	0	0	27	2.54
Roof delay+degradation			-1232		-1102		0					518	**698**	1727					1750	**1800**	1727	
Floor delay										*immediate contact:*		0	**0**	0			*no liner:*		0	**0**	0	
Floor degradation	24	60.96	34	26.9	45.9	15	59.3	1.64	0.170	0.160	0.130	2996	4579	8957	2.54	0.151	0.091	0.017	2996	4579	8957	2.54
Floor delay+degradation			0		0		0					2996	**4579**	8957					2996	**4579**	8957	
Wall delay										*immediate contact:*		0	**0**	0			*no liner:*		0	**0**	0	
Wall degradation	18	45.72	25.5	20.2	34.4	11.3	44.3	1.42	2.118	2.118	0.651	14	19	266	2.54	1.886	1.212	0.087	14	19	266	2.54
Wall delay+degradation			0		0		0					14	**19**	266					14	**19**	266	
Grout - 3.45' delay																						
Grout - 3.45' degradation	273.0	693.4																				
Grout - 3.45' delay+degradation																						
Top saltstone delay																	*Roof:*		518	**698**	1727	
Top saltstone degradation	41.37	105.1							3.45							0.415	0.165	0.032	1549	9801	262774	2.54
Top saltstone delay+degradation																			2068	**10499**	264501	
Column delay																	*Roof or floor min:*		1750	**1800**	1727	
Column degradation*	24	60.96														0.415	0.165	0.032	899	***5686***	152443	2.54
Column delay+degradation																			2649	**7486**	154170	

Table 9-2 Degradation timing for SDU 4 concrete and saltstone (continued).

Degradation mechanism:	Thickness:		Decalcification				Time (yr)			max δ	Limiting		
			A (cm/yr)			A_U (cm/yr)					CE	CV	BE
Component	(in)	(cm)	CE	CV	BE		CE	CV	BE	(cm)	(yr)	(yr)	(yr)
Roof delay				*HDPE-GCL:*			1750	1800	1700		**71**	**144**	**843**
Roof degradation	4	10.16	0.027	0.025	0.019		34605	42811	69211	2.54		Roof	
Roof delay+degradation							36355	44611	70911		**518**	**698**	**1727**
Floor delay				*no liner:*			0	0	0		**0**	**0**	**0**
Floor degradation	24	60.96	0.017	0.016	0.013		516493	584709	885416	2.54		Floor	
Floor delay+degradation							516493	584709	885416		**2996**	**4579**	**8957**
Wall delay				*no liner:*			0	0	0		**0**	**0**	**0**
Wall degradation	18	45.72	0.216	0.216	0.066		2489	2489	26387	2.54		Wall	
Wall delay+degradation							2489	2489	26387		**14**	**19**	**266**
Grout - 3.45' delay				A_U (cm/yr)			2068	10499	264501		**2068**	**10499**	**264501**
Grout - 3.45' degradation	273.0	693.4	5.1E-04	7.6E-05	5.1E-06		1368507	9.1E+06	1.4E+08			Grout-3.45'	
Grout - 3.45' delay+degradation							1.4E+06	**9.1E+06**	1.4E+08		**1.4E+06**	**9.1E+06**	**1.4E+08**
Top saltstone delay											**518**	**698**	**1727**
Top saltstone degradation	41.37	105.1										Top Salt.	
Top saltstone delay+degradation											**2068**	**10499**	**264501**
Column delay											**1750**	**1800**	**1727**
Column degradation*	24	60.96										Column	
Column delay+degradation											**2649**	**7486**	**154170**

segment	start (yr)	end (yr)	segment
grout1	1800	7486	grout12
grout2	7486	13172	grout11
grout3	13172	18858	grout10
grout4	18858	24544	grout9
grout5	24544	30230	grout8
grout6	30230	35916	grout7

Table 9-3 Degradation timing for SDU 2 concrete and saltstone.

Degradation mechanism:			*SA*	*Carb*	*SA*	*Carb*	*SA*	*Carb*	**Sulfate attack**							**Carbonation**					
	Thickness:		CE		CV		BE		**A (cm/√yr)**			**Time (yr)**			**max δ**	**A (cm/√yr)**			**Time (yr)**			**max δ**
Component	(in)	(cm)	(cm)	(cm)	(cm)	(cm)	(cm)	(cm)	CE	CV	BE	CE	CV	BE	(cm)	CE	CV	BE	CE	CV	BE	(cm)
Roof delay									*no clean grout:*			0	**0**	0			*HDPE-GCL:*		1750	1800	1700	
Roof degradation	8	20.32	20.3	0	20.3	0	20.3	0	0.238	0.223	0.182	914	1034	1566	2.54	0.199	0.120	0.023	0	0	0	2.54
Roof delay+degradation			-836		-766		-134					914	**1034**	1566					1750	**1800**	1700	
FloorUMM delay									*immediate contact:*			0	**0**	0			*HDPE-GCL:*		1750	1800	1700	
FloorUMM degradation	12	30.48	30.5	0	30.5	0	29.9	0.56	0.238	0.223	0.182	1371	1552	2306	2.54	0.199	0.120	0.023	0	0	606	10.16
FloorUMM delay+degradation			-379		-248		0					1371	**1552**	2306					1750	**1800**	2306	
Wall delay									*immediate contact:*			0	**0**	0			*HDPE:*		1600	1700	1900	
Wall degradation	8	20.32	20.3	0	20.3	0	20.3	0	0.238	0.223	0.182	914	1034	1566	2.54	0.199	0.120	0.023	0	0	0	2.54
Wall delay+degradation			-686		-666		-334					914	**1034**	1566					1600	**1700**	1900	
Grout delay																						
Grout degradation	264	670.6																				
Grout delay+degradation																						
Column delay									*immediate contact:*			0	**0**	0								
Column degradation	6.20	15.8	15.8	0	15.8	0	15.8	0	0.977	0.863	0.479	42	54	175	2.54							2.54
Column delay+degradation												42	**54**	175								
UMM delay												0	**0**	0					1750	**1800**	1700	
UMM degradation	4	10.16										from above							from above			
UMM delay+degradation												1371	**1552**	2306					1750	**1800**	2306	

Table 9-3 Degradation timing for SDU 2 concrete and saltstone (continued).

Degradation mechanism:			**Decalcification**							**Limiting**		
	Thickness:		**A (cm/yr)**			**Time (yr)**			**max δ**	**CE**	**CV**	**BE**
Component	(in)	(cm)	CE	CV	BE	CE	CV	BE	(cm)	(yr)	(yr)	(yr)
Roof delay				*HDPE-GCL:*		1750	1800	1700		**0**	**0**	**0**
Roof degradation	8	20.32	0.023	0.021	0.017	99434	112567	170459	2.54		Roof	
Roof delay+degradation						101184	114367	172159		**914**	**1034**	**1566**
FloorUMM delay				*HDPE-GCL:*		1750	1800	1700		**0**	**0**	**0**
FloorUMM degradation	12	30.48	0.023	0.021	0.017	149151	168851	255688	2.54		FloorUMM	
FloorUMM delay+degradation						150901	170651	257388		**1371**	**1552**	**2306**
Wall delay					*HDPE:*	1600	1700	1900		**0**	**0**	**0**
Wall degradation	8	20.32	0.023	0.021	0.017	99434	112567	170459	2.54		Wall	
Wall delay+degradation						101034	114267	172359		**914**	**1034**	**1566**
Grout delay			**A_U (cm/yr)**			914	1034	1566		**914**	**1034**	**1566**
Grout degradation	264	670.6	5.1E-04	7.6E-05	5.1E-06	1323392	8.8E+06	1.3E+08			Grout	
Grout delay+degradation						1.3E+06	**8.8E+06**	1.3E+08		**1.3E+06**	**8.8E+06**	**1.3E+08**
Column delay										**0**	**0**	**0**
Column degradation	6.204	15.8									Column	
Column delay+degradation										**42**	**54**	**175**
										0	**0**	**0**
											UMM	
										1371	**1552**	**2306**

Table 9-4 Degradation timing for SDU 6 concrete and saltstone.

Degradation mechanism:			*SA*	*Carb*	*SA*	*Carb*	*SA*	*Carb*	**Sulfate attack**							**Carbonation**						
	Thickness:		CE		CV		BE		**A (cm/√yr)**			**Time (yr)**			**max δ**	**A (cm/√yr)**			**Time (yr)**			**max δ**
Component	(in)	(cm)	(cm)	(cm)	(cm)	(cm)	(cm)	(cm)	CE	CV	BE	CE	CV	BE	(cm)	CE	CV	BE	CE	CV	BE	(cm)
Roof delay									*no clean grout:*			0	**0**	0			*HDPE-GCL:*		1750	1800	1700	
Roof degradation	12	30.48	30.5	0	30.5	0	29.9	0.56	0.238	0.223	0.182	1371	1552	2306	2.54	0.199	0.120	0.023	0	0	606	2.54
Roof delay+degradation			-379		-248		0					1371	**1552**	2306					1750	**1800**	2306	
Floor delay									*immediate contact:*			0	**0**	0			*HDPE-GCL:*		1750	1800	1700	
Floor degradation	12	30.48	30.5	0	30.5	0	29.9	0.56	0.238	0.223	0.182	1371	1552	2306	2.54	0.199	0.120	0.023	0	0	606	2.54
Floor delay+degradation			-379		-248		0					1371	**1552**	2306					1750	**1800**	2306	
Wall delay									*immediate contact:*			0	**0**	0			*no liner:*		0	**0**	0	
Wall degradation	8.93	22.68	13.3	9.34	17.6	5.09	21.7	0.93	0.238	0.223	0.182	600	895	1677	2.54	0.199	0.120	0.023	600	895	1677	2.54
Wall delay+degradation			0		0		0					600	**895**	1677					600	**895**	1677	
Wall delay									*immediate contact:*			0	**0**	0			*no liner:*		0	**0**	0	
Wall degradation	10.72	27.23	16	11.2	21.1	6.12	26.2	1.02	0.238	0.223	0.182	720	1075	2020	2.54	0.199	0.120	0.023	720	1075	2020	2.54
Wall delay+degradation			0		0		0					720	**1075**	2020					720	**1075**	2020	
Wall delay									*immediate contact:*			0	**0**	0			*no liner:*		0	**0**	0	
Wall degradation	13.83	35.12	20.7	14.5	27.2	7.89	34	1.17	0.238	0.223	0.182	929	1386	2617	2.54	0.199	0.120	0.023	929	1386	2617	2.54
Wall delay+degradation			0		0		0					929	**1386**	2617					929	**1386**	2617	
Wall delay									*immediate contact:*			0	**0**	0			*no liner:*		0	**0**	0	
Wall degradation	16.97	43.11	25.4	17.8	33.4	9.68	41.8	1.29	0.238	0.223	0.182	1140	1702	3224	2.54	0.199	0.120	0.023	1140	1702	3224	2.54
Wall delay+degradation			0		0		0					1140	**1702**	3224					1140	**1702**	3224	
Wall delay									*immediate contact:*			0	**0**	0			*no liner:*		0	**0**	0	
Wall degradation	20.01	50.82	29.9	20.9	39.4	11.4	49.4	1.41	0.238	0.223	0.182	1344	2006	3810	2.54	0.199	0.120	0.023	1344	2006	3810	2.54
Wall delay+degradation			0		0		0					1344	**2006**	3810					1344	**2006**	3810	
Grout delay																						
Grout degradation	516	1311																				
Grout delay+degradation																						
Column delay									*immediate contact:*			0	**0**	0								
Column degradation	10.63	27.0	27.0	0	27.0	0	27.0	0	0.977	0.863	0.479	72	92	299	2.54							
Column delay+degradation												72	**92**	299								

Table 9-4 Degradation timing for SDU 6 concrete and saltstone (continued).

Degradation mechanism:	Thickness:		Decalcification							Limiting			Initial thickness		PA t=0 thickness		Times:		
			A (cm/Yr)			Time (yr)			max δ	CE	CV	BE					CE	CV	BE
Component	(in)	(cm)	CE	CV	BE	CE	CV	BE	(cm)	(yr)	(yr)	(yr)	(in)	(cm)	(in)	(cm)	(yr)	(yr)	(yr)
Roof delay				*HDPE-GCL:*		1750	1800	1700		0	0	0							
Roof degradation	12	30.48	0.023	0.021	0.017	149151	168851	255688	2.54		Roof								
Roof delay+degradation						150901	170651	257388		**1371**	**1552**	**2306**							
FloorUMM delay				*HDPE-GCL:*		1750	1800	1700		0	0	0					**-94**	**-140**	**-262**
FloorUMM degradation	12	30.48	0.023	0.021	0.017	149151	168851	255688	2.54		Floor		10.33	26.2	8.93	22.7		Wall ⑤	
FloorUMM delay+degradation						150901	170651	257388		**1371**	**1552**	**2306**					**600**	**895**	**1677**
Wall delay				*no liner:*		0	0	0		0	0	0					**-105**	**-156**	**-293**
Wall degradation	8.93	22.68	0.023	0.021	0.017	110989	125648	190268	2.54		Wall ⑤		12.28	31.2	10.72	27.2		Wall ④	
Wall delay+degradation						110989	125648	190268		**600**	**895**	**1677**					**720**	**1075**	**2020**
Wall delay				*no liner:*		0	0	0		0	0	0					**-123**	**-184**	**-347**
Wall degradation	10.72	27.23	0.023	0.021	0.017	133264	150865	228453	2.54		Wall ④		15.66	39.8	13.83	35.1		Wall ③	
Wall delay+degradation						133264	150865	228453		**720**	**1075**	**2020**					**929**	**1386**	**2617**
Wall delay				*no liner:*		0	0	0		0	0	0					**-141**	**-211**	**-399**
Wall degradation	13.83	35.12	0.023	0.021	0.017	171849	194546	294598	2.54		Wall ③		19.08	48.5	16.97	43.1		Wall ②	
Wall delay+degradation						171849	194546	294598		**929**	**1386**	**2617**					**1140**	**1702**	**3224**
Wall delay				*no liner:*		0	0	0		0	0	0					**-159**	**-237**	**-450**
Wall degradation	16.97	43.11	0.023	0.021	0.017	210956	238818	361638	2.54		Wall ②		22.37	56.8	20.01	50.8		Wall ①	
Wall delay+degradation						210956	238818	361638		**1140**	**1702**	**3224**					**1344**	**2006**	**3810**
Wall delay				*no liner:*		0	0	0		0	0	0							
Wall degradation	20.01	50.82	0.023	0.021	0.017	248702	281549	426346	2.54		Wall ①								
Wall delay+degradation						248702	281549	426346		**1344**	**2006**	**3810**							
Grout delay			A_U (cm/yr)			1371	1552	2306		**1371**	**1552**	**2306**							
Grout degradation	516	1311	5.1E-04	7.6E-05	5.1E-06	2586629	1.7E+07	2.6E+08			Grout								
Grout delay+degradation						2.6E+06	**1.7E+07**	2.6E+08		**2.6E+06**	**1.7E+07**	**2.6E+08**							
Column delay										0	0	0							
Column degradation	10.63	27.0									Column								
Column delay+degradation										**72**	**92**	**299**							

Table 9-5 Degradation timing for SDU 7 Design concrete and saltstone.

Degradation mechanism:			*SA*	*Carb*	*SA*	*Carb*	*SA*	*Carb*	**Sulfate attack**							**Carbonation**						
	Thickness:		CE	CE	CV	CV	BE	BE	**A (cm/√yr)**			**Time (yr)**			**max δ**	**A (cm/√yr)**			**Time (yr)**			**max δ**
Component	(in)	(cm)	(cm)	(cm)	(cm)	(cm)	(cm)	(cm)	CE	CV	BE	CE	CV	BE	(cm)	CE	CV	BE	CE	CV	BE	(cm)
Roof delay									*no clean grout:*			0	**0**	0			*HDPE-GCL:*		1750	1800	1700	
Roof degradation	12	30.48	30.5	0	30.5	0	29.9	0.56	0.238	0.223	0.182	1371	1552	2306	2.54	0.199	0.120	0.023	0	0	606	2.54
Roof delay+degradation			-379		-248		0					1371	**1552**	2306					1750	**1800**	2306	
Floor delay									*immediate contact:*			0	**0**	0			*HDPE-GCL:*		1700	1750	1600	
Floor degradation	24	60.96	51.4	9.54	55	5.97	59.7	1.25	0.238	0.223	0.182	2312	2800	4603	2.54	0.199	0.120	0.023	612	1050	3003	2.54
Floor delay+degradation			0		0		0					2312	**2800**	4603					2312	**2800**	4603	
Wall delay									*immediate contact:*			0	**0**	0			*no liner:*		0	**0**	0	
Wall degradation	10.72	27.23	16	11.2	21.1	6.12	26.2	1.02	0.238	0.223	0.182	720	1075	2020	2.54	0.199	0.120	0.023	720	1075	2020	2.54
Wall delay+degradation			0		0		0					720	**1075**	2020					720	**1075**	2020	
Wall delay									*immediate contact:*			0	**0**	0			*no liner:*		0	**0**	0	
Wall degradation	12.26	31.14	18.3	12.8	24.1	6.99	30	1.1	0.238	0.223	0.182	824	1229	2316	2.54	0.199	0.120	0.023	824	1229	2316	2.54
Wall delay+degradation			0		0		0					824	**1229**	2316					824	**1229**	2316	
Wall delay									*immediate contact:*			0	**0**	0			*no liner:*		0	**0**	0	
Wall degradation	14.92	37.9	22.3	15.6	29.4	8.51	36.7	1.21	0.238	0.223	0.182	1002	1496	2829	2.54	0.199	0.120	0.023	1002	1496	2829	2.54
Wall delay+degradation			0		0		0					1002	**1496**	2829					1002	**1496**	2829	
Wall delay									*immediate contact:*			0	**0**	0			*no liner:*		0	**0**	0	
Wall degradation	17.62	44.76	26.3	18.4	34.7	10	43.4	1.32	0.238	0.223	0.182	1184	1767	3349	2.54	0.199	0.120	0.023	1184	1767	3349	2.54
Wall delay+degradation			0		0		0					1184	**1767**	3349					1184	**1767**	3349	
Wall delay									*immediate contact:*			0	**0**	0			*no liner:*		0	**0**	0	
Wall degradation	20.22	51.37	30.2	21.2	39.8	11.5	50	1.41	0.238	0.223	0.182	1358	2028	3851	2.54	0.199	0.120	0.023	1358	2028	3851	2.54
Wall delay+degradation			0		0		0					1358	**2028**	3851					1358	**2028**	3851	
Grout delay																						
Grout degradation	516	1311																				
Grout delay+degradation																						
Column delay									*immediate contact:*			0	**0**	0								
Column degradation	10.63	27.0	27.0	0	27.0	0	27.0	0	0.977	0.863	0.479	72	92	299	2.54							
Column delay+degradation												72	**92**	299								

Table 9-5 Degradation timing for SDU 7 Design concrete and saltstone (continued).

Degradation mechanism:			Decalcification							Limiting											
	Thickness:		A (cm/Vyr)			Time (yr)			max δ	CE	CV	BE	Initial thickness		t=0 thickness		Times:				
Component	(in)	(cm)	CE	CV	BE	CE	CV	BE	(cm)	(yr)	(yr)	(yr)	(in)	(cm)	(in)	(cm)	CE (yr)	CV (yr)	BE (yr)		
Roof delay				*HDPE-GCL:*		1750	1800	1700		**0**	**0**	**0**									
Roof degradation	12	30.48	0.023	0.021	0.017	149151	168851	255688	2.54		Roof										
Roof delay+degradation						150901	170651	257388		**1371**	**1552**	**2306**									
FloorUMM delay				*HDPE-GCL:*		1700	1750	1600		**0**	**0**	**0**									
FloorUMM degradation	24	60.96	0.023	0.021	0.017	298303	337701	511376	2.54		Floor		12.28	31.2	10.72	27.2					
FloorUMM delay+degradation						300003	339451	512976		**2312**	**2800**	**4603**					**-105**	**-156**	**-293**		
Wall delay				*no liner:*		0	0	0		**0**	**0**	**0**									
Wall degradation	10.72	27.23	0.023	0.021	0.017	133264	150865	228453	2.54		Wall ⑤							Wall ⑤			
Wall delay+degradation						133264	150865	228453		**720**	**1075**	**2020**					**720**	**1075**	**2020**		
Wall delay				*no liner:*		0	0	0		**0**	**0**	**0**									
Wall degradation	12.26	31.14	0.023	0.021	0.017	152382	172507	261226	2.54		Wall ④		13.95	35.4	12.26	31.1		Wall ④			
Wall delay+degradation						152382	172507	261226		**824**	**1229**	**2316**					**824**	**1229**	**2316**		
Wall delay				*no liner:*		0	0	0		**0**	**0**	**0**									
Wall degradation	14.92	37.9	0.023	0.021	0.017	185477	209975	317961	2.54		Wall ③		16.85	42.8	14.92	37.9		Wall ③			
Wall delay+degradation						185477	209975	317961		**1002**	**1496**	**2829**					**1002**	**1496**	**2829**		
Wall delay				*no liner:*		0	0	0		**0**	**0**	**0**									
Wall degradation	17.62	44.76	0.023	0.021	0.017	219008	247934	375443	2.54		Wall ②		19.78	50.2	17.62	44.8		Wall ②			
Wall delay+degradation						219008	247934	375443		**1184**	**1767**	**3349**					**1184**	**1767**	**3349**		
Wall delay				*no liner:*		0	0	0		**0**	**0**	**0**									
Wall degradation	20.22	51.37	0.023	0.021	0.017	251366	284565	430913	2.54		Wall ①		22.60	57.4	20.22	51.4		Wall ①			
Wall delay+degradation						251366	284565	430913		**1358**	**2028**	**3851**					**1358**	**2028**	**3851**		
Grout delay			A_U (cm/yr)			1371	1552	2306		**1371**	**1552**	**2306**									
Grout degradation	516	1311	5.1E-04	7.6E-05	5.1E-06	2586629	1.7E+07	2.6E+08			Grout										
Grout delay+degradation						2.6E+06	**1.7E+07**	2.6E+08		**2.6E+06**	**1.7E+07**	**2.6E+08**									
Column delay										**0**	**0**	**0**									
Column degradation	10.63	27.0									Column										
Column delay+degradation										**72**	**92**	**299**									

Table 9-6 Degradation timing for SDU 7 Design Margin concrete and saltstone.

Degradation mechanism:			*SA*	*Carb*	*SA*	*Carb*	*SA*	*Carb*	**Sulfate attack**							**Carbonation**					
	Thickness:		CE		CV		BE		**A (cm/√yr)**			**Time (yr)**			**max δ**	**A (cm/√yr)**			**Time (yr)**			**max δ**
Component	(in)	(cm)	(cm)	(cm)	(cm)	(cm)	(cm)	(cm)	CE	CV	BE	CE	CV	BE	(cm)	CE	CV	BE	CE	CV	BE	(cm)
Roof delay									*no clean grout:*			0	**0**	0			*HDPE-GCL:*		1700	1750	1600	
Roof degradation	9	22.86	22.9	0	22.9	0	22.6	0.27	0.238	0.223	0.182	1028	1164	1741	2.54	0.199	0.120	0.023	0	0	141	2.54
Roof delay+degradation			-672		-586		0					1028	**1164**	1741					1700	**1750**	1741	
Floor delay									*immediate contact:*			0	**0**	0			*no liner:*		0	**0**	0	
Floor degradation	12	30.48	17.9	12.6	23.6	6.84	29.4	1.08	0.238	0.223	0.182	806	1203	2266	2.54	0.199	0.120	0.023	806	1203	2266	2.54
Floor delay+degradation			0		0		0					806	**1203**	2266					806	**1203**	2266	
Wall delay									*immediate contact:*			0	**0**	0			*no liner:*		0	**0**	0	
Wall degradation	6.16	15.66	9.21	6.45	12.1	3.52	14.9	0.77	0.238	0.223	0.182	414	618	1147	2.54	0.199	0.120	0.023	414	618	1147	2.54
Wall delay+degradation			0		0		0					414	**618**	1147					414	**618**	1147	
Wall delay									*immediate contact:*			0	**0**	0			*no liner:*		0	**0**	0	
Wall degradation	7.82	19.87	11.7	8.18	15.4	4.46	19	0.87	0.238	0.223	0.182	525	784	1464	2.54	0.199	0.120	0.023	525	784	1464	2.54
Wall delay+degradation			0		0		0					525	**784**	1464					525	**784**	1464	
Wall delay									*immediate contact:*			0	**0**	0			*no liner:*		0	**0**	0	
Wall degradation	10.70	27.17	16	11.2	21.1	6.1	26.1	1.02	0.238	0.223	0.182	719	1073	2016	2.54	0.199	0.120	0.023	719	1073	2016	2.54
Wall delay+degradation			0		0		0					719	**1073**	2016					719	**1073**	2016	
Wall delay									*immediate contact:*			0	**0**	0			*no liner:*		0	**0**	0	
Wall degradation	13.61	34.58	20.3	14.2	26.8	7.77	33.4	1.16	0.238	0.223	0.182	915	1365	2577	2.54	0.199	0.120	0.023	915	1365	2577	2.54
Wall delay+degradation			0		0		0					915	**1365**	2577					915	**1365**	2577	
Wall delay									*immediate contact:*			0	**0**	0			*no liner:*		0	**0**	0	
Wall degradation	16.43	41.74	24.5	17.2	32.4	9.37	40.5	1.27	0.238	0.223	0.182	1104	1648	3119	2.54	0.199	0.120	0.023	1104	1648	3119	2.54
Wall delay+degradation			0		0		0					1104	**1648**	3119					1104	**1648**	3119	
Grout delay																						
Grout degradation	516	1311																				
Grout delay+degradation																						
Column delay									*immediate contact:*			0	**0**	0								
Column degradation	8.86	22.5	22.5	0	22.5	0	22.5	0	0.977	0.863	0.479	60	77	249	2.54							
Column delay+degradation												60	**77**	249								

Table 9-6 Degradation timing for SDU 7 Design Margin concrete and saltstone (continued).

Degradation mechanism:			Decalcification							Limiting											
	Thickness:		A (cm/Vyr)			Time (yr)			max δ	CE	CV	BE	Initial thickness		t=0 thickness		Times:				
Component	(in)	(cm)	CE	CV	BE	CE	CV	BE	(cm)	(yr)	(yr)	(yr)	(in)	(cm)	(in)	(cm)	CE (yr)	CV (yr)	BE (yr)		
Roof delay				*HDPE-GCL:*		1700	1750	1600		0	0	0									
Roof degradation	9	22.86	0.023	0.021	0.017	111864	126638	191766	2.54		Roof										
Roof delay+degradation						113564	128388	193366		**1028**	**1164**	**1741**									
FloorUMM delay				*no liner:*		0	0	0		0	0	0									
FloorUMM degradation	12	30.48	0.023	0.021	0.017	149151	168851	255688	2.54		Floor		7.30	18.5	6.16	15.7	**-77**	**-114**	**-212**		
FloorUMM delay+degradation						149151	168851	255688		**806**	**1203**	**2266**									
Wall delay				*no liner:*		0	0	0		0	0	0									
Wall degradation	6.163	15.66	0.023	0.021	0.017	76607	86725	131326	2.54		Wall ⑤		9.12	23.2	7.82	19.9	**-87**	**-130**	**-242**		
Wall delay+degradation						76607	86725	131326		**414**	**618**	**1147**									
Wall delay				*no liner:*		0	0	0		0	0	0									
Wall degradation	7.822	19.87	0.023	0.021	0.017	97220	110061	166664	2.54		Wall ④		12.25	31.1	10.70	27.2	**-104**	**-156**	**-293**		
Wall delay+degradation						97220	110061	166664		**525**	**784**	**1464**									
Wall delay				*no liner:*		0	0	0		0	0	0									
Wall degradation	10.7	27.17	0.023	0.021	0.017	132966	150527	227941	2.54		Wall ③		15.43	39.2	13.61	34.6	**-122**	**-182**	**-343**		
Wall delay+degradation						132966	150527	227941		**719**	**1073**	**2016**									
Wall delay				*no liner:*		0	0	0		0	0	0									
Wall degradation	13.61	34.58	0.023	0.021	0.017	169223	191574	290097	2.54		Wall ②		18.49	47.0	16.43	41.7	**-138**	**-206**	**-390**		
Wall delay+degradation						169223	191574	290097		**915**	**1365**	**2577**									
Wall delay				*no liner:*		0	0	0		0	0	0									
Wall degradation	16.43	41.74	0.023	0.021	0.017	204235	231209	350117	2.54		Wall ①						**1104**	**1648**	**3119**		
Wall delay+degradation						204235	231209	350117		**1104**	**1648**	**3119**									
Grout delay			A_U (cm/yr)			1028	1164	1741		**1028**	**1164**	**1741**									
Grout degradation	516	1311	5.1E-04	7.6E-05	5.1E-06	2586629	1.7E+07	2.6E+08			Grout										
Grout delay+degradation						2.6E+06	**1.7E+07**	2.6E+08		**2.6E+06**	**1.7E+07**	**2.6E+08**									
Column delay										**0**	**0**	**0**									
Column degradation	8.862	22.5									Column										
Column delay+degradation										**60**	**77**	**249**									

Table 9-7 Summary of degradation times.

SDU 1			SDU 4			SDU 2			SDU 6			SDU 7 Design			SDU 7 Design w/Margin		
CE (yr)	CV (yr)	BE (yr)	CE (yr)	CV (yr)	BE (yr)	CE (yr)	CV (yr)	BE (yr)	CE (yr)	CV (yr)	BE (yr)	CE (yr)	CV (yr)	BE (yr)	CE (yr)	CV (yr)	BE (yr)
11	**23**	135	71	**144**	843	0	**0**	0	0	**0**	0	0	**0**	0	0	**0**	0
Roof	6 in		**Roof**	4 in		**Roof**	8 in		**Roof**	12 in		**Roof**	12 in		**Roof**	9 in	
683	**853**	1477	518	**698**	1727	914	**1034**	1566	1371	**1552**	2306	1371	**1552**	2306	1028	**1164**	1741
0	**0**	0	0	**0**	0	0	**0**	0	0	**0**	0	0	**0**	0	0	**0**	0
Floor	24 in		**Floor**	24 in		**FloorUMM**	12 in		**Floor**	12 in		**Floor**	24 in		**Floor**	12 in	
2996	**4579**	8957	2996	**4579**	8957	1371	**1552**	2306	1371	**1552**	2306	2312	**2800**	4603	806	**1203**	2266
0	**0**	0	0	**0**	0	0	**0**	0	0	**0**	0	0	**0**	0	0	**0**	0
Wall	18 in		**Wall**	18 in		**Wall**	8 in		**Wall ⑤**	8.93 in		**Wall ⑤**	10.72 in		**Wall ⑤**	6.16 in	
14	**19**	266	14	**19**	266	914	**1034**	1566	600	**895**	1677	720	**1075**	2020	414	**618**	1147
									0	**0**	0	0	**0**	0	0	**0**	0
									Wall ④	10.72 in		**Wall ④**	12.26 in		**Wall ④**	7.82 in	
									720	**1075**	2020	824	**1229**	2316	525	**784**	1464
									0	**0**	0	0	**0**	0	0	**0**	0
									Wall ③	13.83 in		**Wall ③**	14.92 in		**Wall ③**	10.70 in	
									929	**1386**	2617	1002	**1496**	2829	719	**1073**	2016
									0	**0**	0	0	**0**	0	0	**0**	0
									Wall ②	16.97 in		**Wall ②**	17.62 in		**Wall ②**	13.61 in	
									1140	**1702**	3224	1184	**1767**	3349	915	**1365**	2577
									0	**0**	0	0	**0**	0	0	**0**	0
									Wall ①	20.01 in		**Wall ①**	20.22 in		**Wall ①**	16.43 in	
									1344	**2006**	3810	1358	**2028**	3851	1104	**1648**	3119
683	**853**	1477	2068	**10499**	264501	914	**1034**	1566	1371	**1552**	2306	1371	**1552**	2306	1028	**1164**	1741
Grout	294 in		**Grout-3.4**	273 in		**Grout**	264 in		**Grout**	516 in		**Grout**	516 in		**Grout**	516 in	
1.5E+06	**9.8E+06**	1.5E+08	1.4E+06	**9.1E+06**	1.4E+08	1.3E+06	**8.8E+06**	1.3E+08	2.6E+06	**1.7E+07**	2.6E+08	2.6E+06	**1.7E+07**	2.6E+08	2.6E+06	**1.7E+07**	2.6E+08
			518	**698**	1727												
			Top Salt.	41.37 in													
			2068	**10499**	264501												
			1750	**1800**	1727	0	**0**	0	0	**0**	0	0	**0**	0	0	**0**	0
			Column	24 in		**Column**	6.20 in		**Column**	10.63 in		**Column**	10.63 in		**Column**	8.86 in	
			2649	**7486**	154170	42	**54**	175	72	**92**	299	72	**92**	299	60	**77**	249

10.0 Initial Degradation of Cementitious Materials

Beyond early sulfate attack on SDU 6 and 7 wall concrete (Section 3.5), other early degradation of concrete components is considered in this section.

Cracks were observed in SDU 6 floor concrete in the field, likely due to insufficient moisture during curing. The equivalent hydraulic conductivity of the field-cured SDU 6 floor concrete was inferred by Hang and Flach (2016b, Table 2-4) to be approximately 6.2e-6 cm/s, based on calibration to hydraulic leak testing of the disposal unit in the field. This value is adopted for the initial conductivity of both SDU 6 floor and roof concrete, on the basis that the roof was cured in a similar manner to the floor.

Hang and Flach (2016a) considered the impact of unrepaired floor penetrations due to nail holes, formwork anchors, center pin, and form brackets on SDU 7 floor concrete. Figure 10-1 summarizes their approach for computing an equivalent hydraulic conductivity for the system. “Method 1” is arithmetic averaging followed by harmonic averaging. Alternative “Method 2” is harmonic averaging followed by arithmetic averaging. Equivalent hydraulic conductivity is defined as the geometric average of Methods 1 and 2. This method was reapplied to SDU 7 using updated material properties (Hommel 2018) and dimensions (Watkins 2018) and extended to BE, CV and CE confidence levels. Table 10-1 summarizes the calculation. Although a calculation of the impact of floor penetrations is performed for the SDU 7 Design case, these results are not carried forward because any floor penetrations will be repaired by design. Conversely, floor penetrations are assumed to remain unrepaired for the SDU 7 Design Margin case.

SDU 7 wall concrete may likewise be degraded at PA time zero due to penetrations in the form of wire form anchors and thermocouple trees (Watkins 2018). Because the two types of penetrations differ in depth, the approach of Hang and Flach (2016) is extended from binary to tertiary averaging, as depicted in Figure 10-2. Table 10-2 through Table 10-6 present equivalent hydraulic conductivity estimates for the SDU 7 Design and SDU 7 Design Margin cases. Because wall penetrations for the SDU 7 Design case are assumed to have been repaired at PA time zero or otherwise not compromise the barrier, hydraulic conductivity is unaltered.

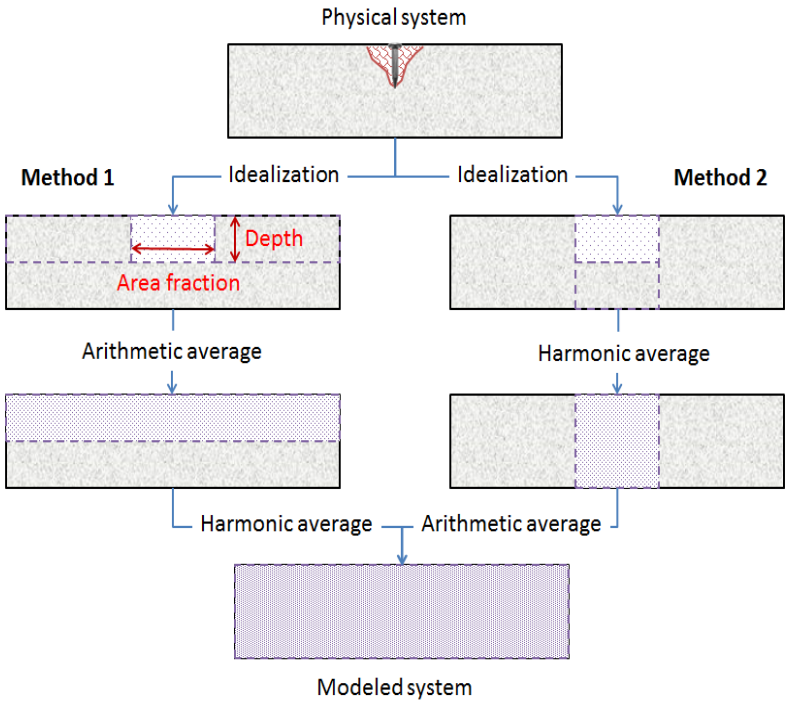

Figure 10-1 Conceptual approach for the equivalent conductivity of floor concrete.

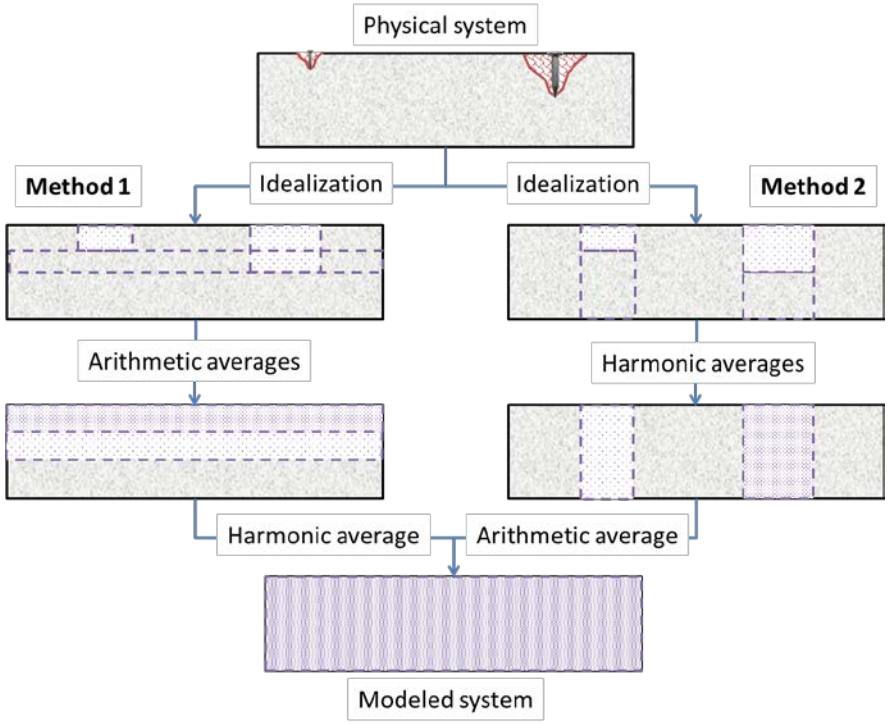

Figure 10-2 Conceptual approach for the equivalent conductivity of wall concrete.

Table 10-1 Equivalent hydraulic conductivity considering SDU 7 floor penetrations.

Case:	BE		CV		CE		Units
	SDU 7	SDU 7 DM	SDU 7	SDU 7 DM	SDU 7	SDU 7 DM	
Floor Thickness	24	12	24	12	24	12	inch
Floor Diameter	375	375	375	375	375	375	ft
Total Floor Area	110447	110447	110447	110447	110447	110447	ft2
Floor Hydraulic Conductivity	6.4E-10	6.4E-10	7.8E-10	7.8E-10	9.1E-10	9.1E-10	cm/s
Penetration Depth	6	8	6	8	6	8	inch
Impacted Area	16.57	22.09	16.57	22.09	16.57	22.09	ft2
Impact Area K	1.5E-01	1.5E-01	1.5E-01	1.5E-01	1.5E-01	1.5E-01	cm/s
Impact Area Fraction	0.015%	0.020%	0.015%	0.020%	0.015%	0.020%	
Intact Area Fraction	99.985%	99.980%	99.985%	99.980%	99.985%	99.980%	
Impacted Depth Fraction	25.00%	66.67%	25.00%	66.67%	25.00%	66.67%	
Intact Depth Fraction	75.00%	33.33%	75.00%	33.33%	75.00%	33.33%	
Method 1							
Arithmetic Average	2.25E-05	3.00E-05	2.25E-05	3.00E-05	2.25E-05	3.00E-05	cm/s
Harmonic Average	8.53E-10	1.92E-09	1.04E-09	2.34E-09	1.21E-09	2.73E-09	cm/s
Ratio to intact condition	1.33	3.00	1.33	3.00	1.33	3.00	
Method 2							
Harmonic Average	8.53E-10	1.92E-09	1.04E-09	2.34E-09	1.21E-09	2.73E-09	cm/s
Arithmetic Average	6.40E-10	6.40E-10	7.80E-10	7.80E-10	9.10E-10	9.10E-10	
Ratio to intact condition	1.00	1.00	1.00	1.00	1.00	1.00	
Modeled System							
Geometric Average	**7.39E-10**	**1.11E-09**	**9.01E-10**	**1.35E-09**	**1.05E-09**	**1.58E-09**	cm/s
Ratio to intact condition	1.15x	1.73x	1.15x	1.73x	1.15x	1.73x	

Table 10-2 Equivalent hydraulic conductivity considering SDU 7 wall segment 5 penetrations.

Case:	BE		CV		CE		Units
	SDU 7	SDU 7 DM	SDU 7	SDU 7 DM	SDU 7	SDU 7 DM	
Wall ⑤ Thickness	12.28	7.30	12.28	7.30	12.28	7.30	inch
Wall Diameter	375	375	375	375	375	375	ft
Wall Height	43	43	43	43	43	43	ft
Total Wall Area	50658	50658	50658	50658	50658	50658	ft2
Ksat, Intact	6.4E-10	6.4E-10	7.8E-10	7.8E-10	9.1E-10	9.1E-10	cm/s
Ksat, Penetrations	1.5E-01	1.5E-01	1.5E-01	1.5E-01	1.5E-01	1.5E-01	cm/s
Penetration Depth 1	0	7.25	0	7.25	0	7.25	in
Area 1	0	16	0	16	0	16	ft2
Penetration Depth 2	0	2	0	2	0	2	in
Area 2	0.00	7.17	0.00	7.17	0.00	7.17	ft2
Method 1							
Area Fraction 1	0	0.000316	0.000000	0.000316	0.000000	0.000316	
Area Fraction 2	0	0.000141	0.000000	0.000141	0.000000	0.000141	
Arithmetic Average A	6.40E-10	6.86E-05	7.80E-10	6.86E-05	9.10E-10	6.86E-05	cm/s
Arithmetic Average B	6.40E-10	4.74E-05	7.80E-10	4.74E-05	9.10E-10	4.74E-05	cm/s
Arithmetic Average C	6.40E-10	6.40E-10	7.80E-10	7.80E-10	9.10E-10	9.10E-10	cm/s
Thickness Fraction A	0	0.27389	0.00000	0.27389	0.00000	0.27389	
Thickness Fraction B	0	0.71895	0.00000	0.71895	0.00000	0.71895	
Thickness Fraction C	1	0.00717	1.00000	0.00717	1.00000	0.00717	
Harmonic Average	6.40E-10	8.92E-08	7.80E-10	1.09E-07	9.10E-10	1.27E-07	cm/s
Ratio to intact condition	1.00	139.32	1.00	139.26	1.00	139.22	
Method 2							
Thickness Fraction 1	0	0.992834	0.000000	0.992834	0.000000	0.992834	
Thickness Fraction 1	0	0.273885	0.000000	0.273885	0.000000	0.273885	
Harmonic Average A	6.4E-10	8.9E-08	7.8E-10	1.1E-07	9.1E-10	1.3E-07	cm/s
Harmonic Average B	6.4E-10	8.8E-10	7.8E-10	1.1E-09	9.1E-10	1.3E-09	cm/s
Harmonic Average C	6.4E-10	6.4E-10	7.8E-10	7.8E-10	9.1E-10	9.1E-10	cm/s
Area Fraction A	0	0.00032	0.00000	0.00032	0.00000	0.00032	
Area Fraction B	0	0.00014	0.00000	0.00014	0.00000	0.00014	
Area Fraction C	1	0.99954	1.00000	0.99954	1.00000	0.99954	
Arithmetic Average	6.40E-10	6.68E-10	7.80E-10	8.14E-10	9.10E-10	9.50E-10	cm/s
Ratio to intact condition	1.00	1.04	1.00	1.04	1.00	1.04	
Modeled System							
Geometric Average	**6.40E-10**	**7.72E-09**	**7.80E-10**	**9.40E-09**	**9.10E-10**	**1.10E-08**	cm/s
Ratio to intact condition	1.00x	12.06x	1.00x	12.06x	1.00	12.05x	

Table 10-3 Equivalent hydraulic conductivity considering SDU 7 wall segment 4 penetrations.

Case:	BE		CV		CE		Units
	SDU 7	SDU 7 DM	SDU 7	SDU 7 DM	SDU 7	SDU 7 DM	
Wall ④ Thickness	13.95	9.12	13.95	9.12	13.95	9.12	inch
Wall Diameter	375	375	375	375	375	375	ft
Wall Height	43	43	43	43	43	43	ft
Total Wall Area	50658	50658	50658	50658	50658	50658	ft2
Ksat, Intact	6.4E-10	6.4E-10	7.8E-10	7.8E-10	9.1E-10	9.1E-10	cm/s
Ksat, Penetrations	1.5E-01	1.5E-01	1.5E-01	1.5E-01	1.5E-01	1.5E-01	cm/s
Penetration Depth 1	0	7.25	0	7.25	0	7.25	in
Area 1	0	16	0	16	0	16	ft2
Penetration Depth 2	0	2	0	2	0	2	in
Area 2	0.00	7.17	0.00	7.17	0.00	7.17	ft2
Method 1							
Area Fraction 1	0	0.000316	0.000000	0.000316	0.000000	0.000316	
Area Fraction 2	0	0.000141	0.000000	0.000141	0.000000	0.000141	
Arithmetic Average A	6.40E-10	6.86E-05	7.80E-10	6.86E-05	9.10E-10	6.86E-05	cm/s
Arithmetic Average B	6.40E-10	4.74E-05	7.80E-10	4.74E-05	9.10E-10	4.74E-05	cm/s
Arithmetic Average C	6.40E-10	6.40E-10	7.80E-10	7.80E-10	9.10E-10	9.10E-10	cm/s
Thickness Fraction A	0	0.21939	0.00000	0.21939	0.00000	0.21939	
Thickness Fraction B	0	0.57589	0.00000	0.57589	0.00000	0.57589	
Thickness Fraction C	1	0.20472	1.00000	0.20472	1.00000	0.20472	
Harmonic Average	6.40E-10	3.13E-09	7.80E-10	3.81E-09	9.10E-10	4.44E-09	cm/s
Ratio to intact condition	1.00	4.88	1.00	4.88	1.00	4.88	
Method 2							
Thickness Fraction 1	0	0.795281	0.000000	0.795281	0.000000	0.795281	
Thickness Fraction 1	0	0.219388	0.000000	0.219388	0.000000	0.219388	
Harmonic Average A	6.4E-10	3.1E-09	7.8E-10	3.8E-09	9.1E-10	4.4E-09	cm/s
Harmonic Average B	6.4E-10	8.2E-10	7.8E-10	1.0E-09	9.1E-10	1.2E-09	cm/s
Harmonic Average C	6.4E-10	6.4E-10	7.8E-10	7.8E-10	9.1E-10	9.1E-10	cm/s
Area Fraction A	0	0.00032	0.00000	0.00032	0.00000	0.00032	
Area Fraction B	0	0.00014	0.00000	0.00014	0.00000	0.00014	
Area Fraction C	1	0.99954	1.00000	0.99954	1.00000	0.99954	
Arithmetic Average	6.40E-10	6.41E-10	7.80E-10	7.81E-10	9.10E-10	9.11E-10	cm/s
Ratio to intact condition	1.00	1.00	1.00	1.00	1.00	1.00	
Modeled System							
Geometric Average	**6.40E-10**	**1.42E-09**	**7.80E-10**	**1.72E-09**	**9.10E-10**	**2.01E-09**	cm/s
Ratio to intact condition	1.00x	2.21x	1.00x	2.21x	1.00x	2.21x	

Table 10-4 Equivalent hydraulic conductivity considering SDU 7 wall segment 3 penetrations.

Case:	BE		CV		CE		Units
	SDU 7	SDU 7 DM	SDU 7	SDU 7 DM	SDU 7	SDU 7 DM	
Wall ③ Thickness	16.85	12.25	16.85	12.25	16.85	12.25	inch
Wall Diameter	375	375	375	375	375	375	ft
Wall Height	43	43	43	43	43	43	ft
Total Wall Area	50658	50658	50658	50658	50658	50658	ft2
Ksat, Intact	6.4E-10	6.4E-10	7.8E-10	7.8E-10	9.1E-10	9.1E-10	cm/s
Ksat, Penetrations	1.5E-01	1.5E-01	1.5E-01	1.5E-01	1.5E-01	1.5E-01	cm/s
Penetration Depth 1	0	7.25	0	7.25	0	7.25	in
Area 1	0	16	0	16	0	16	ft2
Penetration Depth 2	0	2	0	2	0	2	in
Area 2	0.00	7.17	0.00	7.17	0.00	7.17	ft2
Method 1							
Area Fraction 1	0	0.000316	0.000000	0.000316	0.000000	0.000316	
Area Fraction 2	0	0.000141	0.000000	0.000141	0.000000	0.000141	
Arithmetic Average A	6.40E-10	6.86E-05	7.80E-10	6.86E-05	9.10E-10	6.86E-05	cm/s
Arithmetic Average B	6.40E-10	4.74E-05	7.80E-10	4.74E-05	9.10E-10	4.74E-05	cm/s
Arithmetic Average C	6.40E-10	6.40E-10	7.80E-10	7.80E-10	9.10E-10	9.10E-10	cm/s
Thickness Fraction A	0	0.16323	0.00000	0.16323	0.00000	0.16323	
Thickness Fraction B	0	0.42847	0.00000	0.42847	0.00000	0.42847	
Thickness Fraction C	1	0.40830	1.00000	0.40830	1.00000	0.40830	
Harmonic Average	6.40E-10	1.57E-09	7.80E-10	1.91E-09	9.10E-10	2.23E-09	cm/s
Ratio to intact condition	1.00	2.45	1.00	2.45	1.00	2.45	
Method 2							
Thickness Fraction 1	0	0.591696	0.000000	0.591696	0.000000	0.591696	
Thickness Fraction 1	0	0.163227	0.000000	0.163227	0.000000	0.163227	
Harmonic Average A	6.4E-10	1.6E-09	7.8E-10	1.9E-09	9.1E-10	2.2E-09	cm/s
Harmonic Average B	6.4E-10	7.6E-10	7.8E-10	9.3E-10	9.1E-10	1.1E-09	cm/s
Harmonic Average C	6.4E-10	6.4E-10	7.8E-10	7.8E-10	9.1E-10	9.1E-10	cm/s
Area Fraction A	0	0.00032	0.00000	0.00032	0.00000	0.00032	
Area Fraction B	0	0.00014	0.00000	0.00014	0.00000	0.00014	
Area Fraction C	1	0.99954	1.00000	0.99954	1.00000	0.99954	
Arithmetic Average	6.40E-10	6.40E-10	7.80E-10	7.80E-10	9.10E-10	9.10E-10	cm/s
Ratio to intact condition	1.00	1.00	1.00	1.00	1.00	1.00	
Modeled System							
Geometric Average	**6.40E-10**	**1.00E-09**	**7.80E-10**	**1.22E-09**	**9.10E-10**	**1.42E-09**	cm/s
Ratio to intact condition	1.00x	1.57x	1.00x	1.57x	1.00x	1.57x	

Table 10-5 Equivalent hydraulic conductivity considering SDU 7 wall segment 2 penetrations.

Case:	BE		CV		CE		Units
	SDU 7	SDU 7 DM	SDU 7	SDU 7 DM	SDU 7	SDU 7 DM	
Wall ② Thickness	19.78	15.43	19.78	15.43	19.78	15.43	inch
Wall Diameter	375	375	375	375	375	375	ft
Wall Height	43	43	43	43	43	43	ft
Total Wall Area	50658	50658	50658	50658	50658	50658	ft2
Ksat, Intact	6.4E-10	6.4E-10	7.8E-10	7.8E-10	9.1E-10	9.1E-10	cm/s
Ksat, Penetrations	1.5E-01	1.5E-01	1.5E-01	1.5E-01	1.5E-01	1.5E-01	cm/s
Penetration Depth 1	0	7.25	0	7.25	0	7.25	in
Area 1	0	16	0	16	0	16	ft2
Penetration Depth 2	0	2	0	2	0	2	in
Area 2	0.00	7.17	0.00	7.17	0.00	7.17	ft2
Method 1							
Area Fraction 1	0	0.000316	0.000000	0.000316	0.000000	0.000316	
Area Fraction 2	0	0.000141	0.000000	0.000141	0.000000	0.000141	
Arithmetic Average A	6.40E-10	6.86E-05	7.80E-10	6.86E-05	9.10E-10	6.86E-05	cm/s
Arithmetic Average B	6.40E-10	4.74E-05	7.80E-10	4.74E-05	9.10E-10	4.74E-05	cm/s
Arithmetic Average C	6.40E-10	6.40E-10	7.80E-10	7.80E-10	9.10E-10	9.10E-10	cm/s
Thickness Fraction A	0	0.12964	0.00000	0.12964	0.00000	0.12964	
Thickness Fraction B	0	0.34031	0.00000	0.34031	0.00000	0.34031	
Thickness Fraction C	1	0.53005	1.00000	0.53005	1.00000	0.53005	
Harmonic Average	6.40E-10	1.21E-09	7.80E-10	1.47E-09	9.10E-10	1.72E-09	cm/s
Ratio to intact condition	1.00	1.89	1.00	1.89	1.00	1.89	
Method 2							
Thickness Fraction 1	0	0.469945	0.000000	0.469945	0.000000	0.469945	
Thickness Fraction 1	0	0.129640	0.000000	0.129640	0.000000	0.129640	
Harmonic Average A	6.4E-10	1.2E-09	7.8E-10	1.5E-09	9.1E-10	1.7E-09	cm/s
Harmonic Average B	6.4E-10	7.4E-10	7.8E-10	9.0E-10	9.1E-10	1.0E-09	cm/s
Harmonic Average C	6.4E-10	6.4E-10	7.8E-10	7.8E-10	9.1E-10	9.1E-10	cm/s
Area Fraction A	0	0.00032	0.00000	0.00032	0.00000	0.00032	
Area Fraction B	0	0.00014	0.00000	0.00014	0.00000	0.00014	
Area Fraction C	1	0.99954	1.00000	0.99954	1.00000	0.99954	
Arithmetic Average	6.40E-10	6.40E-10	7.80E-10	7.80E-10	9.10E-10	9.10E-10	cm/s
Ratio to intact condition	1.00	1.00	1.00	1.00	1.00	1.00	
Modeled System							
Geometric Average	**6.40E-10**	**8.79E-10**	**7.80E-10**	**1.07E-09**	**9.10E-10**	**1.25E-09**	cm/s
Ratio to intact condition	1.00x	1.37x	1.00x	1.37x	1.00x	1.37x	

Table 10-6 Equivalent hydraulic conductivity considering SDU 7 wall segment 1 penetrations.

Case:	BE		CV		CE		Units
	SDU 7	SDU 7 DM	SDU 7	SDU 7 DM	SDU 7	SDU 7 DM	
Wall ① Thickness	22.60	18.49	22.60	18.49	22.60	18.49	inch
Wall Diameter	375	375	375	375	375	375	ft
Wall Height	43	43	43	43	43	43	ft
Total Wall Area	50658	50658	50658	50658	50658	50658	ft2
Ksat, Intact	6.4E-10	6.4E-10	7.8E-10	7.8E-10	9.1E-10	9.1E-10	cm/s
Ksat, Penetrations	1.5E-01	1.5E-01	1.5E-01	1.5E-01	1.5E-01	1.5E-01	cm/s
Penetration Depth 1	0	7.25	0	7.25	0	7.25	in
Area 1	0	16	0	16	0	16	ft2
Penetration Depth 2	0	2	0	2	0	2	in
Area 2	0.00	7.17	0.00	7.17	0.00	7.17	ft2
Method 1							
Area Fraction 1	0	0.000316	0.000000	0.000316	0.000000	0.000316	
Area Fraction 2	0	0.000141	0.000000	0.000141	0.000000	0.000141	
Arithmetic Average A	6.40E-10	6.86E-05	7.80E-10	6.86E-05	9.10E-10	6.86E-05	cm/s
Arithmetic Average B	6.40E-10	4.74E-05	7.80E-10	4.74E-05	9.10E-10	4.74E-05	cm/s
Arithmetic Average C	6.40E-10	6.40E-10	7.80E-10	7.80E-10	9.10E-10	9.10E-10	cm/s
Thickness Fraction A	0	0.10818	0.00000	0.10818	0.00000	0.10818	
Thickness Fraction B	0	0.28396	0.00000	0.28396	0.00000	0.28396	
Thickness Fraction C	1	0.60786	1.00000	0.60786	1.00000	0.60786	
Harmonic Average	6.40E-10	1.05E-09	7.80E-10	1.28E-09	9.10E-10	1.50E-09	cm/s
Ratio to intact condition	1.00	1.65	1.00	1.65	1.00	1.65	
Method 2							
Thickness Fraction 1	0	0.392138	0.000000	0.392138	0.000000	0.392138	
Thickness Fraction 1	0	0.108176	0.000000	0.108176	0.000000	0.108176	
Harmonic Average A	6.4E-10	1.1E-09	7.8E-10	1.3E-09	9.1E-10	1.5E-09	cm/s
Harmonic Average B	6.4E-10	7.2E-10	7.8E-10	8.7E-10	9.1E-10	1.0E-09	cm/s
Harmonic Average C	6.4E-10	6.4E-10	7.8E-10	7.8E-10	9.1E-10	9.1E-10	cm/s
Area Fraction A	0	0.00032	0.00000	0.00032	0.00000	0.00032	
Area Fraction B	0	0.00014	0.00000	0.00014	0.00000	0.00014	
Area Fraction C	1	0.99954	1.00000	0.99954	1.00000	0.99954	
Arithmetic Average	6.40E-10	6.40E-10	7.80E-10	7.80E-10	9.10E-10	9.10E-10	cm/s
Ratio to intact condition	1.00	1.00	1.00	1.00	1.00	1.00	
Modeled System							
Geometric Average	**6.40E-10**	**8.21E-10**	**7.80E-10**	**1.00E-09**	**9.10E-10**	**1.17E-09**	cm/s
Ratio to intact condition	1.00x	1.28x	1.00x	1.28x	1.00x	1.28x	

11.0 Variation of Equivalent Hydraulic Conductivity with Time

Table 11-1 summarizes hydraulic conductivity recommendations for each SDU at BE, CV and CE confidence levels. The initial values are generally drawn from Hommel (2018), but may also reflect partial degradation at PA time zero due to unrepaired penetrations, suboptimal curing conditions in the field, or early sulfate attack (Sections 3.5, 10.0). The final values are those of backfill soil or Lower Vadose Zone native sediment (Phifer et al. 2006, Table 5-18, K_v), depending on which material adjoins a component. With this selection, the fully-degraded cementitious material functions neither as a barrier nor a conduit to flow, relative to its neighboring geologic material.

As noted in Section 9.1 the degraded thickness Δx is assumed to vary linearly with time for $t > 0$, where t_0 and t_1 in Equation (9-1) are summarized in Table 9-7 (also see Table 9-4 through Table 9-6 for SDU 6 and 7 wall segments). A linear variation with time is appropriate for concrete because δ = 2.54 cm for nearly all components, which is small compared to overall thicknesses. Therefore, degradation fronts advance mostly at a constant rate, per Figure 2-2 and Equation (2-2). For saltstone, advection-controlled decalcification directly produces a constant penetration rate, or linear variation with time. Equation (9-1) can be rewritten in a form valid for all times as

$$f(t) \equiv \frac{\Delta x}{L} = \frac{\min[\max(t, t_0), t_1] - t_0}{t_1 - t_0} \tag{11-1}$$

where $0 \leq f(t) \leq 1$ is the degradation fraction.

Performance Assessment system modeling will treat each concrete and grout component as a homogeneous material with time-varying hydraulic conductivity. Therefore, the equivalent hydraulic conductivity of each degrading component is needed. Equivalent hydraulic conductivity is generally defined as the uniform hydraulic conductivity value that reproduces some integral behavior of a region, such as spatial average liquid flux for a given hydraulic head gradient. A closely related concept is effective hydraulic, a statistical ensemble average. Sanchez-Vila et al. (1995) and Sanchez-Vila et al. (2006) provide a comprehensive review of these mathematical concepts, in the context of groundwater flow applications. For the level of rigor required in this discussion, the two concepts and terms can be used interchangeably.

A well-known example of equivalent hydraulic conductivity K_e is the arithmetic average K_A for flow parallel to perfect homogeneous layers. For a two-layer system

$$K_e = K_A = fK_1 + (1 - f)K_2 \equiv \overline{K} \tag{11-2}$$

Another widely-known example is the harmonic average K_H for flow perpendicular to layers. For two perfect layers,

$$K_e = K_H = \frac{1}{\frac{f}{K_1} + \frac{(1 - f)}{K_2}} = \left(\overline{K^{-1}}\right)^{-1} \tag{11-3}$$

or equivalently

$${K_e}^{-1} = {K_H}^{-1} = f{K_1}^{-1} + (1 - f){K_2}^{-1} = \overline{K^{-1}} \tag{11-4}$$

Matheron (1967) demonstrated that effective hydraulic conductivity is bounded by the arithmetic and harmonic means (Sanchez-Vila et al. 2006):

$$\left(\overline{K^{-1}}\right)^{-1} \leq K_e \leq \overline{K} \tag{11-5}$$

For an isotropic, log-normal, hydraulic conductivity field in two-dimensions, the effective conductivity is the geometric mean K_G of the point values (Gutjahr et al. 1978):

$$K_e = K_G = exp\left[\overline{lnK}\right] \tag{11-6}$$

An equivalent expression is

$$lnK_e = lnK_G = \overline{lnK} \tag{11-7}$$

Arithmetic, harmonic and geometric averaging are special cases of the p-norm (Ababou and Wood 1990) defined by

$${K_e}^p \equiv \overline{K^p} \tag{11-8}$$

where $-1 \leq p \leq +1$ and

$$\begin{array}{ll} p = -1 & \text{harmonic} \\ p \to 0 & \text{geometric} \\ p = +1 & \text{arithmetic} \end{array} \tag{11-9}$$

While integer values correspond to well-known averages, p can also take on non-integer values. Many other examples of effective and equivalent conductivity can be found in the literature (e.g. Sanchez-Vila et al. 2006, Brown and Garrabrants 2017).

The concept depicted in Figure 2-1 is that of a sharp degradation front advancing uniformly and leaving behind fully damaged material, such that the conductivity field is binary and resides in two distinct layers of constant thickness. For this idealized construct, the arithmetic ($p = +1$) and harmonic ($p = -1$) averages are the appropriate equivalent hydraulic conductivities for parallel and perpendicular flow, respectively. However, the ideal of perfect layers and a binary conductivity field is not expected in the field. To some extent, the degradation front will advance non-uniformly and conductivity will vary more continuously between intact and fully damaged states. These non-ideal conditions will lead to a deviation from Equations (11-2) and (11-4).

As a more realistic analog to degrading cementitious materials, consider porous-medium flow through an anisotropic, log-normal, unbounded, hydraulic conductivity field in three dimensions. Suppose the spatial correlation length is the same in directions 1 and 2 ($\lambda_1 = \lambda_2 \equiv \lambda_{12}$) and is an order of magnitude lower in direction 3 (λ_3/λ_{12} = 0.1). In the context of an SDU, directions 1 and 2 are those in the plane of a concrete barrier, and direction 3 is normal to the barrier. In terms of a p-norm, the effective conductivities for parallel and perpendicular flow correspond to $p_{12} = +0.86$ and $p_3 = -0.72$ (Gelhar and Axness 1983, Ababou and Wood 1990, Sanchez-Vila et al. 2006 Equations (46), Phifer et al. 2006 Table 5-6). For a bounded spatial domain with relative extent L/λ = 3, Desbarats (1992) derived equivalent conductivities corresponding to $p_{12} = +0.59$ and $p_3 = -0.33$ (Phifer et al. 2006 Table 5-6). Similarly,

Sarris and Paleologos (2004) estimated $p_{12} = +0.40$ and $p_3 = +0.05$ for L/λ = 8 (Phifer et al. 2006 Table 5-6). For these examples, note that the equivalent conductivity for parallel flow lies between the arithmetic and geometric means, and closer to the arithmetic average. For perpendicular flow, K_e lies between the geometric and harmonic means, and closer to the geometric average.

Brown and Garrabrants (2017) reviewed effective conductivity literature in the context of the Saltstone Disposal Facility, and recommended for simplicity that the geometric mean define the equivalent conductivity of heterogeneous cementitious materials. Considering uncertainties, they argue that the geometric mean adequately approximates theoretical results, and data from experimental columns involving layered soils. For perpendicular flow through cementitious barriers, the geometric mean ($p \rightarrow 0$) is much higher than the harmonic average ($p = -1$) for idealized layers, and biased high compared to the above set of three analogues ($-0.72 \leq p \leq +0.05$). Based on the recommendation of Brown and Garrabrants (2017) and these additional observations, the geometric mean is adopted for equivalent hydraulic conductivity in this study as a simple and defensible assumption when facility performance is driven by flow perpendicular to barriers.

Thus, the equivalent hydraulic conductivity of a partially-degraded thickness is computed as a function of time using Equation (11-1) and the expression

$$K_e(t) = exp\left[f(t) \cdot lnK_1 + \left(1 - f(t)\right) \cdot lnK_2\right] \quad (11\text{-}10)$$

For simplicity, the conductivity field is assumed to be isotropic,

$$K_h(t) = K_v(t) = K_e(t) \quad (11\text{-}11)$$

where the subscripts h and v refer to the horizontal and vertical directions, respectively.

Figure 11-1 illustrates a hypothetical example of Equation (11-10) ($p \rightarrow 0$ or geometric averaging) when $t_0 = 100$ yr, $t_1 = 900$ yr, K_1 = 1.0e-6 cm/s and K_2 = 1.0e-10 cm/s. Also plotted for reference are alternative averages using p = 1 (arithmetic), 0.5, -0.5 and -1 (harmonic).

Table 11-1 Summary of hydraulic conductivities.

SDU 1			SDU 4			SDU 2			SDU 6			SDU 7 Design			SDU 7 Design w/Margin		
CE (cm/s)	CV (cm/s)	BE (cm/s)	CE (cm/s)	CV (cm/s)	BE (cm/s)	CE (cm/s)	CV (cm/s)	BE (cm/s)	CE (cm/s)	CV (cm/s)	BE (cm/s)	CE (cm/s)	CV (cm/s)	BE (cm/s)	CE (cm/s)	CV (cm/s)	BE (cm/s)
2.1E-09	**7.8E-10**	3.1E-10	2.1E-09	**7.8E-10**	3.1E-10	3.2E-10	**1.4E-10**	1.0E-10	6.2E-06	**6.2E-06**	6.2E-06	9.1E-10	**7.8E-10**	6.4E-10	1.6E-09	**1.4E-09**	1.1E-09
Roof	6 in		**Roof**	4 in		**Roof**	8 in		**Roof**	12 in		**Roof**	12 in		**Roof**	9 in	
4.1E-05	**4.1E-05**	4.1E-05	4.1E-05	**4.1E-05**	4.1E-05	4.1E-05	**4.1E-05**	4.1E-05	4.1E-05	**4.1E-05**	4.1E-05	4.1E-05	**4.1E-05**	4.1E-05	4.1E-05	**4.1E-05**	4.1E-05
2.1E-09	**7.8E-10**	3.1E-10	2.1E-09	**7.8E-10**	3.1E-10	3.2E-10	**1.4E-10**	1.0E-10	6.2E-06	**6.2E-06**	6.2E-06	9.1E-10	**7.8E-10**	6.4E-10	1.6E-09	**1.4E-09**	1.1E-09
Floor	24 in		**Floor**	24 in		FloorUMM	12 in		**Floor**	12 in		**Floor**	24 in		**Floor**	12 in	
9.1E-05	**9.1E-05**	9.1E-05	9.1E-05	**9.1E-05**	9.1E-05	9.1E-05	**9.1E-05**	9.1E-05	9.1E-05	**9.1E-05**	9.1E-05	9.1E-05	**9.1E-05**	9.1E-05	9.1E-05	**9.1E-05**	9.1E-05
4.1E-05	**4.1E-05**	1.0E-08	4.1E-05	**4.1E-05**	1.0E-08	3.2E-10	**1.4E-10**	1.0E-10	3.2E-10	**1.40E-10**	1.0E-10	9.10E-10	**7.80E-10**	6.40E-10	1.10E-08	**9.40E-09**	7.72E-09
Wall	18 in		**Wall**	18 in		**Wall**	8 in		**Wall ⑤**	8.93 in		**Wall ⑤**	10.72 in		**Wall ⑤**	6.16 in	
4.1E-05	**4.1E-05**	4.1E-05	4.1E-05	**4.1E-05**	4.1E-05	4.1E-05	**4.1E-05**	4.1E-05	4.1E-05	**4.1E-05**	4.1E-05	4.1E-05	**4.1E-05**	4.1E-05	4.1E-05	**4.1E-05**	4.1E-05
									3.2E-10	**1.40E-10**	1.0E-10	9.10E-10	**7.80E-10**	6.40E-10	2.01E-09	**1.72E-09**	1.42E-09
									Wall ④	10.72 in		**Wall ④**	12.26 in		**Wall ④**	7.82 in	
									4.1E-05	**4.1E-05**	4.1E-05	4.1E-05	**4.1E-05**	4.1E-05	4.1E-05	**4.1E-05**	4.1E-05
									3.2E-10	**1.40E-10**	1.0E-10	9.10E-10	**7.80E-10**	6.40E-10	1.42E-09	**1.22E-09**	1.00E-09
Soils:									**Wall ③**	13.83 in		**Wall ③**	14.92 in		**Wall ③**	10.70 in	
Backfill	**4.1E-05**	cm/s							4.1E-05	**4.1E-05**	4.1E-05	4.1E-05	**4.1E-05**	4.1E-05	4.1E-05	**4.1E-05**	4.1E-05
Native soil	**9.1E-05**	cm/s							3.2E-10	**1.40E-10**	1.0E-10	9.10E-10	**7.80E-10**	6.40E-10	1.25E-09	**1.07E-09**	8.79E-10
									Wall ②	16.97 in		**Wall ②**	17.62 in		**Wall ②**	13.61 in	
									4.1E-05	**4.1E-05**	4.1E-05	4.1E-05	**4.1E-05**	4.1E-05	4.1E-05	**4.1E-05**	4.1E-05
									3.2E-10	**1.40E-10**	1.0E-10	9.10E-10	**7.80E-10**	6.40E-10	1.17E-09	**1.00E-09**	8.21E-10
									Wall ①	20.01 in		**Wall ①**	20.22 in		**Wall ①**	16.43 in	
									4.1E-05	**4.1E-05**	4.1E-05	4.1E-05	**4.1E-05**	4.1E-05	4.1E-05	**4.1E-05**	4.1E-05
2.0E-09	**5.0E-10**	1.0E-10	2.0E-09	**5.0E-10**	1.0E-10	2.0E-09	**5.0E-10**	1.0E-10	2.0E-09	**5.0E-10**	1.0E-10	2.0E-09	**5.0E-10**	1.0E-10	2.0E-09	**5.0E-10**	1.0E-10
Grout	294 in		**Grout-3.4**	273 in		**Grout**	264 in		**Grout**	516 in		**Grout**	516 in		**Grout**	516 in	
4.1E-05	**4.1E-05**	4.1E-05	4.1E-05	**4.1E-05**	4.1E-05	4.1E-05	**4.1E-05**	4.1E-05	4.1E-05	**4.1E-05**	4.1E-05	4.1E-05	**4.1E-05**	4.1E-05	4.1E-05	**4.1E-05**	4.1E-05
			2.0E-09	**5.0E-10**	1.0E-10												
			Top Salt.	41.37 in													
			4.1E-05	**4.1E-05**	4.1E-05												
			1.0E-08	**5.0E-09**	5.0E-09	1.0E-08	**5.0E-09**	5.0E-09	1.0E-08	**5.0E-09**	5.0E-09	1.0E-08	**5.0E-09**	5.0E-09	1.0E-08	**5.0E-09**	5.0E-09
			Column	24 in		**Column**	6.20 in		**Column**	10.63 in		**Column**	10.63 in		**Column**	8.86 in	
			4.1E-05	**4.1E-05**	4.1E-05	4.1E-05	**4.1E-05**	4.1E-05	4.1E-05	**4.1E-05**	4.1E-05	4.1E-05	**4.1E-05**	4.1E-05	4.1E-05	**4.1E-05**	4.1E-05

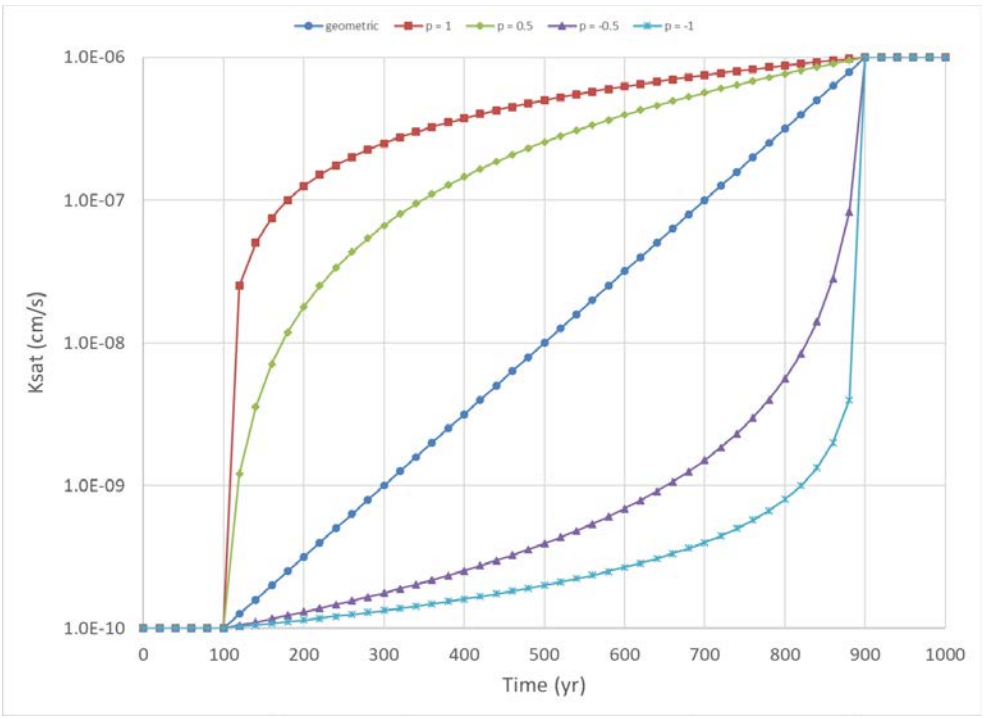

(a)

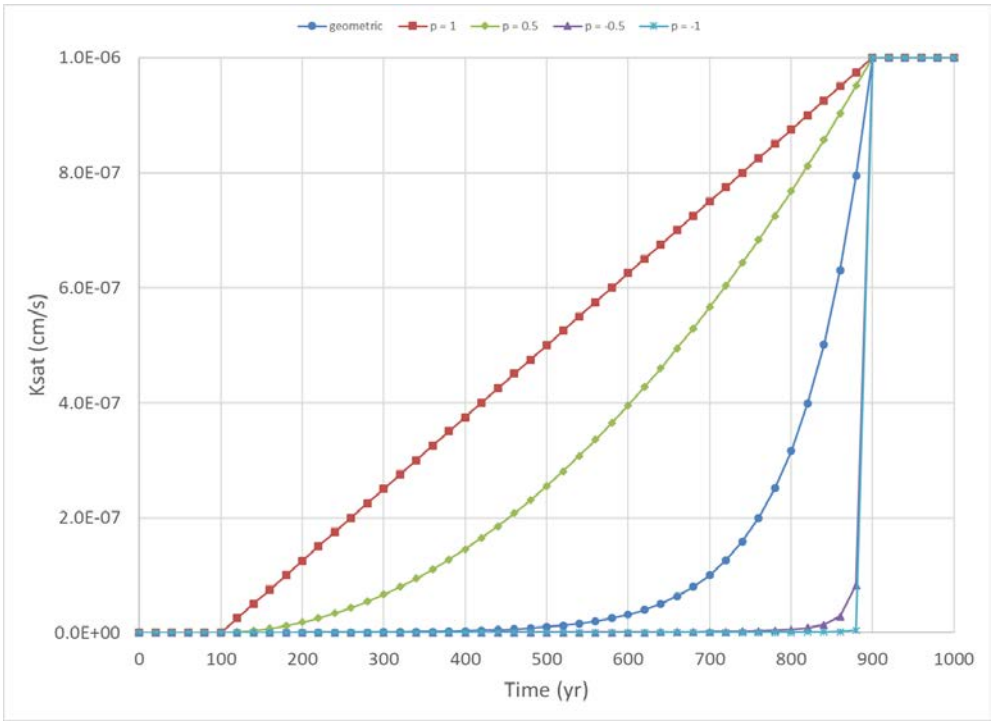

(b)

Figure 11-1 Equivalent hydraulic conductivity example: (a) semi-log plot, (b) linear plot.

12.0 References

Ababou, R. and E. F. Wood. *Comment on "Effective groundwater model parameter values: influence of spatial variability of hydraulic conductivity, leakance, and recharge" by J. J. Gomez-Hernandez and S. M. Gorelick*. Water Resources Research, v26, n8, 1843-1846. 1990.

ACI Committee 222. *Protection of Metals in Concrete Against Corrosion*. committee report ACI 222R-01, September 2001.

Ahmad, S. *Reinforcement corrosion in concrete structures, its monitoring and service life prediction – a review*. Cement & Concrete Composites 25:459-471. 2003.

Arnold, J., D. Kosson, H. van der Sloot, R. DeLapp, P. Seignette, A. Garrabrants and K. Brown. *Characterization of Reference Materials and Related Materials for the Cementitious Barriers Partnership*. CBP-TR-2010-012-1. www.cementbarriers.org. December 2010.

Benson, C. H. and J. M. Benavides. *Predicting Long-Term Percolation from the SDF Closure Cap*. University of Virginia School of Engineering Report No. GENV-18-05, Savannah River Site Report No. SRRA107772-000009. May 2018.

Brown, K. G., J. Arnold, S. Sarkar, G. Flach, H. van der Sloot, J. C. L. Meeussen, and D. S. Kosson. *Modeling Carbonation of High-Level Waste Tank Integrity and Closure*. NUCPERF 2012 Conference, Cadarache, France. November 12-15, 2012.

Brown, K. G. and A. Garrabrants. *Predicting the Hydraulic Conductivity over Time for Degrading Saltstone Vault Concrete – Task 5 (Subcontract Number SRRA110110)*. December 2017.

Brown, K., D. Kosson, A. Garrabrants, S. Sarkar, G. Flach, C. Langton, F. Smith, H. Burns, H. Van Der Sloot, J. Meeussen, E. Garboczi, J. Bullard, P. Stutzman, E. Samson, P. Mallick, L. Suttora, D. Esh, M. Fuhrmann, and J. Philip. *Cementitious Barriers Partnership (CBP): Training and Release of CBP Toolbox Software, Version 1.0 – 13480*. WM2013 Conference, Phoenix, AZ. February 24 – 28, 2013a.

Brown, K., D. Kosson, A. Garrabrants, S. Sarkar, G. Flach, C. Langton, F. Smith, H. Burns, H. Van Der Sloot, J. Meeussen, E. Garboczi, J. Bullard, P. Stutzman, E. Samson, P. Mallick, L. Suttora, D. Esh, M. Fuhrmann, and J. Philip. *Cementitious Barriers Partnership (CBP): Using the CBP Software Toolbox to Simulate Sulfate Attack and Carbonation of Concrete Structures – 13481*. WM2013 Conference, Phoenix, AZ. February 24 – 28, 2013b.

Clodic, L. and A. Meike. *Development of a Database to Model Concrete Dissolution at 25ºC Using the EQ3/6 Geochemical Modeling Code*. Lawrence Livermore National Laboratory report UCRL-ID-132088. August 1997.

Daniel, D. G. and C. L. Lobo. *User's guide to ASTM specification C 94 on ready-mixed concrete*. ASTM Manual Series MNL49. ASTM International. ISBN 9780803145573. 2005.

Desbarats, A. J. *Spatial averaging of hydraulic conductivity in three-dimensional heterogeneous porous media*. Mathematical Geology, v24, n3, 249-267. 1992.

Dixon, K. L. *Moisture Retention Properties of High Temperature Cure ARP/MCU Saltstone Grout*. SRNL-STI-2011-00661, Rev. 0. December 2011.

Drever, J. I. *The Geochemistry of Natural Waters*. 2nd Edition. Prentice-Hall. 1988.

Flach, G. *Degradation of Cementitious Materials for Saltstone Disposal Unit No. 6*. SRNL-L3200-2013-00028. September 16, 2013.

Flach, G. P. *Verification of Sulfate Attack Penetration Rates for Saltstone Disposal Unit Modeling*. SRNL-STI-2015-00236 Rev. 0. May 2015.

Flach, G. P., J. M. Jordan and T. Whiteside. *Numerical Flow and Transport Simulations Supporting the Saltstone Disposal Facility Performance Assessment*. SRNL-STI-2009-00115, Rev. 1. June 2009.

Flach, G. P., D. I. Kaplan, R. L. Nichols, R. R. Seitz and R. J. Serne. *Solid Secondary Waste Data Package Supporting Hanford Integrated Disposal Facility Performance Assessment*. SRNL-STI-2016-00175, Rev. 0. May 2016.

Flach, G. P. and F. G. Smith III. *Degradation of Cementitious Materials Associated with Saltstone Disposal Units*. SRNL-STI-2013-00118 Rev. 2. September 2014.

Fredlund, D. G., and H. Rahardjo. *Soils Mechanics for Unsaturated Soils*. John Wiley, New York. 1993.

Freeze, R. A. and J. A. Cherry. *Groundwater*. Prentice-Hall. 1979.

Gelhar, L. W. and C. L. Axness. *Three-dimensional stochastic analysis of macrodispersion in aquifers*. Water Resources Research, v19, n1, 161-180. 1983.

Gutjahr, A. L., L. W. Gelhar, A. A. Bakr and J. R. MacMillan. *Stochastic analysis of spatial variability in subsurface flows: 2. Evaluation and application*. Water Resour. Res., 14(5), 953–959. 1978.

Hall, C. and W. Hoff. *Water Transport in Brick, Stone and Concrete*. Spon Press, New York. 2002.

Hang, T. and G. P. Flach. *Evaluation of Saltstone Disposal Unit 7 Floor Penetrations*. SRNL-STI-2016-00511, Revision 0. September 2016a.

Hang, T. and G. P. Flach. *Evaluation of Revised Future Saltstone Disposal Unit Locations by PORFLOW Simulations*. SRNL-STI-2016-00534, Revision 0. September 2016b.

Holz, M., S.R. Heil and A. Sacco. *Temperature-dependent self-diffusion coefficients of water and six selected molecular liquids for calibration in accurate 1H NMR PFG Measurements*. Phys. Chem. Chem. Phys. 2. 4740–4742. 2000.

Hommel, S. P. *Recommended Values for Cementitious Degradation Modeling to Support Future SDF Modeling*. SRR-CWDA-2018-00004 Revision 1. August 2018.

Jones, W. E. and M. A. Phifer. *Saltstone Disposal Facility closure cap concept and infiltration estimates*. WSRC-STI-2008-00244, Rev. 0. May 2008.

Langton, C. A. *Chemical Degradation Assessment of Cementitious Materials for the HLW Tank Closure Project (U)*. WSRC-STI-2007-00607 Rev. 0. September 2007.

Langton, C. A. *Chemical Degradation Assessment for the H-Area Tank Farm Concrete Tanks and Fill Grouts*. SRNL-STI-2010-00035 Rev. 0. January 2010a.

Langton, C. A. *Saltstone Characterization and Parameters for Performance Assessment Modeling; SIMCO Technologies, Inc. Task 6 Report Update; SIMCO Technologies, Inc. Subcontract SIMCORD08009 Order AC48992N (U)*. SRNL-STI-2010-00515. August 2010b.

Levitt, M. *Concrete Materials: Problems and Solutions*. Taylor & Francis e-Library. 2003.

Marrero, T. R., and E. A. Mason. *Gaseous Diffusion Coefficients*. J. Phys. Chem. Ref. Data, Vol. 1, No. 1. www.nist.gov/data/PDFfiles/jpcrd1.pdf. 1972.

Matheron, G. *Ele´ments pour une The´orie des Milieux Poruex*. Masson, Paris. 1967.

Matschei, T., B. Lothenbach and F. P. Glasser. *The AFm phase in Portland cement*. Cement and Concrete Research, Vol. 37, Issue 2. pp. 118-130. http://dx.doi.org/10.1016/j.cemconres.2006.10.010. ISSN 0008-8846. February 2007.

Millings, M. R. *Summary of Carbon Dioxide in Water Table Wells and the Vadose Zone at SRS*. Savannah River National Laboratory memorandum SRNL-L3200-2012-00017. May 30, 2012.

Myer, G. E. *Analytical Methods in Conduction Heat Transfer*. McGraw-Hill, New York. 1971.

Papadakis, V. G., C. G. Vayenas, and M. N. Fardis. *A Reaction Engineering Approach to the Problem of Concrete Carbonation*. AIChE Journal, 35:1639-1650. 1989.

Phifer, M. A. *Scoping Study: High Density Polyethylene (HDPE) in Saltstone Service (U)*. WSRC-TR-2005-00101. February 2005.

Phifer, M. A. *Impact of Saltstone Disposal Unit 6 (SDU-6) High Density Polyethylene (HDPE) Thickness*. SRNL-L3200-2013-00025. July 15, 2013.

Phifer, M. A., G. P. Flach, and M. E. Denham. *SRNL Vault 2 Interior Coating Performance Assessment Requirement*. SRNL-ESB-2007-00007. April 30, 2007.

Phifer, M. A., M. R. Millings, and G. P. Flach. *Hydraulic Property Data Package for the E-Area and Z-Area Soils, Cementitious Materials, and Waste Zones*. WSRC-STI-2006-00198. September 2006.

Rast, R., and M. W. Rinker, *Overview of Hanford Single Shell Tank (SST) Structural Integrity - 12123*, WM2012 Conference, February 26 - March 1, 2012.

Richards, B. G. *Measurement of free energy of soil moisture by the psychrometric technique using thermistors, in Moisture Equilibria and Moisture Changes in Soils Beneath Covered Areas: A Symposium*. p. 39-46, Butterworths, Australia. 1965.

Samson, E. *Cementitious Barriers Partnership Task 7 Demonstration of STADIUM® for the Performance Assessment of Concrete Low Activity Waste Storage Structures*. CBP-TR-2010-007-C3, Rev. 0. Cementitious Barriers Partnership, http://cementbarriers.org. 2010.

Samson, E., P. Henocq, and J. Marchand. *Chemical Degradation Review*. Cementitious Barriers Partnership technical report CBP-TR-2009-002-C4 Rev. 0. November 2009.

Sanchez-Vila, X., J. P. Giradi and J. Carrera. *A synthesis of approaches to upscaling of hydraulic conductivities*. Water Resources Research, v31, n4, 867-882. 1995.

Sanchez-Vila, X., A. Guadagnini, and J. Carrera. *Representative Hydraulic Conductivities in Saturated Groundwater Flow*. Reviews of Geophysics, 44, 1-46. 2006.

Sappington, F. C., and M. A. Phifer. *Moisture Content and Porosity of Concrete Rubble Study*. WSRC-TR-2005-00054, Rev. 0. October 2005.

Sarris, T. S. and E. K. Paleologos. *Numerical investigation of the anisotropic hydraulic conductivity behavior in heterogeneous porous media*. Journal of Stochastic Environmental Research & Risk Assessment, v18, 188-197. 2004.

SIMCO Technologies Inc. *Washington Savannah River Company Subcontract no. AC48992N Report; Task 6 – Characterization of a Wasteform Mixture*. SIMCO Technologies Inc., Quebec Canada. June 2010.

SIMCO Technologies Inc. *Washington Savannah River Company Subcontract AC81850N Report – Vault Concrete Characterization*. March 2012.

Simner, S. P. *Proposed Simulant Salt solution for Evaluating the Resistance of SDU Concrete to Chemical Attack*. G-ESR-Z-00018. December 2015.

SRR Closure & Waste Disposal Authority. *Performance Assessment for the Saltstone Disposal Facility at the Savannah River Site*. SRR-CWDA-2009-00017 Rev. 0. October 2009.

SRR Closure & Waste Disposal Authority. *FY2013 Special Analysis for the Saltstone Disposal Facility at the Savannah River Site*. SRR-CWDA-2013-00062 Rev. 2. October 2013.

SRR Waste Disposal Authority. *FY2014 Special Analysis for the Saltstone Disposal Facility at the Savannah River Site*. SRR-CWDA-2014-00002 Rev. 1. June 2014.

Stumm, W. and J. J. Morgan. *Aquatic Chemistry: An Introduction Emphasizing Chemical Equilibria in Natural Waters*. Wiley. 1970.

Task Assistance Request G-TAR-Z-00006. *Update cementitious degradation modeling in support of the SDF modeling*. November 30, 2017.

Tian, K., C. H. Benson, J. M. Tinjum and T. B. Edil. *Antioxidant Depletion and Service Life Prediction for HDPE Geomembranes Exposed to Low-Level Radioactive Waste Leachate*. J. Geotech. Geoenviron. Eng., 143(6): 04017011. 2017.

Tixier, R. and B. Mobasher. *Modeling of Damage in Cement-Based Materials Subjected to External Sulfate Attack. I: Formulation*. Journal of Materials in Civil Engineering. 305-313. July/August 2003a.

Tixier, R. and B. Mobasher. *Modeling of Damage in Cement-Based Materials Subjected to External Sulfate Attack. II: Comparison with Experiments*. Journal of Materials in Civil Engineering. 314-322. July/August 2003b.

Turick, C. E., and C. J. Berry. *Review of Concrete Biodeterioration in Relation to Buried Nuclear Waste*. SRNL-STI-2012-00435, Rev. 0. August 2012.

van Genuchten, M. T. *A closed-form equation for predicting the hydraulic conductivity of unsaturated soils*. Soil Science Society America Journal, vol. 44, no. 5, pp. 892-898. 1980.

Walton, J. C., L. E. Plansky, and R. W. Smith. *Models for Estimation of Service Life of Concrete Barriers in Low-Level Radioactive Waste Disposal*. NUREG/CR-5542. September 1990.

Watkins, D. *Additional Recommended Inputs to PORFLOW Modeling for SDU 7*. SRR-CWDA-2018-00012 Revision 2. August 2018.

Wang, J. S. Y., and T. N. Narasimhan. *Hydrologic Mechanisms Governing Fluid Flow in a Partially Saturated, Fractured, Porous Medium*. Water Resources Research, vol. 21, no. 12. pp. 1861-1874. 1985.

Washington Savannah River Company (WSRC). *Saltstone Disposal Facility Vault 4 Inputs*. SDF-IP-07 Rev. 0. March 2008a.

Washington Savannah River Company (WSRC). *Saltstone Disposal Facility Vault 1 Input*. SDF-IP-05 Rev. 0. April 2008b.

Distribution:

timothy.brown@srnl.doe.gov
michael.cercy@srnl.doe.gov
alex.cozzi@srnl.doe.gov
david.crowley@srnl.doe.gov
david.dooley@srnl.doe.gov
a.fellinger@srnl.doe.gov
samuel.fink@srnl.doe.gov
erich.hansen@srnl.doe.gov
connie.herman@srnl.doe.gov
david.herman@srnl.doe.gov
elizabeth.hoffman@srnl.doe.gov
kevin.fox@srnl.doe.gov
john.mayer@srnl.doe.gov
daniel.mccabe@srnl.doe.gov
nancy.halverson@srnl.doe.gov
frank.pennebaker@srnl.doe.gov
william.ramsey@srnl.doe.gov
luke.reid@srnl.doe.gov
geoffrey.smoland@srnl.doe.gov
michael.stone@srnl.doe.gov
boyd.wiedenman@srnl.doe.gov
bill.wilmarth@srnl.doe.gov
Records Administration (EDWS)
tom.butcher@srnl.doe.gov
tim.coffield@srs.gov
thomas.danielson@srnl.doe.gov
james.dyer@srnl.doe.gov
gregory.flach@srnl.doe.gov
kerri.crawford@srs.gov
luther.hamm@srnl.doe.gov
thong.hang@srnl.doe.gov
steven.hommel@srs.gov
ginger.humphries@srs.gov
vijay.jain@srs.gov
daniel.kaplan@srnl.doe.gov
dien.li@srs.gov
barry.lester@srs.gov
jeremiah.mangold@srs.gov
larry.romanowski@srs.gov
kent.rosenberger@srs.gov
roger.seitz@srnl.doe.gov
ira.stewart@srs.gov
kevin.tempel@srs.gov
steven.thomas@srs.gov
david.watkins@srs.gov
jennifer.wohlwend@srnl.doe.gov